CHAPTER 12

BED CONFIGURATIONS GENERATED BY WATER FLOWS AND THE WIND

INTRODUCTION

1 A striking characteristic of the transport of granular sediment over a bed of the same material by a turbulent flow of fluid is that in a wide range of conditions the bed is molded into topographic features, called bed forms, on a scale that is orders of magnitude larger than the grains. Little ripples at one's feet at the seashore, or on a dry river bed, or in the desert, and gigantic dunes in the desert and (even more common, but not apparent to the casual observer) in large rivers and the shallow ocean—all of these are examples of bed forms. Generations of scientists and engineers have marveled at the rich and confusing variety of these features.

2 First I will introduce some terminology. The overall bed geometry that exists at a given time in response to the flow (the ***bed configuration***) is composed of individual topographic elements (***bed forms***). The aggregate or ensemble of similar bed configurations that can be produced by a given mean flow over a given sediment bed is the ***bed state***: The bed configuration differs in detail from time to time, and the bed state can be considered to be the average over the infinity of configurations that are possible under those conditions. The term ***bed phase*** can be used for recognizably or qualitatively different kinds of bed configurations which are produced over some range of flow and sediment conditions and which are closely related in geometry and dynamics. Finally, the term ***bedform*** (one word) is widely used, indiscriminately, for all four of the foregoing aspects of the bed geometry.

3 Bed configurations that are common in natural flow environments can be generated by purely unidirectional flows, combined flows, and purely oscillatory flows. I pointed out in Chapter 6 that even purely oscillatory flows in natural flow environments can be more complex than those with only one oscillatory flow component, and that a wide range of oscillatory flows can be superimposed on a unidirectional current. (This would be a good point at which to go back and review the nature of oscillatory and combined flows.)

4 You can well imagine, then, how wide a range of bed configurations we should expect to have to deal with if we endeavor to make an inclusive survey of bed configurations. The enormous range of flows that can generate bed configurations, together with the complex dynamics of the response of the bed, makes for highly varied geometry of the resulting bed configurations. In one sense, though, this is fortunate for sedimentologists, because it provides a great variety of different sedimentary structures which can be used in attempting to make paleoflow interpretations!

5 Both engineers and geologists have been making laboratory experiments on bed forms for over one hundred years, as well as watching their movement in natural flow environments. Understanding of unidirectional-flow bed configurations is fairly good by now, although by no means perfect. Work on oscillatory-flow bed configurations is less well advanced, I think owing to the difficulty of arranging oscillatory flows with long oscillation periods in the laboratory. Finally, combined-flow bed configurations have still not been much studied.

6 If the flow changes with time, the bed configuration adjusts in response. In natural flows, equilibrium between the bed and the flow is the exception rather than the rule: usually the bed configuration lags behind the change in the flow. Such disequilibrium is a major element of complexity that makes relationships among bed phases much more difficult to decipher, but its effects are very important in natural flow environments.

7 In the natural environment most bed forms are seen in sands, but they are produced in silts and gravels as well. Of greatest interest to geologists, oceanographers, and hydraulic engineers are bed forms produced by flows of air or water over mineral sediments with equant grain shape, but a far wider range, important in many engineering applications, can be produced by flows of other fluids with other densities and viscosities over sediments less dense or more dense than the common mineral sediments.

8 Many natural scientists believe (and I am among them) that there must be enormous numbers of Earth-like planets throughout the universe. The field of extraterrestrial planets is a rapidly growing field nowadays, and it would not surprise me to learn, in the not too distant future, that such Earth-like planets are being discovered. In studying a physical phenomenon like bed configurations, there is an element of danger in restricting our consideration only to the few points in the spectrum of density ratios with which we have at hand: sand in water on Earth; sand in air on Earth; sand in the Martian atmosphere of the Venusian atmosphere; see Figure 8-5, in Chapter 8). In a sense, there is nothing special about those particular points in the spectrum!

9 Apart from their intrinsic scientific interest, bed forms are important in both geology and engineering. Large subaqueous bed forms many meters high can be obstacles to navigation, and their movement can be a threat to submarine structures. Engineers are interested in bed configurations partly because they play an important role in determining the sediment transport rate, but perhaps mainly because of their importance in determining the resistance which a channel presents to a flow. For example, predicting the depth of flow in a channel built with a given slope and designed to carry a given water discharge necessitates knowing the bed configuration to be expected. Sedimentologists have given attention to bed configurations mostly because of their role in the development of stratification in sedimentary deposits; bed forms are one of the most useful tools available for interpreting ancient sedimentary environments.

10 The status of observations on bed configurations is good, but there is much room for further improvement. It is easy to observe bed configurations in

steady unidirectional and simple bidirectional oscillatory flows in laboratory channels and tanks. But there is still a great need for further laboratory work, in part because the usually small width-to-depth ratios of tanks and flumes tend to inhibit full development of the three-dimensional aspects of the bed geometry, but also, and more importantly, because not much work has been done with multidirectional oscillatory flows, and, especially, combined flows. And even the largest of laboratory experiments are restricted to flow depths at the lower end of the range of natural flow depths. In nature, on the other hand, observations on bed configurations are limited by practical and technical difficulties, and the flows that produce them are usually more complicated.

UNIDIRECTIONAL-FLOW BED CONFIGURATIONS

Introduction

11 Bed configurations made by unidirectional flows have been studied more than those made by oscillatory flows and combined flows. They are formed in rivers and in shallow marine environments with strong currents, and also in engineering flows like outdoor canals and channels of various kinds, as well as in pipes and conduits carrying granular materials.

12 In shallow marine environments, even symmetrically reversing tidal currents produce bed forms that look much like those in truly unidirectional flows, presumably because the current in each direction flows for a long enough time for the bed to respond to what it feels as a unidirectional flow. In asymmetrical tidal currents, the bed forms show net movement and asymmetry in the direction of the stronger flow, but they suffer interesting modifications by the weaker flow in the other direction.

A Flume Experiment on Unidirectional-Flow Bed Configurations

13 To get an idea of the bed configurations produced by a steady uniform flow of water over a sand bed, and the succession of different kinds of bed configurations that appear as the flow strength is increased, imagine making a series of exploratory flume experiments on sand with a mean size between 0.2 mm and 0.5 mm.

14 Build a large open channel consisting of wood or metal, with a rectangular cross section (Figure 11-1). The channel might be about one meter wide and a few tens of meters long. Install a pump and some piping to take the water from the downstream end and recirculate it to the upstream end of the channel. You might mount the whole channel on a set of screw jacks near the upstream end, so that you can change the slope of the channel easily, but this is not really necessary. It would also be nice to make at least one sidewall of the channel out of glass or transparent plastic, for good viewing of the bed configurations.

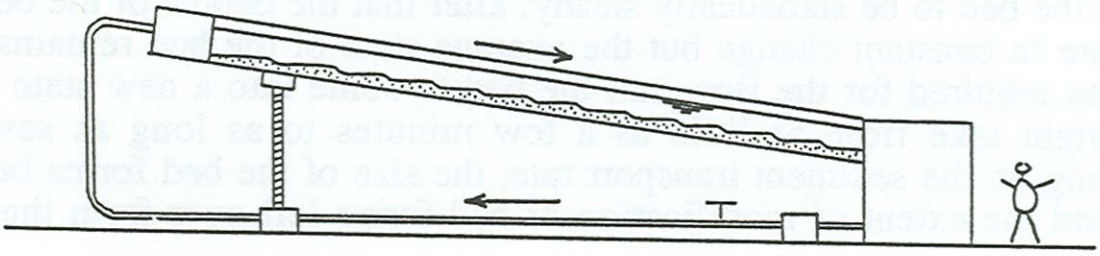

Figure 12-1. A home-made flume for studying bed configurations in unidirectional flow.

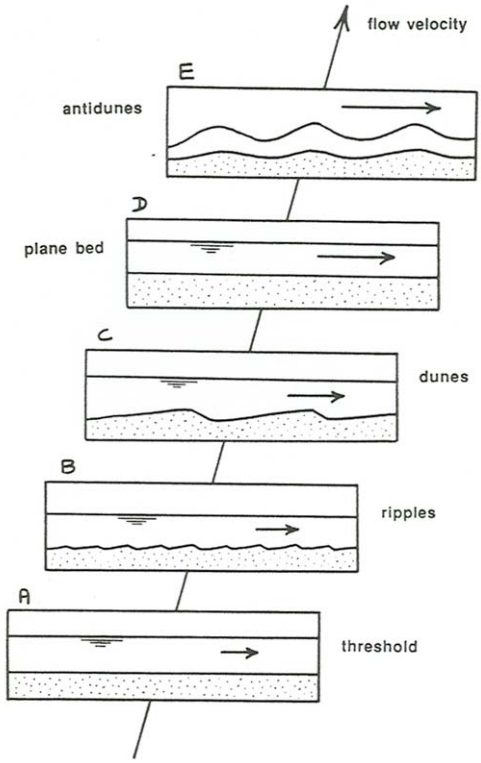

Figure 12-2. The sequence of bed phases with increasing flow velocity at a given flow depth, for medium sand.

15 Place a thick layer of sand on the bottom of the channel and then pass a series of steady and uniform flows over it. Arrange each run to have the same mean flow depth (as great as the flume will allow, ideally at least a large fraction of a meter, but a decimeter or two would suffice) and increase the mean flow velocity slightly from run to run.

16 In each run, let the flow interact with the bed long enough for the state of the bed to be statistically steady or unchanging. After that time the details of the bed configuration change constantly but the average state of the bed remains the same. The time required for the flow and the bed to come into a new state of equilibrium might be as little as a few minutes or as long as several days, depending on the sediment transport rate, the size of the bed forms that develop, and the extent of modification of bed forms that remained from the preceding run.

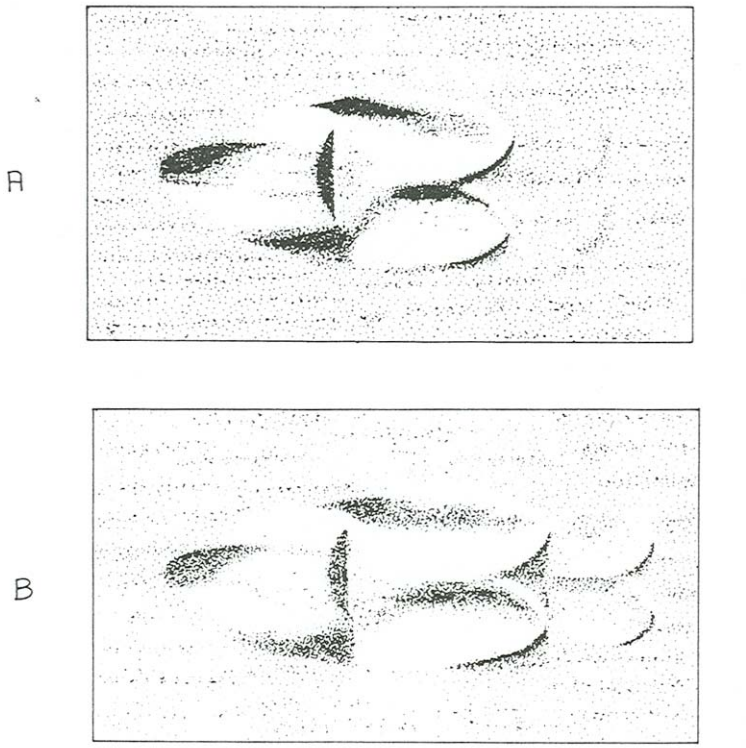

Figure 12-3. Two stages in the development of a train of ripples from a planar sand bed. Flow is from left to right, and light is from the upper left. The view is straight down on the sand bed. The depression in the left part of the pictures was made by dragging a rod along the bed. The mound thus produced was modified by the flow to become a ripple. (From photographs similar to those shown in Southard and Dingler, 1971.)

17 You could speed the attainment of equilibrium somewhat by continually adjusting the slope of the channel to maintain uniform flow as the bed roughness changes (the rougher the bed, the steeper the water-surface slope for a given water discharge), but these adjustments are not necessary, because the flow itself adjusts the bed for uniform flow by erosion at one end and deposition at the other.

18 If you are impatient for results, the way to make bed forms develop most rapidly is to start with an irregular sediment bed, but it is more instructive to start with a planar bed. (You can easily arrange a planar bed by passing a straight horizontal scraper blade along the bed. If you mount the blade on a carriage that slides on the straight upper edges of the flume walls, with a little care you obtain a beautifully planar bed.) Now turn the pump on and gradually increase the flow velocity.

Ripples:

19 After you exceed threshold conditions (Figure 12-2A), wait for a short time, and the flow will build very small irregularities at random points on the bed, not more than several grain diameters high, from which small ripples develop spontaneously.

20 You can help bed forms to develop on the planar bed by poking your finger into the bed at some point to localize the first appearance of bed forms. The flow soon transforms the little mound you made with your finger into a flow-molded bed form. The flow disturbance caused by this bed form scours the bed just downstream, and piles up enough sediment for another bed form to be produced, and so on until a beautiful widening train of downstream-growing bed forms is formed (Figure 12-3). Trains of bed forms like this, starting from various points on the bed, soon join together and pass through a complicated stage of development, finally to become a fully developed bed configuration (Figure 12-2B). The stronger the grain transport, the sooner the bed forms appear, and the faster they approach equilibrium. These bed forms, which I will later classify as ***ripples***, show generally triangular shapes in cross sections parallel to the flow.

21 At this point I should introduce some terms for the geometry of ripples and other bed forms of similar shape; see Figure 12-4. The region around the highest point on the ripple profile is the ***crest***, and the region around the lowest point is the ***trough***. The upstream-facing surface of the ripple, extending from a trough to the next crest downstream, is the ***stoss surface***, and the downstream-facing surface, extending from a crest to the next trough downstream, is the ***lee surface***. A well defined and nearly planar segment of the lee surface, called the ***slip face***, is usually a prominent part of the profile. The top of the slip face is marked by a sharp break in slope called the ***brink***. There is often but not always a break in slope at the base of the slip face also. The top of the slip face is not always the highest point on the profile, and the base of the slip face is not always the lowest point on the profile.

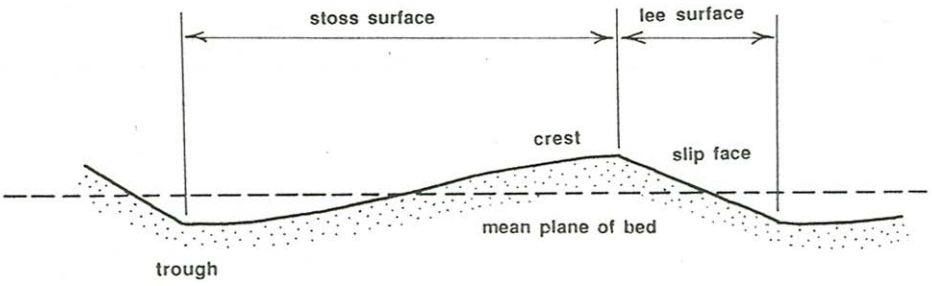

Figure 12-4. Terminology for ripple geometry in flow-parallel profile.

---

22 The stoss surfaces of ripples are gently sloping, usually less than about 10° relative to the mean plane of the bed, and their lee surfaces are steeper, usually at or not much less than the angle of repose of the granular material in water. Crests and troughs are oriented dominantly transverse to the mean flow but are irregular in detail in height and arrangement. The average spacing of ripples is of the order of 10–20 cm, and the average height is a few centimeters. The ripples move downstream, at speeds orders of magnitude slower than the flow itself, by erosion of sediment from the stoss surface and deposition of sediment on the lee surface.

23 The field of ripples is commonly *three-dimensional*, rather than *two-dimensional* as it would be if the ripples were regular and straight-crested. (This terminology has the potential to be confusing. It is common in fluid dynamics to apply the term *two-dimensional* to any feature that looks the same in all flow-parallel cross sections. That is true for perfectly regular ripples, with straight, flow-normal crests and troughs that are of the same height all along the ripple.) Most current ripples show great variability in their pattern of crests and troughs, as well as in crest heights and trough depths.

Dunes:

24 At a flow velocity that is a moderate fraction of a meter per second, ripples are replaced by larger bed forms usually called ***dunes*** (Figure 12-2C). Dunes are fairly similar to ripples in geometry and movement, but they are at least an order of magnitude larger. The transition from ripples to dunes is complete over a narrow range of only a few centimeters per second in flow velocity. Within this transition the bed geometry is complicated: the ripples become slightly larger, with poorly defined larger forms intermingled, and then abruptly the larger forms become better organized and dominate the smaller forms. With increasing flow velocity, more and more sediment is transported over the dunes as suspended load. If your flume is large enough, the dunes become large enough under some conditions of sand size and flow velocity for smaller dunes to be superimposed on larger dunes.

Plane Bed:

25 With further increase in flow velocity the dunes become lower and more rounded, over a fairly wide interval of flow velocity, until finally they disappear entirely, giving way to a ***planar bed surface*** over which abundant suspended load as well as bed load is transported (Figure 12-2D). Judging from the appearance of the bed after the flow is abruptly brought to a stop, the transport surface is very nearly planar, with relief no greater than a few grain diameters, although this subtle relief, reflecting the existence and movement of very low-relief bed forms, is thought by some to be responsible for the generation of planar lamination under conditions of net aggradation of the bed (see Chapter 16). Because the bed is obscured by abundant bed load and suspended load, it is difficult to observe the mode of grain transport over the planar bed except through the sidewall of the flume.

Antidunes:

26 As the flow velocity is increased still further, subdued standing waves appear on the water surface, and the resulting pattern of higher and lower near-bed flow velocity causes the bed to be molded correspondingly into a train of waves that are in phase with the water-surface waves. Under certain conditions these coupled bed waves and surface waves increase in amplitude and become unstable: they move slowly upstream and at the same time grow in amplitude, until they become so steep that they break abruptly, throwing much sediment into suspension (Figure 12-2E). The bed and the water surface then revert to a planar or nearly planar condition, whereupon the waves build again and the cycle is repeated. Because of their upstream movement these forms are called ***antidunes***, so named by G.K. Gilbert (1914) in his pioneering flume experiments on sediment transport and bed configurations.

27 In an approximate way, the condition for development of antidunes is that the upstream speed of propagation of surface water waves is about the same as the mean velocity of flow, so that the surface water waves have only a small speed relative to the channel bottom. The speed of shallow-water surface waves is well known to be $(gd)^{1/2}$ (see Chapter 6), where g is the acceleration of gravity and d is the water depth. The condition for development of antidunes is therefore

$$U \approx (gd)^{1/2} \tag{12.1}$$

or, dividing both sides by the right side to make the terms dimensionless,

$$\frac{U}{(gd)^{1/2}} \approx 1 \tag{12.2}$$

So conditions are favorable for the development of antidunes when the mean-flow Froude number approaches one. Of course, there must be an underlying

instability in the first place to make the antidunes grow in amplitude when in-phase bed waves develop under the water-surface waves.

28 An instructive variation on your exploratory flume experiment is to increase the flow depth by a factor of two and cover the entire flow with a rigid planar sheet parallel to the mean plane of the bed. The flow structure in the lower half of the closed duct formed in this way is very nearly the same as that in the original open-channel flow (before surface waves set in), except for some differences in the largest-scale eddies in the outer layer owing to the possibility of large eddies making their way across the center plane of the flow, in the case of the closed duct. Now make the same sequence of runs with the top cover in place. You would find the same succession of bed configurations (Figure 12-5) except for one major difference: standing waves and antidunes would not appear, and plane-bed transport would be observed up to indefinitely high flow velocities. This demonstrates that the dynamics of antidunes is unrelated to the dynamics of ripples, dunes, and plane bed: antidunes are dependent upon the presence of the free surface, whereas ripples and dunes are independent of the presence of the free surface.

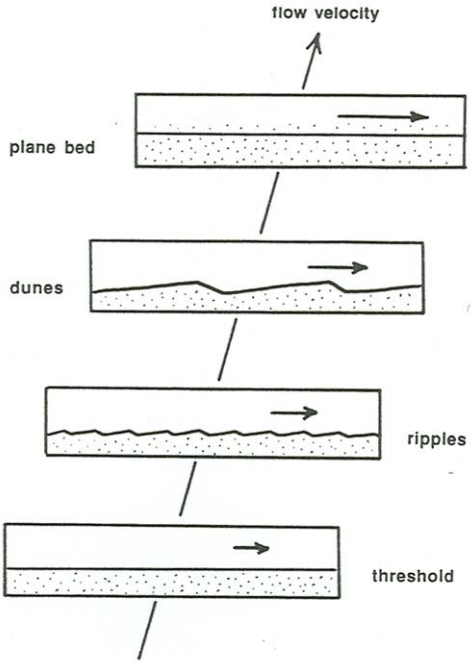

Figure 12-5. Sequence of bed phases as a function of flow velocity over medium sand in a closed conduit.

29 Now for a list of the most important variables associated with the fluid, the sediment, and the flow that define the bed state. Once we know the important variables, we can then develop a useful corresponding set of dimensionless variables and plot the positions of bed states observed in the laboratory and in natural flows in a graph with these dimensionless variables along the axes, to identify the fields or regions of existence or stability of the various bed phases. Although that does not address the dynamics behind the various bed phases—a fascinating and complicated matter, about which the last word is nowhere near having been said (see a later section in this chapter)—it provides a useful basis for paleoflow interpretations on the part of sedimentary geologists who work with the ancient sedimentary record, because the various bed configurations are commonly preserved in the record at least partly intact.

30 As is usual for work with real sediments in nature, even for equilibrium bed states in steady flows the number of variables is depressingly infinite, because an infinite number of variables are needed to describe the joint probability distribution of sediment density, grain size, and grain shape that is associated with any natural sediment. To obtain useful results we have to make some simplifying assumptions. We will assume that the sediment has only a single density and fairly equant particle shape, is subangular to subrounded rather than highly angular or perfectly well rounded, and is moderately well sorted but not unisize. Those assumptions might seem overly restrictive, but they describe most natural sands and fine gravels rather well: most natural sediments have densities not much different from that of quartz and are of approximately equant grain shape. Then the sediment can be characterized fairly well by just the average size D and the density ρ_s. Ignoring the size distribution is not as good an assumption; we should include the sorting σ in the analysis, but few studies have been made on the effect of sorting on bed configuration. The submerged weight per unit volume γ' of the sediment must be included in addition to ρ_s to take account of particle weight as well as particle inertia.

31 As usual, ρ and μ are needed to characterize the fluid. Two variables are needed to describe the flow: a flow-strength variable, and the flow depth d. Keeping in mind the discussion of flow variables in Chapter 8, we will first use U, which will lead to an unambiguous description in a three-dimensional graph, and then τ_0, which will lead to a two-dimensional graph with considerable overlapping of phase fields, although we will see that with an appropriate method for drag partition, to separate the skin friction from the total bed shear stress, a much better two-dimensional representation is possible.

32 Using first U as the flow-strength variable,

$$\text{bed state} = f(U, d, D, \rho, \mu, \gamma', \rho_s) \tag{12.3}$$

By dimensional analysis the seven variables chosen in an earlier section as being the most natural in characterizing the bed state can be grouped into four

dimensionless variables that equally well characterize the bed state, in the sense that to every combination of the four dimensionless variables there is one and only one dimensionless bed state. Many such sets of dimensionless variables, all equivalent, are possible. Perhaps the simplest set, and certainly the most meaningful in terms of the physics of the flow, is the mean-flow Reynolds number $\rho Ud/\mu$, a mean-flow Froude number $\rho^{1/2}U/(\gamma' d)^{1/2}$ written using γ', the relative roughness d/D, and the density ratio ρ_s/ρ. Another set, more useful sedimentologically in that it segregates U, d, and D into separate variables (Southard 1971; Harms et al. 1982; Southard and Boguchwal 1990), is

$$\text{Dimensionless flow depth } d^o = d(\rho\gamma'/\mu^2)^{1/3}$$

$$\text{Dimensionless flow velocity } U^o = U(\rho^2/\mu\gamma')^{1/3}$$

$$\text{Dimensionless sediment size } D^o = D(\rho\gamma'/\mu^2)^{1/3}$$

$$\text{Density ratio } \rho_s/\rho \qquad (12.4)$$

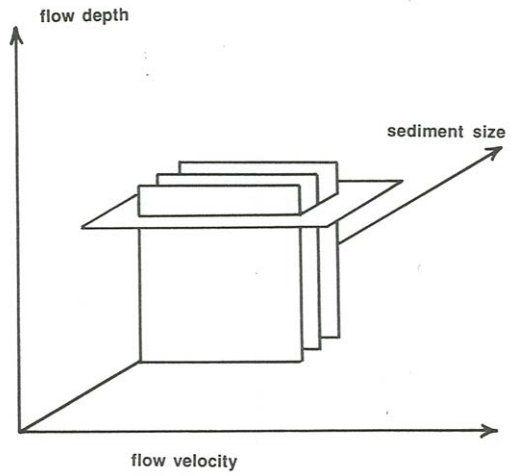

Figure 12-6. The depth–velocity–size diagram for unidirectional-flow bed phases, showing three depth–velocity sections and one velocity–size section.

33 For a given density ratio ρ_s/ρ, data on bed states obtained for equilibrium flume runs in steady uniform flow and for field observations in flows thought to be reasonable approximations to steady uniform flow can be plotted in a three-dimensional graph with d^o, U^o, and D^o along the axes (Figure 12-6). I will call this three-dimensional graph the *dimensionless depth–velocity–size diagram*. Each bed state that is observed in a flume or in a natural flow can be viewed as one of an infinite number of realizations of a single dimensionless bed

state. The corresponding dimensionless depth d^o, dimensionless velocity U^o, and dimensionless sediment size D^o for that dimensionless bed state can be computed from the given data on d, U, D, ρ, and μ and plotted in the graph. The stability fields for the various bed phases occupy certain volumes (three-dimensional regions) in this graph, and the volumes should fill space exhaustively and non-overlappingly. Boundaries between bed phases are three-dimensional surfaces or transitional zones. The graph has to be in three dimensions, but you can see its nature fairly well by making two-dimensional sections through it. Such a graph is loosely analogous to the phase diagrams that petrologists use to represent the thermodynamic equilibrium of mineral phases. Bed-phase stability graphs are a good way of systematizing and unifying disparate data on bed states in a wide variety of flows and sediments.

34 By virtue of the role of fluid density and fluid viscosity in the dimensional analysis on which the dimensionless variables in Equations 12.4 are based, the dimensionless depth–velocity–size diagram is implicitly standardized for water temperature. It is therefore possible to label the axes of the graph in an alternative way by using depths, velocities, and sizes referred to some arbitrary hypothetical water temperature. In compiling literature data for a depth-velocity-size diagram, I chose a reference temperature of 10°C as being reasonably representative of a wide range of natural subaqueous environments with flow-generated bed configurations in sands; otherwise there is nothing special about it. Using Equations 12.4 I computed from the original data the values of the 10°C depth d_{10}, the 10°C velocity U_{10}, and the 10°C size D_{10} for a flow of 10°C water dynamically equivalent to the actual flow, in the sense that it corresponds to the same set of values of d^o, U^o, and D^o. This is easily done (Southard and Boguchwal, 1990) for each variable by formulating the dimensionless value both from the given conditions and from the 10°C conditions, setting the two equal,

$$
\begin{aligned}
d^o &= d\left(\frac{\rho\gamma'}{\mu^2}\right)^{1/3} = d_{10}\left(\frac{\rho_{10}\gamma'_{10}}{\mu_{10}{}^2}\right)^{1/3} \\
U^o &= U\left(\frac{\rho^2}{\mu\gamma'}\right)^{1/3} = U_{10}\left(\frac{\rho_{10}{}^2}{\mu_{10}\gamma'_{10}}\right)^{1/3} \\
\mathrm{D^o} &= d\left(\frac{\rho\gamma'}{\mu^2}\right)^{1/3} = D_{10}\left(\frac{\rho_{10}\gamma'_{10}}{\mu_{10}{}^2}\right)^{1/3}
\end{aligned}
\qquad (12.5)
$$

and then solving for the 10°C value on the assumption that the slight variation of ρ with temperature can be neglected (the error being by a factor of only 1.003 even for 30° water):

$$d_{10} = d\left(\frac{\mu_{10}}{\mu}\right)^{2/3}$$

$$U_{10} = U\left(\frac{\mu_{10}}{\mu}\right)^{1/3} \qquad (12.6)$$

$$D_{10} = D\left(\frac{\mu_{10}}{\mu}\right)^{2/3}$$

35 In the rest of this chapter, depth, velocity, and sediment size referred to 10°C water temperature in this way are called 10°C-equivalent depth, velocity, and sediment size. Note in Equations 12.5 and 12.6 that because the factor in parentheses on the right side of the equations is raised to the 2/3 power for d and D but to the 1/3 power for U, a change in water temperature and therefore μ/ρ produces a greater change in effective flow depth and sediment size than in effective flow velocity.

36 The dimensionless depth–velocity–size diagram presented in a later section from literature data was drawn by computing d^o, U^o, and D^o for all the data points and plotting those points in a three-dimensional graph with d^o, U^o, and D^o along the axes. But then the three axes were converted to the 10°C-equivalent quantities d_{10}, U_{10}, and D_{10} by the procedure outlined above. The interior of the graph remains unchanged, but the graph becomes more useful by providing a concrete representation of depths, velocities, and sediment sizes. The values of d^o, U^o, and D^o associated with any point in the graph can be obtained using Equations 12.5. Figure 12-7 allows easy conversion between actual values of depth, velocity, and sediment size and dimensionless depth, velocity, and sediment size for two water temperatures, 0°C and 30°C.

37 If you want to use the dimensionless depth–velocity–size diagram to find the depth, velocity, and size of a bed state at some water temperature other than 10°C that corresponds to a certain point (i.e., a certain dimensionless bed state) in the diagram, you have to use Equations 12.6 in reverse:

$$d = d_{10}\left(\frac{\mu}{\mu_{10}}\right)^{2/3}$$

$$U = U_{10}\left(\frac{\mu}{\mu_{10}}\right)^{1/3} \qquad (12.7)$$

$$D = D_{10}\left(\frac{\mu}{\mu_{10}}\right)^{2/3}$$

Because the particular bed state and the corresponding hypothetical 10°C bed state are rigorously similar (geometrically, kinematically, and dynamically), dependent variables with the dimensions of length, like bed-form height or spacing, are in the same ratio between the two states as d/d_{10} or D/D_{10}, found from Equations 12.5, 12.6, or 12.7 to be

$$\frac{d}{d_{10}} = \left(\frac{\mu}{\mu_{10}}\right)^{2/3} \qquad (12.8)$$

and dependent variables with the dimensions of velocity, like the speed of bed-form movement, are in the same ratio between the two states as U/U_{10}, found likewise from Equations 12.5, 12.6, or 12.7 to be

$$\frac{U}{U_{10}} = \left(\frac{\mu}{\mu_{10}}\right)^{1/3} \tag{12.9}$$

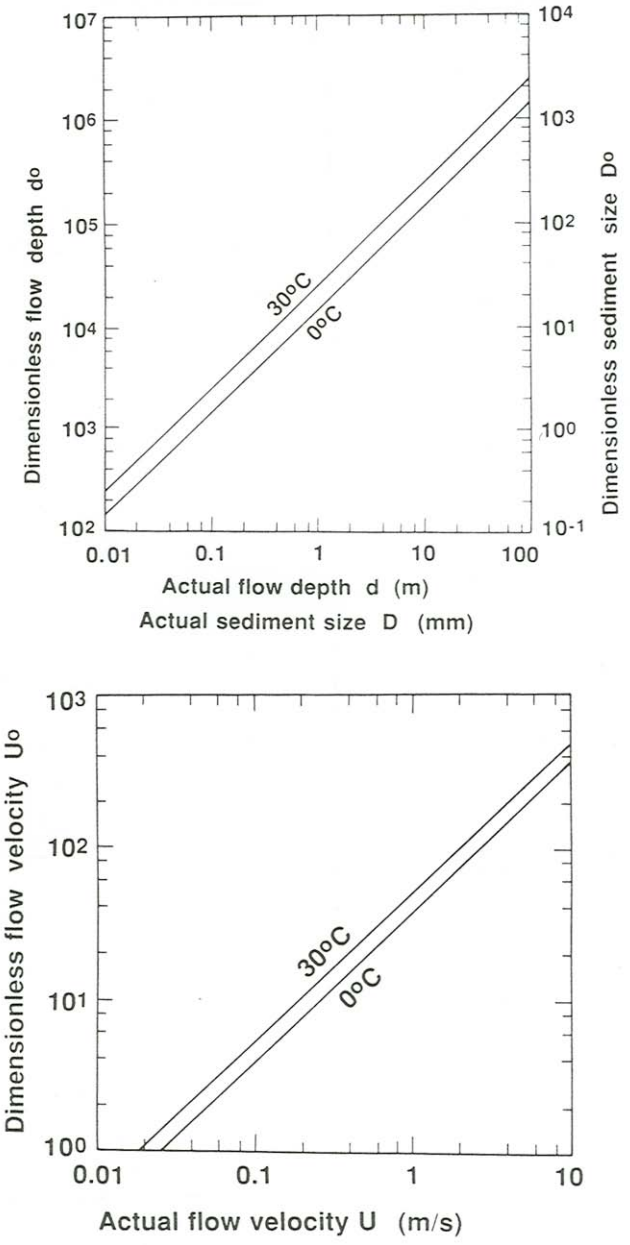

Figure 12-6. Graph for converting between actual flow depth, flow velocity, and particle size, and dimensionless flow depth, flow velocity, and particle size.

38 It is difficult for the mind to translate values for dimensionless flow depth, flow velocity, and sediment size into real combinations of flow and sediment. In water flows on the Earth's surface, with water temperatures from 0°C to 30°C and a range of actual flow depths from 0.01 m to 10 m, dimensionless flow depth ranges from about 10^2 to almost 10^6. Likewise, in the same range of water temperature, for actual flow velocities from 0.1 m/s to a few meters per second, dimensionless flow velocity ranges from about 5 to about 150, and for actual sediment sizes from a few hundredths of a millimeter to a few centimeters, dimensionless sediment size ranges from about 0.5 to about 750.

Hydraulic Relationships

Depth–Velocity–Size Diagram

39 Figures 12-8, 12-9, 12-10, and 12-11 show what the depth–velocity–size diagram for quartz sand in water looks like, on the basis of laboratory experiments made by many investigators. The experiments have been made mainly at flow depths less than a meter. It is much more difficult to obtain data points from deeper natural flows, and none are included in these figures; see below for further discussion of bed configurations in deeper flow depths.

40 I have labeled the axes in Figures 12-8 through 12-11 not with the dimensionless variables but with the actual values of flow velocity U, flow depth d, and sediment size D that correspond to the respective dimensionless variables for an arbitrary reference water temperature of 10°C. This provides a concrete feeling for flow and sediment conditions while preserving the interior features of the dimensionless graph. Ignoring the water temperature would lead to considerable scatter in the data points, and would obscure the strong regularities shown by the dimensionless diagram.

41 Figures 12-8 and 12-9 show three depth–velocity sections for sediment sizes of 0.10–0.14 mm, 0.40–0.50 mm, and 1.30–1.80 mm. Figure 12-8 shows data points from many experimental studies, and Figure 12-9 is a schematic version of Figure 12-8. Figures 12-10 and 12-11 show a velocity–size section for a flow depth of 0.25–0.40 m. Figure 12-10 shows data points, and Figure 12-11 is a schematic version. Figures 12-8 through 12-11 are from Boguchwal and Southard (1990).

42 The section for 0.10–0.14 mm sand (Figures 12-8A, 12-9A) shows fields only for ripples, upper-regime plane bed, and antidunes. All the boundaries here and in the other two graphs in Figures 12-8 and 12-9 slope upward to the right. The boundary between ripples and plane bed slopes in that sense because the deeper the flow the greater the velocity needed for a given bed shear stress. The boundary between plane bed and antidunes slopes in that sense because it is well represented by the condition that the Froude number $U/(gd)^{1/2}$ is equal to one, as discussed above. The latter boundary is shown to truncate the former, because (though data are scanty) as the Froude number approaches one, antidunes develop irrespective of the preexisting configuration. This relation holds true also, and more clearly, for coarser sediments (Figures 12-8B, 12-8C, 12-9B, 12-10C).

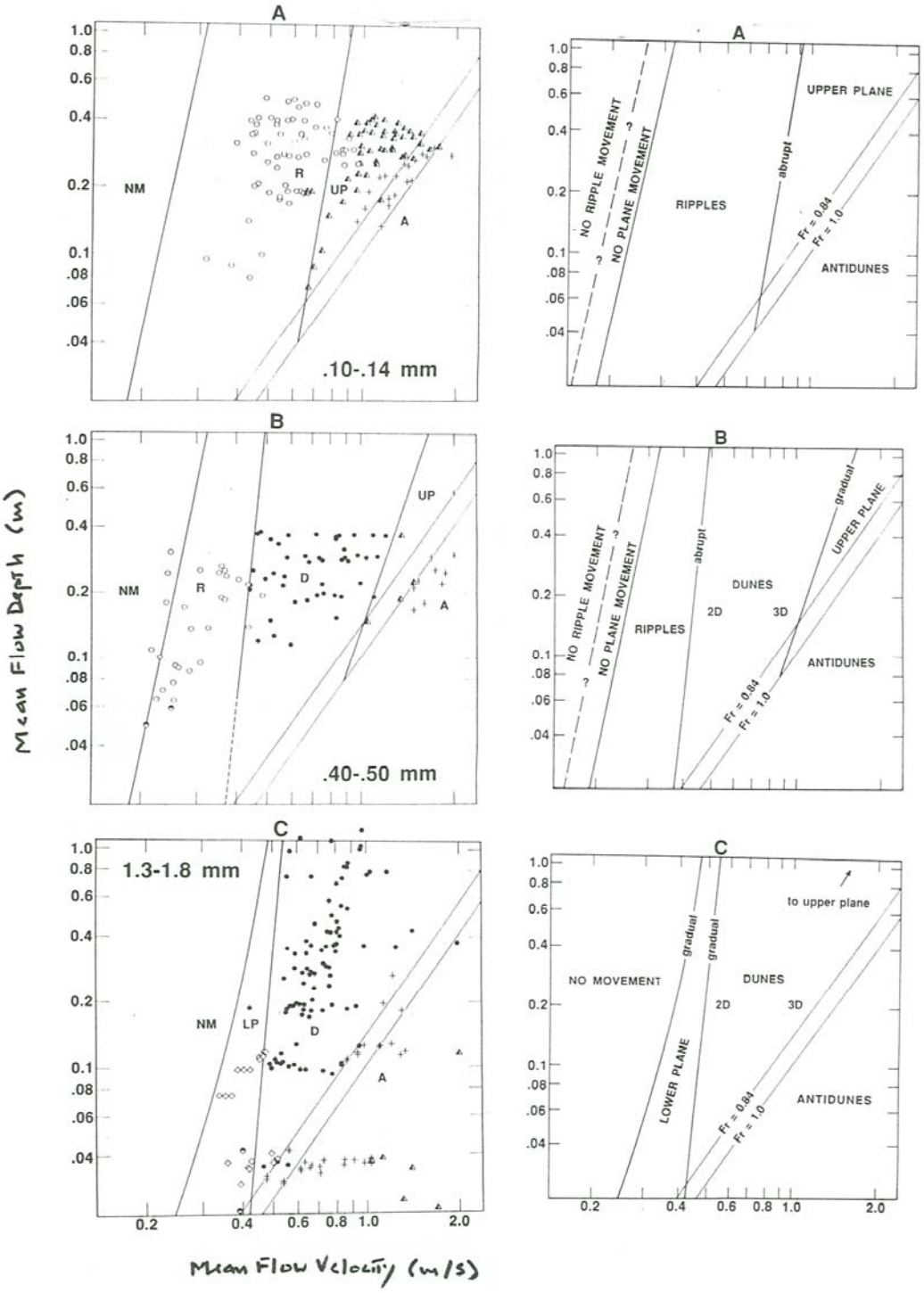
A
1.0
0.8
0.6
0.4
0.2
0.1
.08
.06
.04
NM
R
UP
A
.10-.14 mm
A
UPPER PLANE
NO RIPPLE MOVEMENT
? ? ?
NO PLANE MOVEMENT
RIPPLES
abrupt
Fr = 0.84
Fr = 1.0
ANTIDUNES
B
NM
R
D
UP
A
.40-.50 mm
B
gradual
UPPER PLANE
NO RIPPLE MOVEMENT
? ? ?
NO PLANE MOVEMENT
abrupt
DUNES
2D
3D
RIPPLES
ANTIDUNES
Fr = 0.84
Fr = 1.0
C
1.3-1.8 mm
NM
LP
D
A
0.2
0.4
0.6
0.8
1.0
2.0
C
to upper plane
gradual
gradual
NO MOVEMENT
DUNES
2D
3D
LOWER PLANE
ANTIDUNES
Fr = 0.84
Fr = 1.0
Mean Flow Depth (m)
Mean Flow Velocity (m/s)

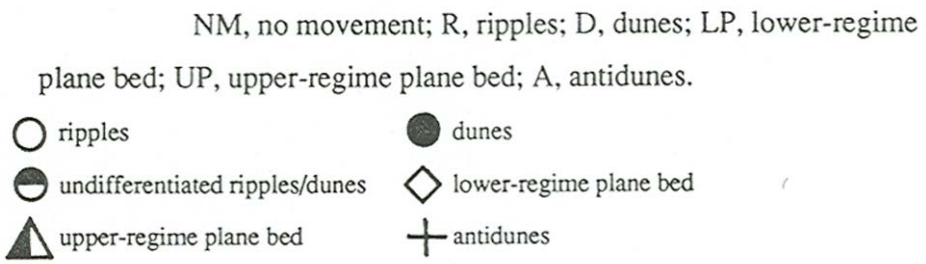

Figure 12-8 (previous page, left column). Bed phases in graphs of mean flow depth vs. mean flow

Figure 12-9 (previous page, right column. Schematic versions of the graphs in Figure 12-8.

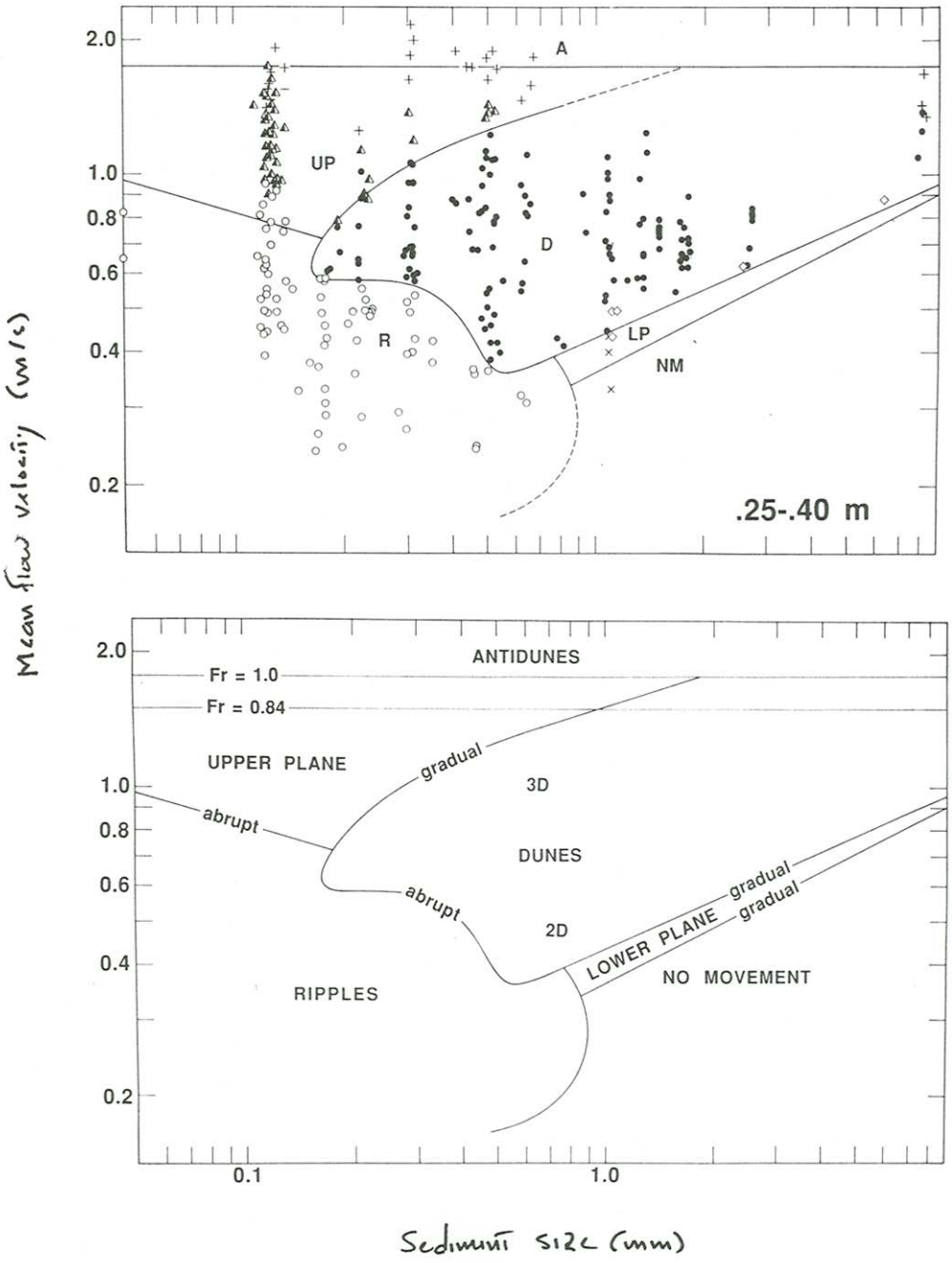

Figure 12-10 (upper). Bed phases in a graph of mean flow velocity vs. mean sediment size, for a mean flow depth of 0.25–0.40 m.

Figure 12-11 (lower). Schematic version of the graph in Figure 12-10.

43 Figure 12-8A (and Figure 12-8B, for medium sands, as well) show two kinds of boundary between movement and no movement. To the right is the curve for incipient movement on a plane bed, and to the left is the boundary that defines the minimum velocity needed to maintain preexisting ripples at equilibrium. It is clear that the latter boundary lies to the left of the former, but the existing data are not good enough to define the positions of these boundaries well. (Only the former boundary is shown in Figures 12-8A and 12-9B.)

44 The section for 0.40–0.50 mm sand (Figures 12-8B, 12-9B) shows an additional field for dunes between the fields for ripples and for plane bed. The boundary between dunes and plane bed clearly slopes less steeply than the boundary between ripples and dunes. For depths less than about 0.05 m it is difficult to differentiate between ripples and dunes, because dunes become severely limited in size by the shallow flow depth. The appearance and expansion of the dune field with increasing sediment size pushes the lower termination of the plane-bed field to greater depths and velocities, nearly out of the range of most flume work. The antidune field truncates not only the ripple field, as with finer sands, but the dune field as well.

45 In the section for 1.30–1.80 mm sand (Figures 12-8C, 12-9C), a lower-regime plane bed replaces ripples at low flow velocities. Upper-regime plane bed is still present in the upper right, but few flume data are available. Upper-regime plane beds succeed antidunes with increasing velocity and decreasing depth in the lower right; apparently the bed becomes planar once again as the Froude number becomes sufficiently greater than one. The left-hand boundary in Figures 12-8C and 12-9C represents the threshold for sediment movement on a plane bed. Sections for even greater sediment size are qualitatively similar to the section shown in Figures 12-8C and 12-9C.

46 In the velocity–size section for flow depths of 0.25–0.40 m (Figures 12-10, 12-11), ripples are the stable bed phase for sediment sizes finer than about 0.8 mm. The range of flow velocity for ripples becomes narrower with increasing sediment size, and the ripple field finally ends against the fields for plane beds with or without sediment movement. Relationships in this region are difficult to study because in these sand sizes and flow velocities a long time is needed for the bed to attain equilibrium. In medium sands ripples give way abruptly to dunes with increasing flow velocity, but, in finer sediment, ripples give way (also abruptly) to plane bed. Although not well constrained, the ripple–plane boundary rises to higher velocities with decreasing sediment size.

47 Dunes are stable over a wide range of flow velocities in sediments from medium sand to indefinitely coarse gravel. Both the lower and upper boundaries of the dune field rise with increasing flow velocity, and both are gradual transitions rather than sharp breaks. For sediments coarser than about 0.8 mm there is a narrow field below the dune field for lower-regime plane bed; the lower boundary of this field is represented by the curve for threshold of sediment movement on a plane bed.

48 There is one *triple point* among ripples, dunes, and upper plane bed at a sediment size of about 0.2 mm, and another among ripples, dunes and lower plane

bed at a sediment size of about 0.8 mm. The coverage of data around these two triple points constrains the bed-phase relationships fairly closely. Between these two triple points the dune field forms a kind of indented salient pointing toward finer sediment sizes. The boundary between ripples and upper plane bed seems to pass beneath the dune field at the upper left triple point to emerge again at coarser sediment size and lower flow velocity as the boundary between ripples and lower plane bed at the lower right triple point.

49 Other velocity–size sections, for other flow depths, show the same qualitative relationships as Figures 12-10 and 12-11. With increasing flow depth the lower boundary of the antidune field rises very rapidly, and antidunes are unimportant in flows greater than a few meters deep. All the other boundaries rise more slowly with increasing flow depth. There is also some change in the shape of the dune field with increasing flow depth.

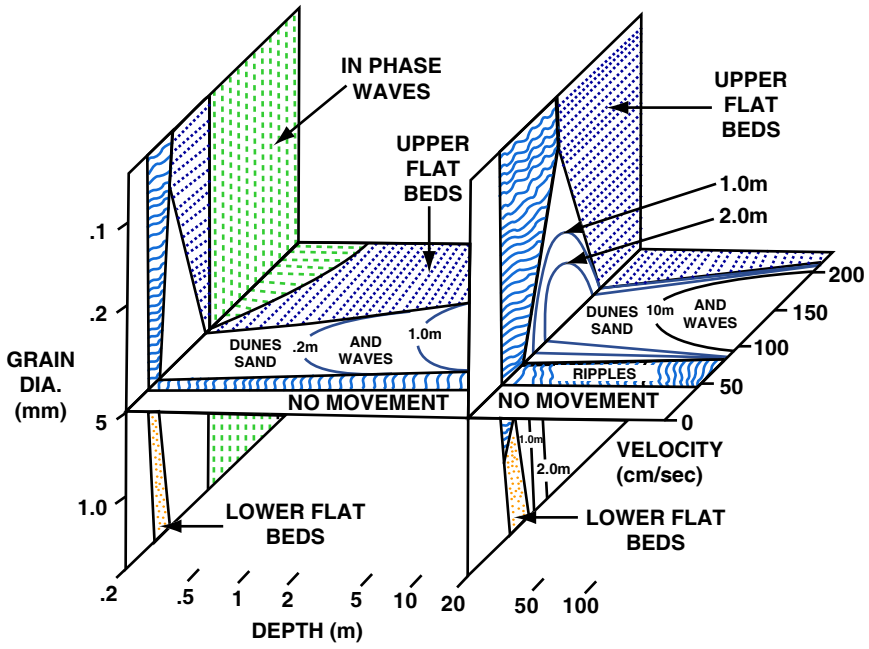

Figure by MIT OpenCourseWare.

Figure 12-12. Schematic depth–velocity–size diagram showing bed-phase stability field for bed phases in steady unidirectional water flows with a wide range of flow depths in flumes and natural environments. (From Rubin and McCulloch, 1980.)

50 Numerous observations of bed configurations in natural environments in which sands are subjected to fairly steady unidirectional flows indicate that the stability relationships of bed configurations in deeper flows are a straightforward extrapolation of the depth–velocity–size diagram discussed above. Ripples are almost the same in shallow flows and deep flows, but dunes in deep flows are much larger than dunes in shallow flows. Figure 12-12, after Rubin and McCulloch (1980), shows an extrapolation of the depth–velocity–size diagram to much greater flow depths based on data from several studies in natural flow environments.

51 There must be a definite average dune height and spacing associated with each point in the existence field for dunes in the depth–velocity–size diagram. Unfortunately, few experimental studies have reported dune dimensions systematically. Figures 12-13 and 12-14 make use of data on dune spacings and heights from the best data set, that of Guy et al. (1966), in a crude attempt to contour dune spacings and heights in the depth–velocity–size diagram. Figures 12-13A and 12-13B show contours of dune spacing and height in a depth–velocity section for a sediment size of 0.30–0.40 mm, and Figures 12-14A and 12-14B show contours of dune spacing and height in a velocity–size section for a flow depth of 0.25–0.40 m.

52 In the depth-velocity section (Fig. 12-13A), dune spacing increases from lower left to upper right, with increasing depth and velocity. In the velocity-size section (Fig. 12-14A), dune spacing increases from lower right to upper left with increasing velocity and decreasing sediment size; the greatest spacings are at the upper-plane-bed boundary and a sediment size of between 0.2 and 0.3 mm. Dune height shows a different and more complicated behavior. In the depth–velocity section (Fig. 12-13B), dune height increases monotonically with increasing depth but shows an increase and then a decrease with increasing flow velocity at constant depth. In the velocity–size section (Fig. 12-14B), there is an elongated core of greatest heights extending from near the left-hand extremity of the dune field, at the finest sizes of about 0.2 mm, rightward to sizes of 0.5 to 0.6 mm. Heights seem to decrease in all directions from that core, most rapidly with decreasing flow velocity.

53 The sections in Figures 12-13 and 12-14 intersect each other at right angles at the dashed line shown on both sections. You have to imagine the contours as cuts through a family of curved surfaces in three dimensions filling the dune field in the depth–velocity–size diagram.

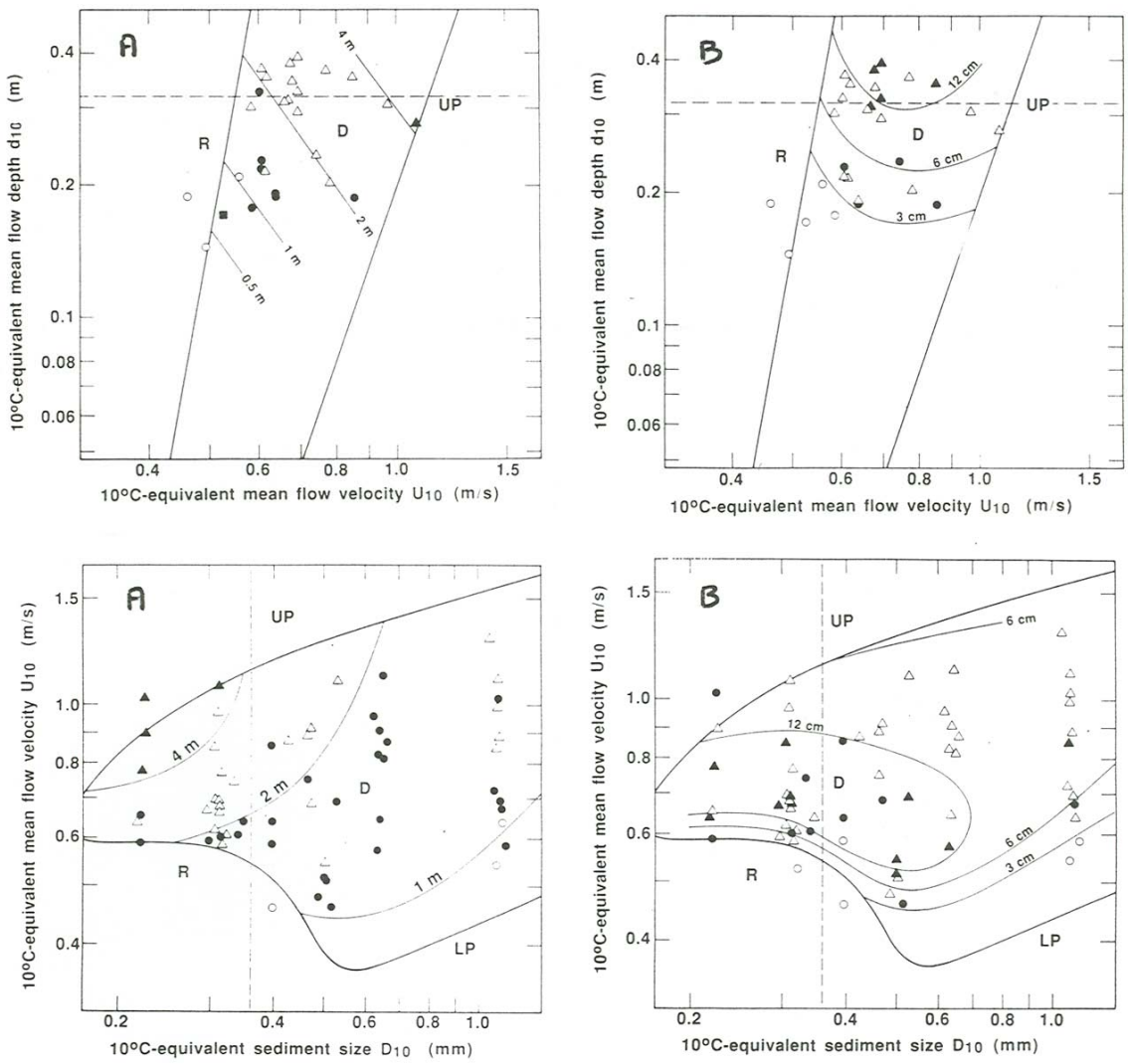

Figure 12-13. Contoured data on **A)** dune spacing and **B)** dune height from Guy et al. (1966) in a depth–velocity section for a range of sediment size of 0.30–0.40 m, with bed-phase stability fields taken from Figure 12-8. Symbols for dune spacing: solid squares, < 0.5 m; open circles, 0.5–1 m; solid circles, 1-2 m; open triangles, 2-4 m; solid triangles, > 4 m. Symbols for dune height: open circles, < 3 cm; solid circles, 3–6 cm; open triangles, 6–12 cm; solid triangles, > 12 cm. The dashed line shows the intersection of the sections represented by Figures 12-8 and 12-10 in the depth–velocity–size diagram.

Figure 12-14. Contoured data on **A)** dune spacing and **B)** dune height from Guy et al. (1966) in a velocity–size section for a range of flow depths of 0.25–0.40 m, with bed-phase boundaries taken from Figure 12-10. Symbols for dune spacing: open circles, < 1 m; solid circles, 1–2 m; open triangles, 2–4 m; solid triangles, > 4 m. Symbols for dune height: open circles, < 3 cm; solid circles, 3–6 cm; open triangles, 6–12 cm; solid triangles, > 12 cm. The dashed line shows the intersection of the sections represented by Figures 12-8 and 12-10 in the depth–velocity–size diagram.

Diagrams with Bed Shear Stress

54 So far we have looked at the hydraulic relationships of bed phases using the mean flow velocity U as the flow-strength variable. Most investigators have chosen to use the bed shear stress τ_o rather than U. What do the same relationships look like in graphs using the bed shear stress τ_o? One thing we can say right away about such graphs is that the effect of flow depth is much less: the effect of the substantial change in velocity with flow depth for a given bed shear stress is no longer relevant, and all that is left is the smaller effect on the bed shear stress of changes in bed-form geometry with flow depth. A single suitably nondimensionalized two-dimensional graph of bed shear stress against sediment size should therefore be expected to represent bed states reasonably well. Simons and Richardson (1966) seem to have been the first to use such a plot, although in the dimensional form of τ_o vs. D. A later and more comprehensive of plots of this kind was given by Allen (1982, Vol. 1, p. 339–340), who plots Shields parameter and dimensionless (temperature-standardized) stream power against dimensionless (temperature-standardized) sediment size.

55 Boundary shear stress can be nondimensionalized in various ways. The conventional way is to form a dimensionless variable containing τ_o and D, namely $\tau_o/\gamma' D$, usually called the Shields parameter (see Chapter 9). One can also work with a dimensionless form of the stream power $\tau_o U$, on the theory that the sediment transport depends most fundamentally upon stream power. Another alternative is $\tau_o(\rho/\gamma'^2\mu^2)^{1/3}$, which I call here the dimensionless boundary shear stress T^o. The disadvantage with T^o is that it does not embody the physics of the phenomenon nearly as well as the Shields parameter, but the advantage is that, when T^o is used with D^o, τ_o and D do not appear together in the same dimensionless variable. We will work with this last alternative, because it lends itself more directly to temperature standardization, which is important in the range of conditions for which Reynolds-number effects cannot be neglected, and also because sediment-size effects are thereby manifested entirely through the dimensionless sediment size $D(\rho\gamma'/\mu^2)^{1/3}$.

56 Figure 12-15 is a plot of T^o vs. D^o showing the stability fields for the various bed phases. The same data sources were used as for the depth–velocity–size graph discussed above, except that fewer studies were used because some studies that reported the mean flow velocity did not report the energy slope, so τ_o could not be computed. Only runs made at depths greater than 0.06 m were used. In all, 1204 runs were used. 10°C-equivalent flow depths d_{10} range from 0.06 m up to the deepest reported in the sources used, a little greater than 1 m (by Nordin 1976). Figure 12-16 is a schematic version of Figure 12-15.

57 The value of τ_o for each run was corrected for sidewall effects by the method proposed by Vanoni and Brooks (1957). (For a summary of this method, see Vanoni 1975, p. 152–154.) The result is an estimate of the shear stress τ_{ob} acting on the sediment bed only. Because the bed is always rougher than the sidewalls (except for dynamically smooth flow over a planar granular bed), and the width/depth ratio is never infinite, this estimate of τ_{ob} is always greater than the boundary shear stress averaged over the wetted perimeter of the flow, which is

found from the experimental data by use of the resistance equation for steady uniform flow in an open channel, $\tau_o = \rho g A S/p$, where A is the cross-sectional area of the flow and p is the wetted perimeter of the flow. For bed states with rugged flow-transverse bed forms in flows with small width/depth ratios, τ_{ob} can be almost half again as large as τ_o.

58 The axes of the graph in Figure 12-15 are not labeled with T^o and D^o but with D_{10} and $(\tau_{ob})_{10}$, the sidewall-corrected bed shear stress standardized to a water temperature of 10°C. As with depth, velocity, and size in an earlier section, $(\tau_{ob})_{10}$ is related to τ_{ob} by the equation

$$(\tau_{ob})_{10} = \tau_{ob}\left(\frac{\mu_{10}}{\mu}\right)^{2/3} \qquad (12.10)$$

obtained by equating values of T^o for 10°C and for the given conditions and solving for $(\tau_{ob})_{10}$ on the assumption that ρ and γ' do not vary with temperature.

59 Scatter or overlapping of points for different bed phases is much greater in Figure 12-15 than in the various sections through the dimensionless depth–velocity–size diagram, for two main reasons:

- It is well known that because the form resistance, which is the dominant contribution to the total bed shear stress over rugged flow-transverse bed forms, disappears in the transition from ripples to upper plane bed or from dunes to upper plane bed, the total bed shear stress actually decreases with increasing mean flow velocity in these transitions before it increases again. For that reason, there is a certain range of τ_{ob} for which three different values of U are possible; see Figure 8-10, back in Chapter 8. In a plot of τ_{ob} against D, this means that there is an approximately horizontal band across the graph in which values of U, and thus also their associated bed phases, overlap or fold onto one another. In Figure 12-15 this is shown as a field of overlapping dunes, upper plane bed, and antidunes, labeled V, and a field of overlapping ripples, upper plane bed, and antidunes, labeled VI.

- Accurate measurement of water-surface slope S, and therefore τ_o, is understandably less accurate than measurement of U: water-surface slopes are small, so long channels and careful surveying are needed, and in any case the slope varies with time around some long-term average as the details of the bed configuration fluctuate, so long time series of S are needed for good accuracy. These problems with the slope presumably affect all of Figure 12-15, but they are noticeable only at bed-phase boundaries that should not be affected by the shear-stress ambiguity noted above, like the boundary between ripples and dunes or the boundary between lower plane bed and dunes.

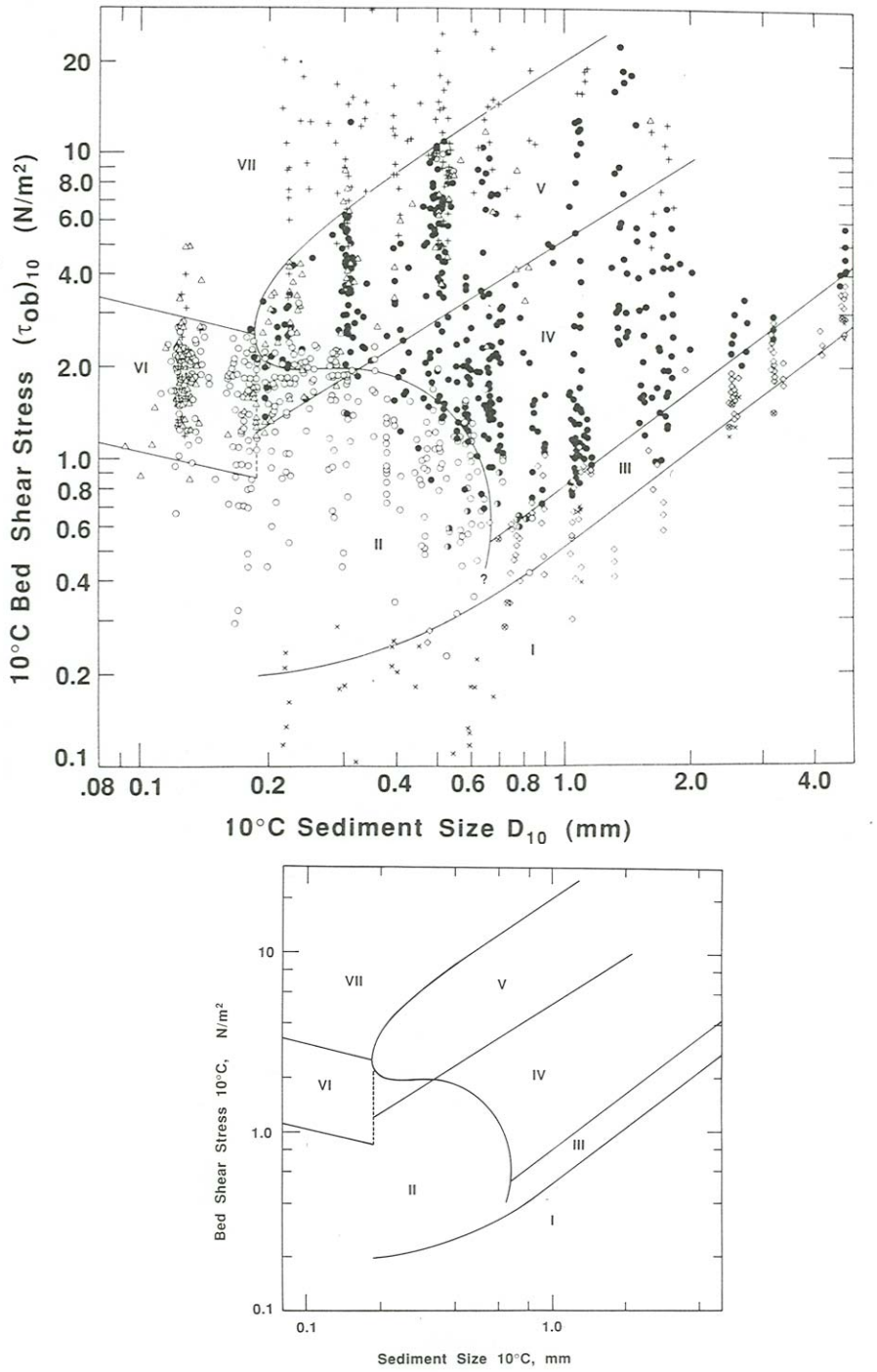

Figure 12-15. Bed phases in a dimensionless (temperature-standardized) plot of sidewall-corrected bed shear stress vs. sediment size for bed phases. labels for regions: I, no movement on plane bed; II, ripples; III, lower plane bed; IV, dunes; V overlap region of dunes, upper plane bed, and antidunes; VI, overlap region of ripples, upper plane bed, and antidunes; VII overlap region of upper plane bed and antidunes.

Figure 12-16. Schematic version of Figure 12-15.

60 The effects of data scatter and phase-field overlap make partitioning Figure 12-15 into existence fields for the various bed phases not a straightforward matter. The more straightforward results for the depth–velocity–size diagram were used as a guide in developing a rational partition.

61 Because of the moderate degree of scatter of ripple and dune points, the boundary between ripples (Region II) and dunes (Region IV) can be located only in a general way. The overall shape of the boundary was made qualitatively similar to that in the depth–velocity–size diagram (Figures 12-8 through 12-11). It is reasonable to suppose that this boundary continues downward past the question mark and then leftward to define the minimum shear stress for existence of ripples, as in Figures 12-10 and 12-11. Because few investigators have attempted to identify the weakest flows for which preexisting ripples are maintained as flow strength is very gradually decreased while equilibrium is maintained, existing data are inadequate to define the position of this extension. Either the plane-bed threshold curve is eclipsed by the lower part of the ripple field, as in Figures 12-10 and 12-11, or the lower boundary of the ripple field is at bed shear stresses entirely above those for the plane-bed threshold curve. The threshold curve itself is not extended leftward because of this uncertainty.

62 Interpretation of the remaining boundaries is based upon the existence of a minimum sediment size of about 0.15–0.20 mm for existence of dunes, as shown clearly by left-pointing "nose" of the dune field in the velocity–size sections through the depth–velocity–size diagram together with the effect of the τ_0 ambiguity on the relations among ripples, dunes, and plane beds. As in the velocity–size sections through the depth–velocity–size diagram, the ripple–dune boundary in Figure 4-17 is interpreted to pass leftward through an inflection point and then curve upward and again rightward, passing through the sediment-size minimum for dunes, to become the upper limit of dune stability (between Regions V and VII).

63 Owing to the shear-stress ambiguity there is a substantial range of shear stresses below this upper boundary for dunes for which either dunes or plane bed can exist. The lower limit of this overlap region (Region V) is shown as a straight line sloping downward to the left. Neither the shape nor the position of this line is well constrained by the data. By its nature, this boundary must end leftward at the minimum sediment size for the existence of dunes; it is therefore connected upward to the point of minimum sediment size by a vertical dashed line. In the small unlabeled region with approximately triangular shape (bounded below by this lower limit of upper-plane-bed stability, above by the upper limit of ripple stability, and to the left by the leftward limit of dune stability), ripple and dune points overlap.

64 To the left of the minimum sediment size for dunes, ripple pass directly into upper plane bed with increasing flow strength, and again there is a broad region of overlap of ripples and upper plane bed (Region VI). In this region the vertical span of the overlap region is about as great as the span of available data, so the two boundaries sloping downward to the right here (the upper showing the

maximum shear stresses for existence of ripples, and the lower showing the minimum shear stresses for existence of plane beds) are poorly constrained. The slopes of these lines were chosen only by analogy with that of the boundary between ripples and upper plane bed in the velocity–depth sections of the depth–velocity–size diagram; both their slope and their parallelism are arbitrary.

65 The upper of these two boundaries, giving the upper limit for ripples, is shown to end at the sediment-size minimum for dunes (i.e., the point of vertical tangent at the leftward extremity of the dune field), although this is not a necessity: the intersection could just as well lie somewhat above or somewhat below that point. In any case, the second of these boundaries, representing the lower limit for existence of upper plane beds, must terminate rightward at the same sediment size—hence the vertical dashed line connecting the two boundaries. Because the intersection should not be expected to be exactly at the minimum sediment size for dunes, this vertical dashed line should actually be at a slightly different and greater sediment size from the vertical dashed line, mentioned above, that connects the two analogous curves for dunes at greater sediment sizes. So there must really be *two* vertical dashed lines, very close together. Existing data, extensive as they are, are inadequate to locate the two corresponding sediment sizes with certainty, and they are shown as a single vertical dashed line in Figure 12-15.

66 Points for antidunes appear throughout Regions VI and VII and in the upper part of Region V in Figure 12-15. Presumably the reason there is no boundary between upper plane bed and antidunes in what is labeled as Region VII in Figure 12-15 is that the transition from upper plane bed to antidunes with increasing flow velocity at the flow depths characteristic of many flume experiments takes place at bed shear stresses well below those of Region VII.

67 The consequences of lumping all flow depths into the single plot represented by Figure 12-15 are substantial only for antidunes, because the onset of antidunes depends upon the mean-flow Froude number. Plots of $(\tau_{ob})_{10}$ vs. D_{10} for the individual depth categories used in plotting the depth–velocity–size diagram show a systematic, although still scattered, rise in the position of the minimum shear stresses for antidunes as flow depth increases. Other effects of flow depth on the positions of the various boundaries in $(\tau_{ob})_{10}$–D_{10} plots are so minor as to be swamped by the data scatter.

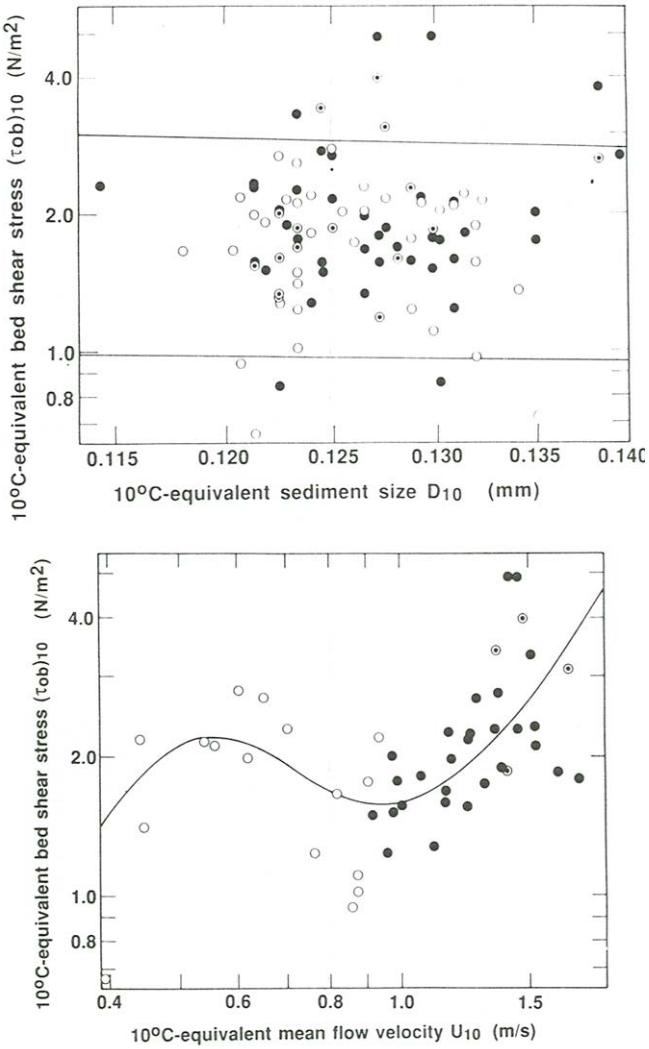

Figure 12-17. Dimensionless (temperature-standardized) plot of sidewall-corrected bed shear stress vs. sediment size for a narrow range of sediment sizes from the data of Willis et al. (1972) to show more clearly the details of the left-hand part of Figure 12-15. Symbols: solid circles, upper plane bed; bull's-eye circles, antidunes; open circles, ripples.

Figure 12-18. Dimensionless (temperature-standardized) plot of sidewall-corrected bed shear stress vs. mean flow velocity from the data of Willis et al. (1972). Symbols are the same as in Figure 12-17.

68 The welter of overlapped points for ripples, upper plane bed, and antidunes for sediment sizes around 0.12 mm, mostly from the work of Willis et al. (1972), is difficult to distinguish in Figure 12-15, so all the runs made in that study for which slope was reported are replotted in Figure 12-17 with the sediment-size axis stretched relative to the shear-stress axis. The straight lines represent the minimum shear stresses for ripples and the minimum shear stresses for upper plane beds, taken from Figure 12-15. The thorough blending of points for the three phases is clear. Figure 12-18, a plot of 10°C-equivalent bed shear stress against 10°C-equivalent mean flow velocity for those same points, shows why the points in Figure 12-17 are so scrambled. Despite the considerable scatter, there clearly is first an increase, then a decrease, and then again an increase in shear stress with increasing velocity, as shown by the curve that represents very approximately the trend of the data points. The range in shear stress between the local minimum and the local maximum in that curve, together with the inevitable scatter in the shear stresses themselves, is sufficient for substantial mixing of the points.

69 The plot in Figure 12-15 could be transformed into a plot of Shields parameter against dimensionless sediment size, or into a plot of dimensionless flow power against dimensionless sediment size (neither of which is shown here), but with no obvious advantages for sedimentological interpretation. These plots would be qualitatively different in certain ways from those presented by Allen (1982) because of the influence of the results from the depth–velocity–size diagram on our method of partitioning Figure 12-15.

70 Van den Berg and van Gelder (1993) introduced a bed-phase stability diagram (Figure 12-19) based on boundary shear stress that in large part removes the difficulties discussed above. The horizontal axis is the dimensionless sediment size used above, and the vertical axis is a Shields parameter modified in such a way that the bed shear stress is represented by the part generated by the particle roughness rather than the form drag associated with bed forms. The strategy is to express the bed shear stress in terms of a Chézy coefficient (see Chapter 4) that is a function of the ratio of water depth to D_{90}, the ninetieth-percentile particle size. This largely circumvents the dominance of form drag in the presence of rugged bed forms. You can see from the diagram that there is much less ambiguity in partitioning of existence fields than in Figure 12-15, but there is still considerable overlap between dunes and upper plane bed, suggesting that the method for drag partitioning is still less than perfect. Nonetheless, Figure 12-19 is a great improvement over earlier existence diagrams based on bed shear stress.

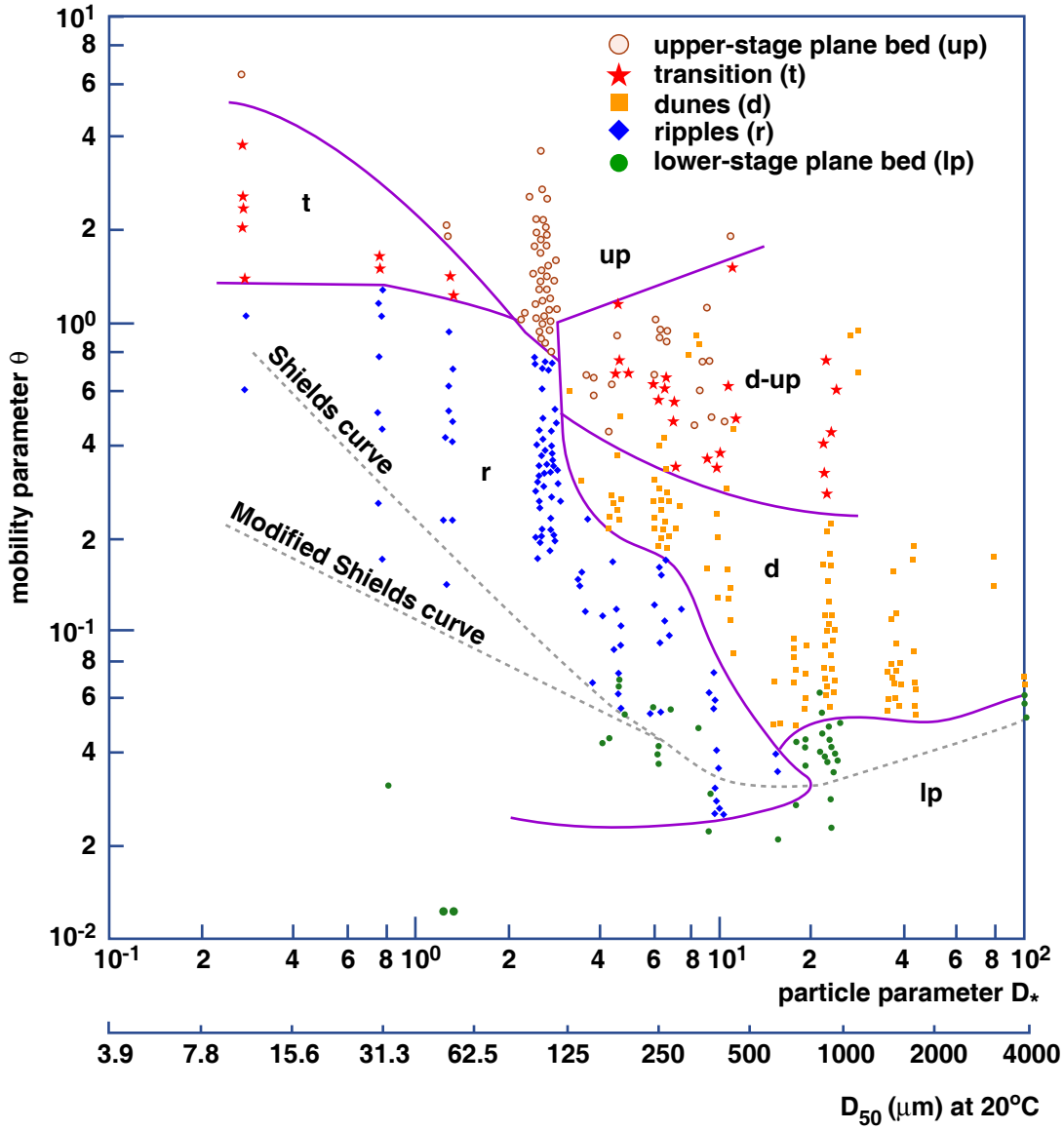

Figure by MIT OpenCourseWare.

Figure 12-19. Existence fields for bed phases in a dimensionless plot of modified Shields parameter vs. dimensionless sediment size. (From van den Berg and van Gelder, 1993.)

Flow Regimes

71 This is the place to be more specific about the terms ***lower flow regime*** and ***upper flow regime*** I have used a few times already. Simons and Richardson (1963) proposed that bed phases be classified into a lower flow regime and an upper flow regime on the basis of the transition from the rugged ripple-like bed phases (ripples and dunes) formed at relatively low flow strengths and the less rugged bed phases (upper plane bed and antidunes) formed at high flow strengths (Figure 12-20A). The motivation for this classification was not so much the sharp distinction in bed geometry in itself as the great decrease in flow resistance in

passing from the lower flow regime to the upper flow regime. Geologists have found the distinction useful not only in terms of the differing bed geometry but also in terms of the consequent great difference in sedimentary structures produced: with the minor exception of lower-regime plane beds, lower-regime conditions give rise to cross-stratified structures, whereas upper-regime conditions give rise mostly to planar lamination—although antidunes produce cross-stratification as well: see Chapter 15.

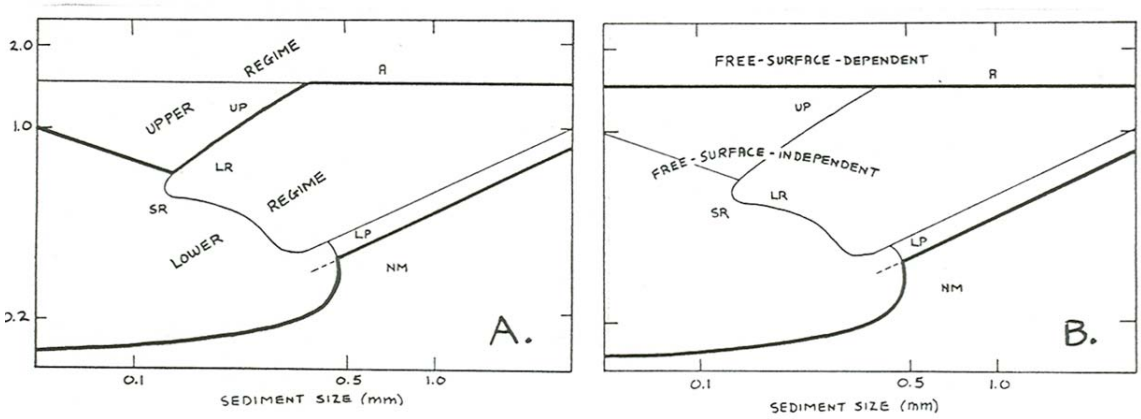

Figure 12-20. Two ways of classifying bed phases into flow regimes. **A)** Velocity–size diagram for a flow depth of about half a meter (See Figure 12-10) showing the customary division into an upper flow regime and a lower flow regime based on the transition from ripple and dune bed phases to upper plane bed or antidunes. **B)** The same velocity–size diagram showing an alternative division into a lower group of bed phases (lower plane bed ripples, dunes, and upper plane bed) whose dynamics are independent of the presence of a free surface and an upper bed phase (antidunes) whose dynamics are dependent upon the presence of a free surface.

72 In terms of bed-configuration dynamics, it is also natural to divide bed phases into two groups in a different way on the basis of the importance of a free surface (Figure 12-20B). Ripples, dunes, and plane bed are bed phases whose occurrence is independent of the existence of a free surface: recall that in the exploratory flume experiments described earlier in this chapter the existence of ripples was not affected by placing a board over the water surface. These bed phases could therefore be termed *free-surface-independent* bed phases. Antidunes, on the other hand, are dependent upon the existence of a free surface, and could therefore be termed a *free-surface-dependent* bed phase.

73 Flow over ripples and dunes is dominated by ***flow separation***, a phenomenon whereby the flow separates from the solid boundary in the region where the boundary curves away from the general upstream flow direction. The general picture of separated flow over a ripple or a dune is shown in Figure 12-21, and in more cartoonlike form in Figure 12-22. When the flow reaches the crest it continues to move in the

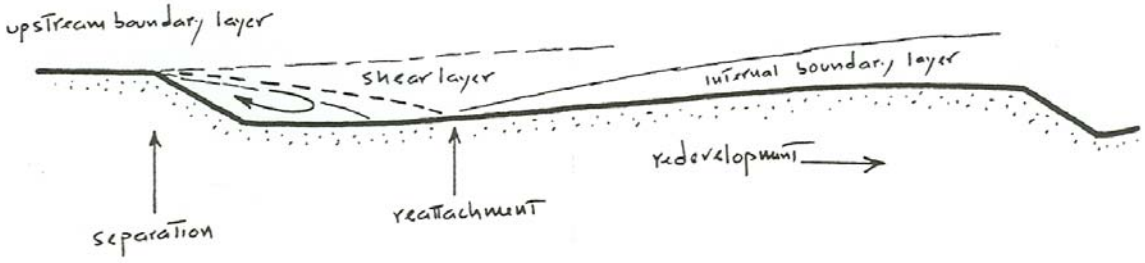

Figure 12-21. Flow structure over ripple or dune bed forms. (Schematic, but not much vertical exaggeration.)

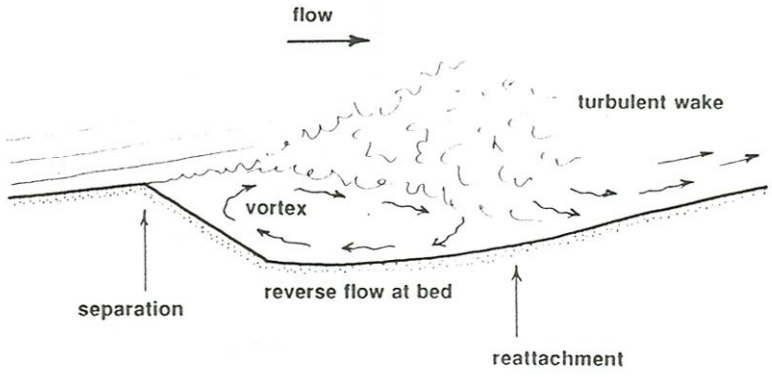

Figure 12-22. A version of Figure 4-23 that is less schematic but has some vertical exaggeration.

same direction rather than bending downward to follow the contour of the bed. Strong turbulence develops along the surface of strong shear, called the ***shear layer***, which represents the contrast between the high velocity in the separated flow and the low velocity in the shelter of the bed form. This turbulence expands both upward and downward, and at some position downstream of the crest the turbulent shear layer meets the sediment bed. The flow is said to ***reattach*** to the bed at that point. Downstream of reattachment, the flow near the bed is directed

downstream once again. Upstream of reattachment, in what is called the ***separation vortex***, the bed feels a weak flow in the reverse direction.

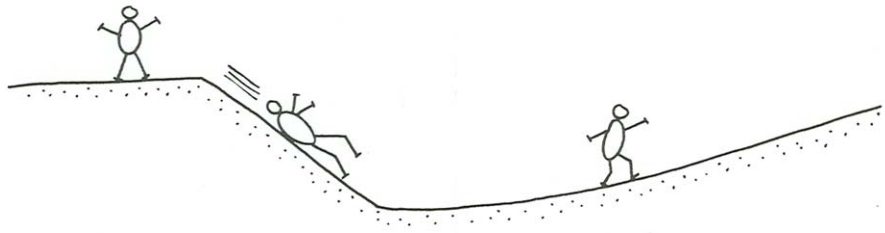

Figure 12-23. A field trip on a dune.

74 Take a tour of a ripple or dune profile by starting at a crest, sliding down the slip face, and then walking across the trough and up the stoss surface of the next bed form downstream (Figure 12-23). The flow you would feel differs greatly along the profile. With the appropriate equipment you could actually do this on a large dune in a river or a tidal current, or more easily on a subaerial dune when the wind is blowing. Refer to Figures 12-21 and 12-22 as you read the next paragraph.

75 As you move down the slip face and into the trough you would feel a weak, irregular, eddying current in the opposite direction. Near the reattachment line you would feel the full effect of the turbulence in the shear layer. In the reattachment zone the strong eddies generated in the shear layer impinge upon the bed and flatten out against it to cause temporarily very high local shear stresses. You would feel strong puffs or gusts of flow trying to push you this way and that. But even though the shear stress is high at certain points and certain times, it is nearly zero on the average. As you continue to walk up the slope toward the next crest, the flow velocity and therefore the boundary shear stress would gradually increase, because the flow is crowded upward, but the intensity of the turbulence would lessen.

Velocity Profiles over Ripples

76 The material in the latter part of Chapter 4 on velocity profiles over rough beds is useful here in dealing with vertical profiles of time-average velocity over fields of ripple-shaped bed forms, large or small. It is natural to think about such profiles in two different ranges of height above the bed: well above the ripples, and close to the bed.

77 Think first about the velocity profile above a plane parallel to the mean bed level and one to two ripple heights above the ripple crests. Unless the ripple height is such a large fraction of the flow depth that the whole flow accelerates

and decelerates as it passes over the ripples, such a velocity profile is almost the same wherever it is taken, because at this height the upward-diffusing wake turbulence generated by flow separation at ripple crests is well blended spatially. In the following paragraphs we will use the adjective *integrated* for such profiles (cf. Paola, 1983). These profiles characterize layers of the flow that blanket entire fields of bed forms without varying at the scale of those bed forms.

78 First we need to do a little more with velocity profiles near the bed in dynamically rough flows, as a continuation of Chapter 4. This additional material deals with the inner layer not far above the tops of the particles, which we skipped in Chapter 4.

79 For sand-size bed roughness the lowermost part of the inner layer, not far above the tops of the grains, is not much more than a few millimeters thick, but for water flowing over gravels or for wind blowing over large ground-surface roughness it may be decimeters or even meters thick, and no sophisticated, miniaturized velocity meters are needed to include it in measured velocity profiles. At positions this close to the bed there is a troublesome problem that we have avoided up to now: where ia the origin for y? It seems reasonable to suppose that the $y = 0$ level lies somewhere between the bases and the tops of the surface particles. A natural choice would be the average surface elevation—the spatial average of the heights, normal to the mean plane of the bed, at which a solid surface is first encountered in descending onto the bed. You will see, however, that this does not produce the best fit of velocity to Equations 4.41 or 4.42 of Chapter 4. And it is not a very practical choice anyway. With close-packed granular roughness, the plane through the tops of the grains (which itself is not very well defined) is usually taken as the $y = 0$ level for velocity measurements.

80 For a given dimensionless distance y^+ from the boundary, u/u_* is not the same in rough and smooth flow, because the second term on the right side of Equation 4.39 always has a value different from B in Equation 4.34. But the shape and slope of the velocity profile are the same: if you differentiate Equation 4.39 for the rough-flow velocity profile with respect to y, you get

$$\frac{du}{dy} = \frac{Au_*}{y} \tag{12.11}$$

which is exactly the same as Equation 4.33 for flow over a smooth bottom. You might expect, however, that, at positions closer down to the tops of the grains, the grains have some effect on the shape as well as the position of the velocity profile, making the shape different from the smooth-flow case. In other words, when y is not much greater than D, the velocity gradient depends not only on τ_o, ρ, and y but also on D:

$$\frac{du}{dy} = f(\tau_o, \rho, y, D) \tag{12.12}$$

or in dimensionless form,

$$\frac{u}{u_*}\frac{du}{dy} = \mathrm{f}\left(\frac{D}{y}\right) \tag{12.13}$$

81 It is convenient to extract the same constant A from the function on the right in Equation 12.13, so that the effect of proximity to the bed grains can be viewed as a correction function by which the right side of Equation 12.11 must be multiplied:

$$\frac{du}{dy} = \frac{Au_*}{y} f\left(\frac{D}{y}\right) \tag{12.14}$$

82 There is no simple way of dealing with the physics behind the correction function $f(D/y)$ in Equation 12.14. The only thing we can say with certainty is that as y gets smaller (and D/y gets larger) the correction gets larger. To investigate the correction function further we can expand it as a power series in D/y (Monin and Yaglom, 1971; remember that any function can be approximated in this way by an appropriate power series.) Equation 12.14 can then be written

$$\frac{du}{dy} = \frac{Au_*}{y}\left[1 + a\frac{D}{y} + b\left(\frac{D}{y}\right)^2 + \ldots\right] \tag{12.15}$$

83 As the boundary is approached from above, and the correction gets larger, the term $a(D/y)$, the dominant term while the correction is still small, gets less important relative to terms of higher order in D/y. In the following we will consider only positions higher than one to two diameters above the tops of the roughness elements. Measurements are seldom made closer to the bed anyway, because to get a representative value for the mean velocity a large number of profiles must be taken at different places relative to the roughness elements and then spatially averaged.) To conform to the usual practice in dealing with the grain-proximity correction, we will recast Equation 12.15 into a slightly different form by introducing a new variable $y\text{-}y_1$ for the vertical coordinate, where y_1 is a small constant that's in the same ballpark as D itself. We also need the following algebraic identity:

$$\frac{1}{y} = \left(\frac{1}{y\text{-}c}\right)\left(\frac{y\text{-}c}{y}\right) = \left(\frac{1}{y\text{-}c}\right)\left(1\text{-}\frac{c}{y}\right) \tag{12.16}$$

where y is some variable and c is a constant. Then, replacing $1/y$ in Equation 12-15 with the right side of the identity above and letting the constant be y_1,

$$\begin{aligned}\frac{du}{dy} &= \frac{Au_*}{y\text{-}y_1}\left(1\text{-}\frac{y}{y_1}\right)\left[1 + \mathrm{a}\frac{D}{y} + \mathrm{b}\left(\frac{D}{y}\right)^2 + \ldots\right] \\ &= \frac{Au_*}{y\text{-}y_1}\left(1\text{-}\frac{y_1}{y} + a\frac{D}{y} + \text{terms in } \frac{1}{y^2} \text{ etc.}\right)\end{aligned} \tag{12.17}$$

Neglecting terms of order higher than $1/y$ on the right side, Equation 12.17 becomes

$$\frac{du}{dy} = \frac{Au_*}{y\text{-}y_1}\left(1+\frac{aD\text{-}y_1}{y}\right) \tag{12.18}$$

84 We are at liberty to adjust the definition of y_1 at the outset in such a way that $y_1 = aD$; then Equation 12-18 becomes

$$\frac{du}{dy} = \frac{Au_*}{y\text{-}y_1} \tag{12.19}$$

Equation 12.19 can be integrated in the same way as the rough-flow equivalent of Equation 4.33 in Chapter 4 to be in the same form as Equation 4.34,

$$\frac{u}{u_*} = A\ln\frac{y\text{-}y_1}{D} + B' \tag{12.20}$$

and Equation 12.20 can be manipulated into the same form as Equation 4.42 in Chapter 4, with y_o and no separate constant of integration,

$$\frac{u}{u_*} = A\ln\frac{y\text{-}y_1}{y_o} \tag{12.21}$$

(For details see Middleton and Southard, 1984, Appendix 4.)

85 Equations 12.20 and 12.21 are the conventional way of dealing with the correction function $f(D/y)$ that appears in Equation 12.14. Shifting the origin of the y coordinate by the small quantity y_1 usually straightens out the velocity profile in a semilog plot down to positions not far above the tops of the roughness elements. What is commonly done with wind-velocity profiles above the land surface is to take $y = 0$ at the base of the roughness elements—the ground on which the observer is standing—and then find the value of y_1 which when subtracted from y gives the best straight-line fit of data to Equation 12.21. The distance y_1 (often denoted by d) is called the ***displacement height*** or the ***zero-plane displacement***. The situation is a little different with close-packed granular roughness, which is of greater interest here: usually the velocity profile is measured with respect to the tops of the grains, and then the apparent origin for y is lowered to produce the best straight-line fit to Equation 12.21. (The plane through the tops of the grains is not ideally well defined, but it is impossible to define a dynamically natural plane that represents the bases of the grains in a full bed of loose sediment.) So the value of y_1 depends not only on the physics of the problem but also on the y origin chosen at the outset. For a wide variety of roughness geometries, the distance y_1 has been found to be between 0.2 and 0.4 roughness diameters below the tops of the roughness elements (Jackson, 1981).

86 The physical significance of the displacement height y_1 has never been clear. There is some experimental evidence that the height y_1 above the origin is the level in the flow at which the boundary shear stress τ_o appears to act (Thom, 1971). The horizontal component of the force per unit area the flow exerts on its bed has not only a magnitude but also a line of action. In other words, if we could measure τ_o with enough accuracy and detail we would find that it appears to act on some plane parallel to the bed. (Presumably this plane would lie somewhere

between the bases and tops of the roughness elements.) Choose an arbitrary plane above or below the bed and find the moment M per unit bed area associated with the force τ_o per unit bed area. Dividing M by τ_o gives a quantity with the dimensions of length, and this length is just the distance above or below the arbitrary plane at which τ_o acts. Jackson (1981) reasons that this distance is none other than the displacement height y_1.

87 Now, finally, back to velocity profiles over bed forms. In the following, the subscript t denotes variables associated with the total bed shear stress, and the subscript s denotes variables associated with the skin friction. If the flow depth is large relative to the ripple height the lower part of the integrated profile (and with little error the upper part also) is well described by Equation 12.21, the law of the wall for rough boundaries written here using the subscript t,

$$\frac{u}{(u_*)_t} = A \ln \frac{y-(y_1)_t}{(y_o)_t} \tag{12.22}$$

88 The boundary shear stress $(\tau_o)_t$ concealed in $(u_*)_t$ in Equation 12.22 is the total shear stress the flow exerts on the rippled bed. If you were to invent a good way of measuring pressure and viscous shear stress at every point on the bed, you would have to average over an area much larger than the scale of the ripples to get a representative value for $(\tau_o)_t$. Most of $(\tau_o)_t$ is form drag exerted on the ripples, not local stress exerted on the granular bed surface—called skin friction. This latter skin-friction component of the total drag would be largely viscous drag, if flow in the immediate vicinity of the bed is dynamically smooth, or it may itself be largely form drag, if the flow in the vicinity of the bed is dynamically rough. By analogy with the results in Chapter 4 for granular roughness, the roughness length $(y_o)_t$ associated with the integrated velocity profile in Equation 12.22 is proportional to the height of the ripples and is a small fraction thereof, the exact value depending on the shape (and most importantly the steepness) of the ripples. The displacement height $(y_1)_t$ is such that the origin for the velocity profile lies somewhat below the ripple crests. As the ratio of flow depth to ripple height decreases (but not to the point where there is no longer an integrated profile) it becomes more difficult to distinguish between inner and outer layers of the flow, but the wall-law representation is still a good approximation.

89 Now look at the velocity profile near the bed at points on the stoss surface of a given ripple. At points well downstream from reattachment the velocity profile near the bed follows the law of the wall also, because of the upward development of the internal boundary layer at the expense of the turbulent wake downstream of separation. If the boundary Reynolds number based on the skin friction $(\tau_o)_s$ and the local granular roughness height is larger than about 10 the flow in the internal boundary layer is dynamically rough, and the velocity profile is given by

$$\frac{u}{(u_*)_s} = A \ln \frac{y-(y_1)_s}{(y_o)_s} \tag{12.23}$$

where $(\tau_o)_s$ in the shear velocity $(u_*)_s$ is a local boundary shear stress that can be viewed as averaged over an area that is large compared with the granular roughness but small compared with the ripples themselves. We will use the adjective *local* for profiles of this kind, because they apply only to particular points on the ripple. The profile in Equation 12.23 is characterized by values of roughness length $(y_o)_s$ and displacement height $(y_1)_s$ associated with the granular roughness, and both of these are smaller than the corresponding values associated with the integrated wall-law profile in Equation 12.22.

90 If the local boundary Reynolds number is much smaller, less than about 5, the local velocity profile is represented instead by the law of the wall for smooth flow, Equation 4.35 in Chapter 4,

$$\frac{u}{(u_*)_s} = A \ln \frac{\rho (u_*)_s y}{\mu} + B \tag{12.24}$$

where B has a value of about 5.1, as noted in Chapter 4. In this case the skin friction on the stoss surface of the ripple is mostly viscous drag rather than granular form drag. At intermediate boundary Reynolds numbers the velocity profile is represented by the law of the wall for transitionally rough flow. This can be put into the same form as the rough-flow profile, Equation 12.23, but with y_n then a function of the local boundary Reynolds number as well as the roughness height, and the skin friction is partly viscous drag and partly form drag. Whether the local flow in the growing boundary layer is smooth or rough, however, $(u_*)_s$ in Equations 12.23 or 12.24 is much smaller than $(u_*)_t$ in Equation 12-22, because whatever its nature the skin friction on the ripple surface is much smaller than the form drag on the ripples.

91 The local wall-law profile varies with distance up the stoss surface: as the flow in the internal boundary layer accelerates up the slope, the skin friction $(\tau_o)_s$ increases, as does the height to which the profile is applicable. You can be sure, however, that in a simple dimensional semilog plot with $\log y$ on the vertical axis and u on the horizontal axis the slopes of the straight lines that represent the local wall-law profile are always much greater than the slope of the single straight line for the integrated wall-law profile that holds well above the level of the crests of the ripples, because $(u_*)_t$ is much larger than $(u_*)_s$; see Figure 12-24, which summarizes the relationship between the integrated profile and the local profile above a given point on the stoss surface of a ripple. In between the regions of applicability of the local wall-law profile near the bed and the integrated wall-law profile well above the ripples is a complicated region of the flow in which the velocity grades from one profile to the other. This region thins downstream along the stoss surface but is not consumed completely even when the flow reaches the next ripple crest downstream.

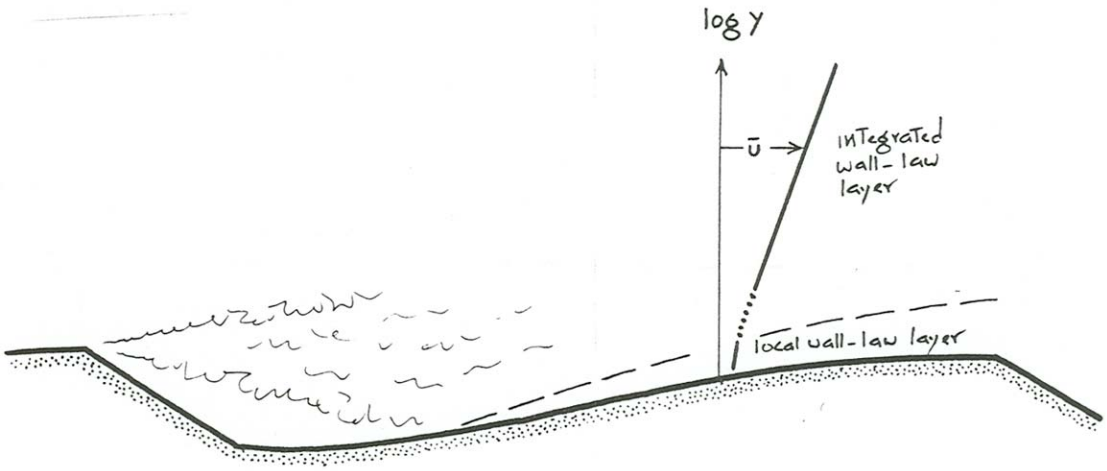

Figure 12-24. Relationship between the integrated wall-law layer and the local wall-law layer developed over a dune bed.

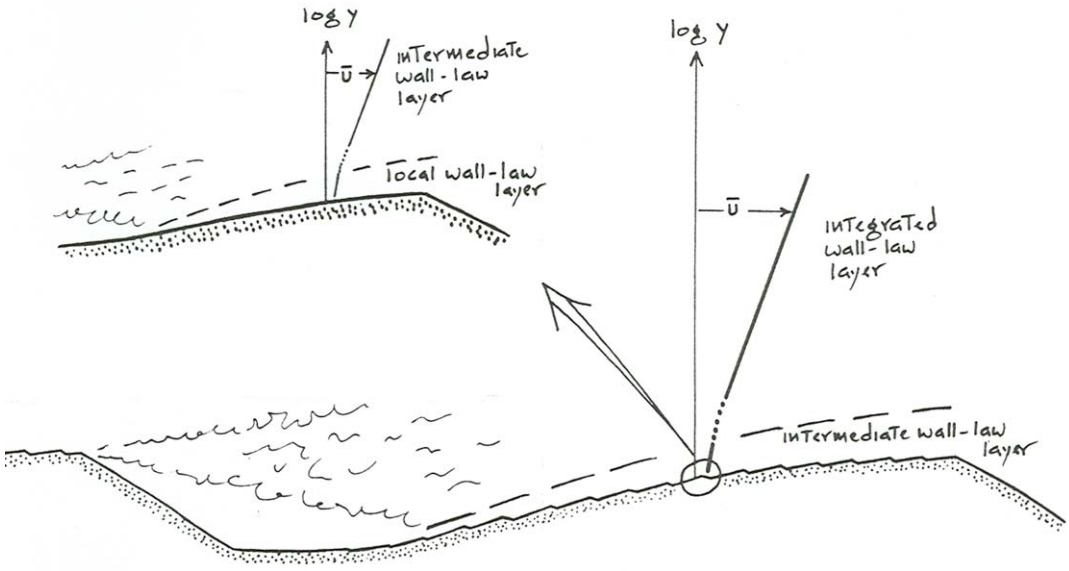

Figure 12-25. Intermediate wall-law layer developed over a dune bed on which smaller dunes are superimposed on larger dunes. The intermediate layer acts as an integrated layer with respect to the smaller dunes but as a local layer with respect to the larger dunes.

---

92 Where small dunes are superimposed on much larger dunes, the foregoing line of reasoning can be taken a step further. Large internal boundary layers develop on the stoss surfaces of the larger dunes in just the same way that small internal boundary layers develop on the smaller dunes. The smaller dunes, of which there presumably are a great number on the stoss face of each larger dune, act as local roughness beneath the internal boundary layer that develops up

the stoss surface of each larger dune. There is therefore a layer of the flow well above the crests of the smaller dunes but still well below the crests of the larger dunes in which the velocity follows an intermediate wall-law profile (Figure 12-25). This intermediate profile looks simultaneously like an integrated (although slowly varying) profile to a small observer stationed on one of the smaller dunes but like a local profile to a large observer stationed on one of the larger dunes. This profile is characterized by values of u_*, y_o, and y_1 intermediate between those of the integrated profile over the large dunes and those of the local profile over the smaller dunes. From the standpoint of the large dunes the intermediate value of u_* represents a local boundary shear stress, so in a sense it is skin friction even though form drag predominates over viscous drag. At the same time, the viscous drag and smaller-scale form drag associated with the sediment grains on the surfaces of the smaller dunes represent skin friction relative to the smaller dunes.

93 The same ideas can even be extended to very large dunes (which many would call sand waves) on which two orders of smaller dunes with two greatly different scales are superimposed. There are then two different intermediate layers of the flow, of the kind just described, each with its own wall-law profile characterized by its own set of values of u_*, y_o, and y_1: one that is local relative to the largest dunes (the sand waves themselves) but integrated relative to the larger superimposed dunes and one that is local relative to the larger superimposed dunes but integrated relative to the smaller superimposed dunes.

94 You could take velocity profiles at a large number of points along the profile of one or more of the largest dunes present on the bed and average them all together to obtain a spatially averaged velocity profile. In a sense this spatially averaged profile represents the entire flow. Such averaging is not entirely satisfactory, for two reasons:

- Owing to growth of the internal boundary layer, the near-bed part of the velocity profile varies with position along the dune profile (even aside from the gross changes caused by separation and reattachment in the vicinity of the trough).

- Because the origin plane for the integrated wall-law region associated with dunes of a given order is parallel to the mean plane of the bed in the vicinity of those dunes, whereas the origin for the individual profiles is naturally taken at the bed surface itself, the base of the integrated wall-law profile is encountered at different heights in different places. The latter problem is not as serious as it seems, however, because at the height of even the lowest of such integrated wall-law regions, points at rather different heights plot close to each other on a logarithmic vertical axis. Provided that the ratio of spacing to height of the dunes of each order is large, so that separation bubbles occupy only a small fraction of the area of the bed, the spatially averaged profile in a semilog plot of height against velocity shows a series of straight-line segments connected by smooth transitions, just like the individual profiles—although the transitions are likely to be more gradual, for the two reasons noted above. The values for boundary shear

stress obtained from these straight-line segments in the spatially averaged profile represent the spatial averages of the boundary shear stresses associated with each order of bed form present, ranging upward in scale from the grain roughness itself. For further details on such spatially averaged velocity profiles over dunes, see Smith and McLean (1977).

Sediment Movement over Ripples and Dunes

95 The mode of sediment transport varies greatly from place to place over the ripple or dune profile. A repetition of your traverse, this time to watch the sediment movement, would be instructive. See Figure 12-26 for a key to the material discussed below. Start at the reattachment zone, where the time-average bed-load transport rate is near zero. Strong eddies in the reattaching shear layer impinge upon the bed to cause strong but sporadic grain transport. At low mean-flow velocities, sediment is shifted this way and that on the bed in local pulses that strike seemingly at random. This is the site of first suspension of sediment as flow velocity gradually increases: swirls of sediment are put into suspension in puffs and gusts, and then the grains either settle directly back to the bed or are dispersed up into the flow.

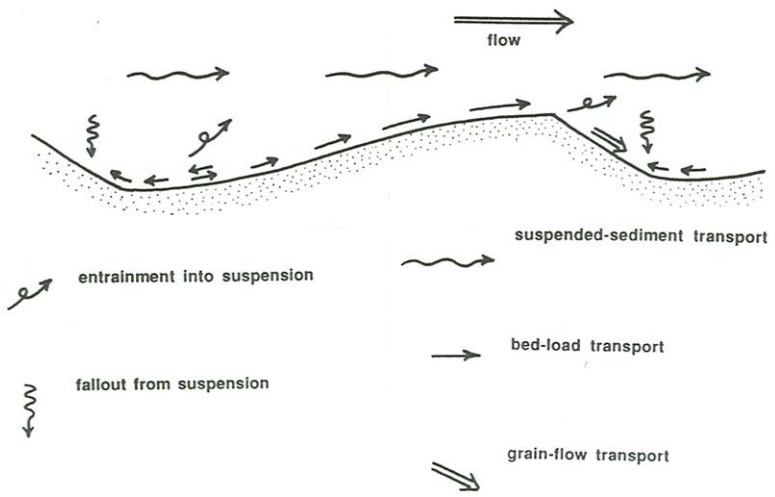

Figure 12-26. Modes of sediment movement over ripples or dunes.

96 Downchannel from reattachment the pulses of movement are directed more and more consistently downchannel and gradually give way to more uniform grain movement up the stoss slope. In the other direction they cease to be important just a short distance upchannel from reattachment, because flow in the separation vortex behind the bed form is relatively weak.

97 Particle movement up the stoss surface is much like that on a planar sediment bed: it is in the form of isolated puffs at low mean-flow velocities, and in the form of a continuous sheet at higher velocities. With increasing velocity the bed-load movement is obscured by sediment suspended from the trough or from upstream ripples. Dunes often have ripples or even smaller dunes superimposed on their stoss slopes; this should not surprise you, because such bed forms develop wherever they have sufficient space and suitable flow conditions.

98 At low flow velocities all of the sediment that is transported as bed load to the brink is deposited there. This sediment tends to build the stoss surface forward over the top of the lee surface. The sediment slips down the lee surface as a kind of grain flow to try to restore a stable angle of repose. Grain flow is localized and sporadic when the rate of delivery is slow but widespread and continuous at higher flow velocities. The result is a nearly planar slip face, with a break in slope not only at the top but also at the base, where the slip face builds forward onto the surface of the trough downstream.

99 At higher flow velocities some fraction of the transported grains are carried beyond the crest above the separation surface, to settle through the complicated turbulent flow field in the wake of the ripple and land at various points (Figure 12-27): on the slip face, in the trough, on the stoss surface of the next ripple downstream, or even on some ripple much farther downstream. Where the grains land depends on several factors: the flow velocity, the settling velocity, the height of the grains above the bed as they pass over the brink, and which eddies the grains happen to fall through.

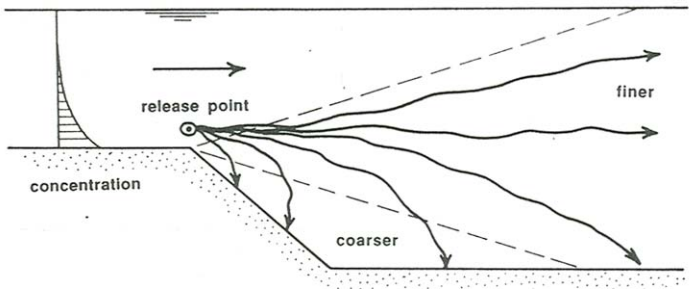

Figure 12-27. Trajectories of sediment particles passing through a given point (the "release point") above the crest or a ripple or a dune.

100 When the ripple geometry is three-dimensional, many troughs show no well defined separation vortex, and patterns of flow and sediment transport are not as simple as outlined above. The bed surface near the base of the lee slope nonetheless usually feels flows that are much weaker than over the stoss slope, although these flows may have a substantial cross-stream component. Transverse

flow in the lee of the dunes often makes ripples in troughs and on lee slopes, with crests oriented at a large and variable angle to the dune crests.

The Movement of Ripples and Dunes

101 Ripples and dunes move downstream, at speeds that are orders of magnitude slower than the flow speed, by erosion on the stoss surface and deposition on the lee surface. It is surprisingly difficult to characterize this downstream movement, partly because the bed forms change their profiles with time but even more importantly because any given bed form has a finite lifetime: it is born, it moves, and it eventually dies, usually within a travel distance equal to only a small multiple of the bed-form spacing, something like 5–10 spacings. The moderately regular arrangement of ripples in a still photograph is deceiving. This section says some things about the nature and analysis of movement of ripples and dunes.

102 A fundamental characteristic of ripples is that they move downstream at some velocity U_B, by erosion on the stoss surface and deposition on the lee surface. This velocity is of interest because

- it is an index of bed-load transport rate, because we have seen that most of the bed load moving on a ripple bed is cycled within the same ripple, and
- it is one of the determinants of the stratification geometry produced by ripple movement.

This section addresses the measurement of U_B, along with some results, and also its use in estimating sediment transport rates. A discussion of its role in the geometry of sedimentary structures would take us too far afield; see papers by Allen (1970), Ashley et al. (1982), Rubin and Hunter (1982), and Harms et al. (1982, Chapter 3).

103 It is surprisingly difficult to characterize the downstream movement of ripples. If each ripple had an unchanging streamwise profile, U_B would be both well defined and readily measurable. Because most ripples have a fairly sharp break in slope at the brink, it is usually no problem to follow a distinguishable point on the profile as the ripple moves. But the profile shape changes as the pattern of sediment transport over the ripple changes, even if the profile area stays the same. This usually causes the position of the brink to change relative to the center of area of the ripple over just a short distance of movement, so even the position of a well defined point on the profile does not necessarily represent well the position of the ripple. Moreover, the profile area of a ripple itself is changed by several processes, which can act concurrently:

- intensification of scour in a trough and deposition of the eroded sediment on the stoss surface or farther downstream;

- transfer of sediment from one ripple to another by either bed-load transport or suspended-load transport;
- overriding of one ripple by the next ripple upstream;
- division of one ripple into two, as a new trough develops on the stoss surface of a ripple as a result of some change in upstream flow pattern.

The last two processes imply that ripples do not live forever: they come into being, move for some distance that is usually a small number of ripple spacings, and then disappear.

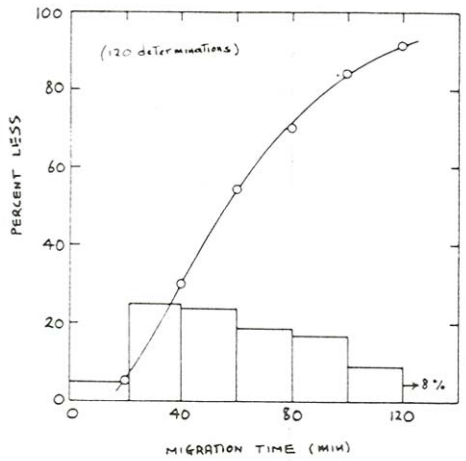

Figure 12-28. Histogram and cumulative curve of times for passage of two successive ripple crests past a fixed point, for 0.38 mm sand in a flow with mean flow depth 0.3 cm and mean flow velocity 29.2 cm/s. (Data are from Southard et al., 1980.)

---

104 A good way to apprehend the transitory existence of individual ripples is to generate a train of ripples in your flume and photograph them with a time-lapse movie camera as they move downstream. When you viewed the film at normal speed you would see the ripples doing all sorts of crazy things that are hard to appreciate by real-time viewing; the moderately regular succession of ripples when viewed in a still picture is deceiving. Two other instructive things you could do are described in the following paragraphs.

105 You might stock up on sandwiches and caffeine, occupy a station somewhere along the channel, and for a large number of ripples measure the time T_r needed for two successive ripple crests to pass the station. After getting some rest you could then plot a cumulative distribution of T_r. (When multiplied by the spacing of the passing ripple, the inverse of T_r is a good representation of U_B.)

Figure 12-28, measured by Southard et al. (1980), is such a curve. Note the wide range in passage times. It was found that hundreds of ripples would have had to be measured to obtain a stable cumulative curve, although substantially fewer were sufficient for a stable mean value.

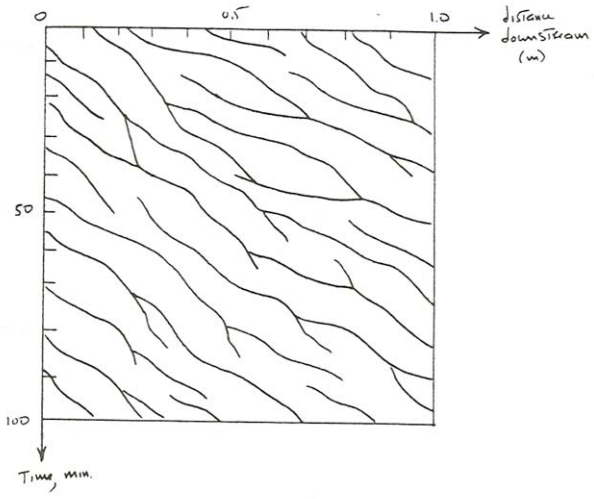

Figure 12-29. Positions of ripples in a space–time plot. The curves show positions of ripple crests as a function of time and downstream position. The flow is steady and uniform, and the bed state is unchanging on average. (Schematic.)

---

106 To quantify the variability in ripple movement you might enlist a large number of volunteers to stand along the transparent sidewall and be responsible for keeping track of the positions of the ripples as a function of time. A plot of position vs. time would look like Figure 12-29, from which you can see that

- for a given ripple U_B varies widely and irregularly with time;
- a given ripple exists for a distance of movement that is only a few ripple spacings;
- ripples usually are born by division of one large ripple into two smaller ones, and usually die by becoming smaller and slower and then being overridden by a faster-moving ripple (on the average, deaths equal births).

Despite all of this variability, when considered as an aggregate the lines in the graph have a definite average slope, which is probably the best measure of U_B.

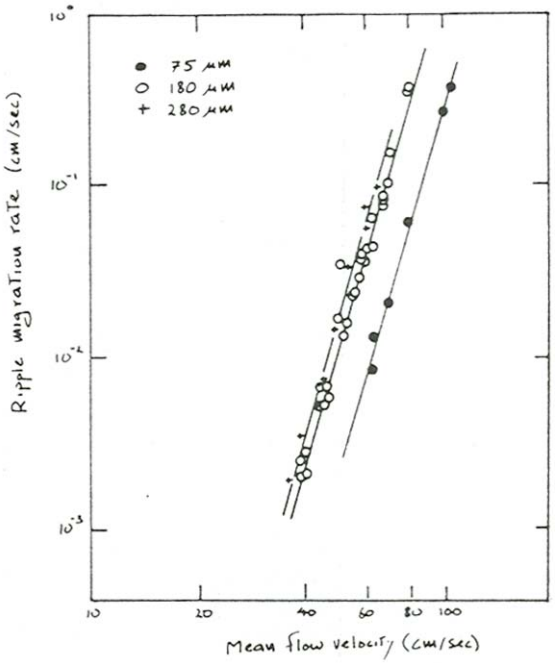

Figure 12-30. Plot of bed-form speed U_B vs. mean flow velocity U in uniform flow for three sand sizes. (Data are from Dillo, 1960.)

---

107 You should expect U_B to increase steeply with mean flow velocity U for a given sand, because, as you will learn in Chapter 12, bed-load transport rate increases steeply with flow strength and most of the bed load remains within individual ripples. The magnitude of this increase depends, however, on the concurrent change in ripple size, because the larger the ripple, the slower it moves for a given bed-load transport rate. The effect should therefore be most pronounced for ripples, which vary little in size with flow conditions and sediment size. Systematic data on bed-form velocity as a function of flow strength and sediment size are surprisingly scarce, presumably owing to the difficulty of accurate measurement. Figure 12-30, a plot of U_B vs. U for three different sand sizes (Dillo, 1960), shows that U_B increases sharply with U for a given sand size, as expected. Note, however, that ripples in coarser sands move faster than ripples in finer sands. The reason for this seemingly anomalous behavior is unclear. There seem to be two possibilities:

- The volume transport of sand as traction load in the accelerating flow over the stoss face of the ripple might be greater in coarser sand than in finer sand at a given mean flow velocity.

- The ripples in the coarser sand may have been smaller than in the finer sand, so that U_B is greater even though bed-load transport rate might have been smaller.

108 In the absence of suspension, particles are cycled through individual bed forms. Think about a particle in the interior of a moving bed form (a ripple or a dune). The particle is of course stationary relative to the substrate. As the bed forms moves, the particle finds itself closer and closer to the stoss surface. When it become exposed at the surface, it is entrained, moves up to the brink as part of the bed load, and then slumps or slides down the lee slope, stopping at some point on the slope (or at its base), there to be buried by later lee-side deposition to become entombed again, temporarily, within the body of the bed form.

108 To the extent that the moving sediment is cycled within bed forms, the bed-load transport rate can be expressed in terms of the speed of movement of the bed forms. For ripples this is a good approximation, because bed-load transport rate is usually zero or nearly so at some point in the trough. Only if bed-load transport rate is nowhere zero over the bed-form profile, as is generally the case with antidunes, is this not true. To derive an expression for the bed-load transport rate associated with bed-form movements, consider a train of identical bed forms in which bed-load transport rate is zero in the troughs (Figure 12-31). The ripples have cross-sectional area A and spacing (i.e., repeat distance of cross-section geometry) L. The time needed for passage of a bed form past a given point is T_r. The rate q_f, expressed per unit width normal to the flow, at which volume of sediment is moved downstream by bed-load transport within the ripples (remember that this involves stripping of sediment from the stoss surface, dumping at the crest, and slumping down the lee surface) is the same as the rate of downstream shift of the ripple cross section, except for a correction factor discussed below. A good way of thinking about this is to consider that the entire cross-sectional area of the ripple passes a given point on the bed in time $T_r = L/U_B$, so the average rate of passage of cross-sectional area past the point during this time is A/T_r, or, eliminating T_r, AU_B/L. So

$$q_f = K_1 \frac{AU_B}{L} \tag{12.25}$$

For a more elegant derivation of this result, see Simons et al. (1965).

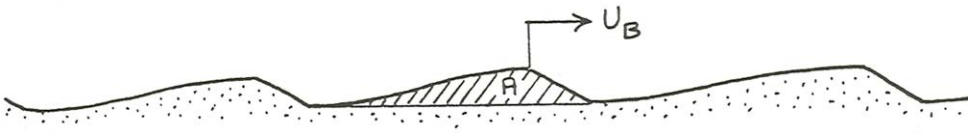

Figure 12-31. Definition sketch for derivation of a relationship for bed-form transport rate.

109 The correction factor K_1 is needed because the transport rate is expressed as solids volume whereas bed volume is expressed as bulk volume, solids plus void space. It is easy to derive a relationship between solids volume V_s and bulk volume V_b in a sediment sample. Because voids volume and solids volume add up to total volume in a sediment,

$$V_v + V_s = V_b \tag{12.26}$$

where V_v is voids volume. Also, the porosity k is defined as

$$\lambda = \frac{V_v}{Vb} \tag{12.27}$$

Combining Equations 12.26 and 12.27 to eliminate V_v gives the relationship between solids volume and bulk volume:

$$V_b = \frac{1}{1-\lambda}\ V_s \tag{12.28}$$

110 Because λ in equant and fairly well sorted sediments is on the order of 0.2–0.4, depending on both sorting and packing, the porosity correction factor $1/(1-\lambda)$ is always positive and a little larger than one. Using Equation 12.28, Equation 12.25 becomes

$$q_f = \frac{1}{1-\lambda}\ \frac{A U_B}{L} \tag{12.29}$$

111 In the rest of this chapter $1/(1-\lambda)$ will be written K_1 for convenience. If the bed forms have the shape of end-to-end triangles with height H, then $A = HL/2$ and Equation 12.29 becomes

$$q_f = K_1 \frac{HU_B}{2} \tag{12.30}$$

112 Rubin and Hunter (1982) proposed that q_f be called the ***bed-form transport rate*** and that the remainder of the bed-load transport rate, the part that bypasses the bed forms rather than being cycled within the same bed form, be called the ***throughgoing transport rate***.

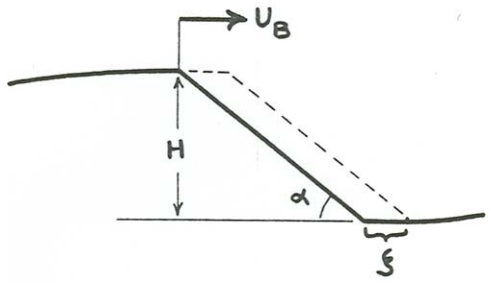

Figure 12-32. Definition sketch for derivation of a relationship for bed-load transport rate at the crest of a ripple or dune.

---

113 The bed-load transport rate (call it q_{sb}) is greatest at the crests of ripples. An expression for q_{sb} at a ripple crest can be derived on the assumption that all the bed load arriving at the crest is dumped there to slump down the lee face and build it forward (Figure 12-32). The slip-face angle is α and the horizontal distance of slip-face outbuilding is ζ. As before, ripple velocity is U_B and ripple height is H. The principle is that q_{sb} at the crest is equal to the time rate of addition of bulk sediment volume on the slip face. Because the increment in volume of the slip-face deposit is just the thickness of the slip-face deposit, $\zeta \sin\alpha$, times the length down the slip face, $H/\sin\alpha$,

$$
\begin{aligned}
q_{sb} &= K_1 \frac{d}{dt}\left[(\zeta \sin\alpha \frac{H}{\sin\alpha}\right] \\
&= K_1 \frac{d(\zeta H)}{dt} \\
&= K_1 H \frac{d\zeta}{dt} \\
&= K_1 H U_B
\end{aligned}
\qquad (12.31)
$$

114 By comparison of Equations 12.30 and 12.31 we have the neat result that, for ripples with triangular cross-section, bed-load transport at the crests is exactly twice the average value. This result seems first to have been derived by Bagnold (1941).

2D DUNES AND 3D DUNES

115 It has become widely stated, in the literature on unidirectional-flow dunes, that at low flow strengths in the dune range the dunes tend to be straight-crested, with fairly even crest elevations and trough elevations. Such bed forms are referred to as *two-dimensional* (2D), in the accepted hydrodynamic sense that

the geometry of the features can be represented by a single flow parallel cross section extending unchanged across the width of the flow. In contrast, at high flow strengths in the dune range the dunes show much greater crest curvature, much less crest continuity, and much greater variability in trough depths. Such bed forms are said to be *three-dimensional* (3D). Correspondingly, large-scale cross stratification produced by the movement of dunes is recognized as either two-dimensional, interpreted as representing relatively low flow strengths in the dune regime, or three-dimensional, interpreted as representing relatively high flow strengths—as you will see in Chapter 15. Recently, however, Venditti et al. (2005), on the basis of a systematic set of flume experiments using well sorted half-millimeter sand, claim that at low flow strengths in the dune regime initially 2D dunes eventually evolve into 3D dunes—a finding that is inconsistent with much of the earlier flume studies on dunes. The issue is not yet settled.

Dynamics of Unidirectional-Flow Bed Configurations

Introduction

116 How is it that a turbulent flow molds a bed of loose sediment into stable bed forms? The subject of bed-configuration dynamics has long been one of frustration and controversy. The fundamental difficulty is easy to state: it has to do with the difficulty of specifying adequately how sediment transport rate varies from place to place over a geometrically irregular transport surface. Before elaborating, I should make clear what I mean by the sediment transport rate at a point. I will address more fully in the following chapter the rate at which sediment is transported past a given cross section of the flow, in solids volume per unit width of the flow; it is usually denoted by q_S. Here we need to think about how the "point" value of the volumetric transport rate, which you can view as the sediment transport rate over an arbitrarily small local area of the bed (again expressed per unit width of flow), varies from point to point on a nonplanar sediment bed. I will denote this by q_S also.

117 The velocity profile and the local bed shear stress (i.e., the skin friction) at some point on a nonplanar sediment bed, and their time variation, are not likely to be the same as at a point on a featureless planar bed with the same discharge and depth above it. This is because the details of forces and motions in accelerating and decelerating boundary layers are substantially different than in non-accelerating boundary layers. You have already seen this for the grossly non-uniform flows around bluff bodies like spheres and cylinders, but the effect is substantial even when much smaller accelerations or decelerations are caused by mild streamwise gradients in fluid pressure. The structure of the flow above any point tends to be inherited from upstream as the flow adjusts toward new conditions, so the flow at the given point depends in a complicated way on the shape of the bed for a long distance upstream. So even if q_S could be assumed to be in local equilibrium with the spatially varying flow, it could not be specified in any simple way as a function of position. Furthermore, q_S is likely not to be in equilibrium with local flow conditions, because a finite distance is needed for load to be dropped out or picked up as transport capacity changes. This distance

should be expected to be greater for suspended load than for bed load, but it cannot be assumed to be negligible even for the latter.

118 The development of bed forms depends on the variation in q_S over the bed-form profile. In turn, q_S depends on the flow, and if an adequate expression for q_S as a function of position could be found it could be combined with the kinematic constraint imposed by conservation of sediment volume to give an equation that could be solved for the evolution of any initial bed geometry to a steady equilibrium geometry. But q_S cannot be specified so simply: as you have seen, the local sediment transport rate is itself a function of the bed configuration for which we are trying to solve.

119 In the face of this depressing prospect, many investigators have attempted with some limited success to glean physical understanding of the dynamics of bed configurations by making various simplifying assumptions that allow q_s to be expressed in a form that leads to mathematically tractable equations. Not many of these attempts have led to greatly improved understanding of the problem. This is a field of endeavor marked by an understandable scarcity of satisfying or useful results.

120 In this section I will concentrate not so much on a detailed review of the literature on bed-configuration dynamics as on the physical effects related to the existence, shape, size, and movement of bed forms. I will deal with each of these four aspects of dynamics in the following sections. The aim is to give you some appreciation of the potential and limitations of the various approaches to the problem of bed-configuration dynamics. It turns out to be easier to account qualitatively for shape and movement than for existence and size. As a necessary preliminary I will first derive the sediment conservation equation, a kinematic relation expressing conservation of sediment volume (or mass) that has to hold in any sediment-transporting system.

Sediment Conservation Equation

121 In any flow that transports sediment, the volume or mass of transported sediment must be conserved. This requirement leads to a purely kinematic relationship that has to hold irrespective of the dynamics of sediment transport. I will concentrate on a two-dimensional flow (one that varies in two dimensions only, downstream and upward from the bed but not in the cross-stream direction), but the principle is the same for a flow that varies in all three directions.

122 Consider a small rectangular region R of the sediment bed, with unit width normal to the flow and with length Δx in the flow direction (Figure 12-33). The area of R is Δx because of the unit width. Denote by h the elevation of the bed above some arbitrary horizontal datum plane. Transport of sediment at any cross section can be expressed by q_S, the volumetric sediment transport rate per unit width of flow; this may include sediment moving as bed load or in suspension. (In Chapter 12, the symbol q_s is used for the unit transport rate expressed as mass rather than as volume.) Let the depth-averaged volume

concentration of the load be C. (Strictly, C includes the concentration of bed load as well as suspended load.) The difference between q_S at the downstream boundary of R, $(q_S)_{out}$, and at the upstream boundary of R, $(q_S)_{in}$, is Δq_S:

$$(q_S)_{out} - (q_S)_{in} = \Delta q_S \tag{12.32}$$

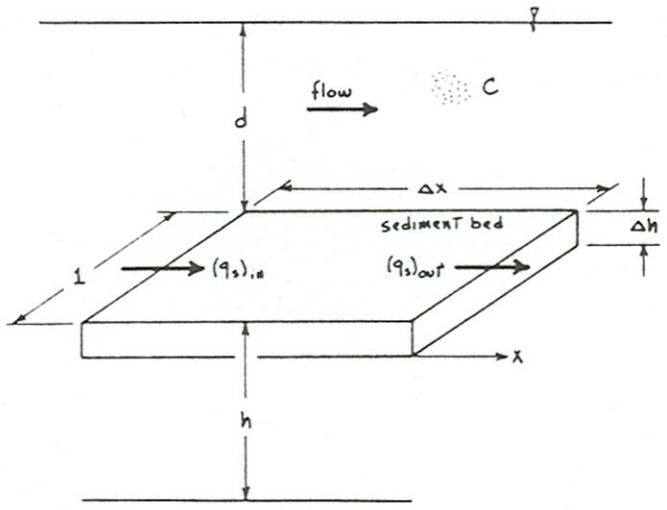

Figure 12-33. Definition sketch for derivation of the sediment conservation equation.

123 Any change Δh in bed elevation during some time interval Δt is caused by storage of sediment in R (deposition, or aggradation) or removal of sediment from R (erosion, or degradation). This change can be viewed as the sum of two contributions. One of these, Δh_S, is caused by downstream change in q_S: if q_S is greater across the upstream face than across the downstream face of R, then sediment must be stored in R, but if q_S is smaller, then sediment must be removed from storage in R. The other contribution, Δh_t, is caused by temporal change in C: if the concentration of transported sediment is decreasing with time, then there must be deposition on all areas of the bed, but if the concentration is increasing, then there must be erosion (assuming that sediment is not being added to the flow from above). The bulk volume $\Delta h_S \Delta x$ of aggraded or degraded bed in R due to downstream variation in q_S is equal to Δt times $(q_S)_{in} - (q_S)_{out}$, the rate of sediment storage due to the difference in transport rates across the upstream and downstream boundaries of R, with a correction for the porosity effect (Equation 12.28):

$$h_S \Delta x = \Delta t[(q_S)_{in} - (q_S)_{out}] = -K_1 \Delta q_S \Delta t \tag{12.33}$$

124 The porosity correction factor $1/(1-\lambda)$, again denoted by K_1, is needed because the volume of transported sediment is measured in solids volume whereas volume of bed sediment is measured in bulk volume, solids plus void space. The bulk volume of aggraded bed in R due to temporal variation in C is equal to minus the total change in volume of suspended sediment above R, again corrected for the porosity effect:

$$\Delta h_t \Delta x = -K_1 d \Delta C \Delta x \tag{12.34}$$

where d is flow depth. Using Equations 12.33 and 12.34, the average rate of change of bed elevation with time over R, $\Delta h/\Delta t$, can now be written

$$\frac{\Delta h}{\Delta t} = \frac{\Delta h_S}{\Delta t} + \frac{\Delta h_t}{\Delta t}$$

$$= -K_1 \left(\frac{\Delta q_S}{\Delta x} + d \frac{\Delta C}{\Delta t} \right) \tag{12.35}$$

In the limit, as $\Delta x \rightarrow 0$, Equation 12.35 becomes

$$\frac{\partial h}{\partial t} = -K_1 \left(\frac{\partial q_S}{\partial x} + d \frac{\partial C}{\partial t} \right) \tag{12.36}$$

125 The differential equation (Equation 12.36) is a volume-balance relationship that must hold at every point on the bed regardless of the sediment-transport dynamics. It relates the time rate of change of bed elevation at a point, $\partial h/\partial t$, to the downstream rate of change of sediment transport rate at that point, $\partial q_S/\partial x$, and the time rate of change of total suspended-sediment concentration in the flow, $\partial C/\partial t$. It is usually called the ***sediment conservation equation***, or the ***sediment continuity equation***. Its use is essential in thinking about the temporal changes in bed geometry consequent upon spatial changes in transport rate. If C does not change with time, Equation 12.36 becomes

$$\frac{\partial h}{\partial t} = -K_1 \frac{\partial q_S}{\partial x} \tag{12.37}$$

Rate of change of bed elevation is thus directly proportional to minus the downstream rate of change of sediment transport rate. If q_S decreases downstream for any reason, the bed is aggraded; if q_S increases downstream, the bed is degraded.

Movement of Bed Forms

126 Armed with the sediment conservation equation and all that has been said about flow and sediment transport in turbulent boundary layers, what can we do about accounting for the existence, size, shape, and movement of loose-sediment bed forms? Look first at *movement*, because that is the most

straightforward. Consider a hypothetical bed form like that in Figure 12-34A, one element in a train of similar bed

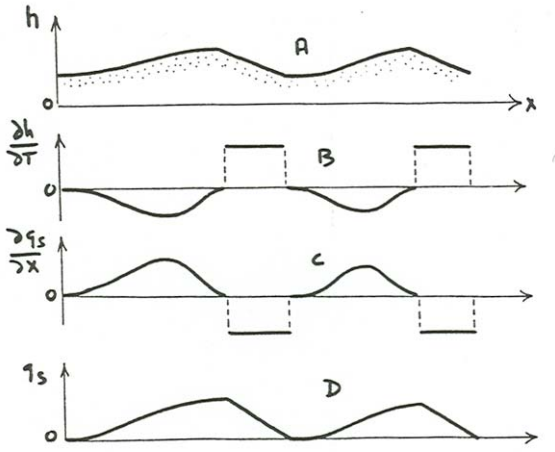

Figure 12-34. Variation of **A)** h, **B)** $\partial h/\partial t$, **C)** $\partial q_s/\partial x$, and **D)** q_s over a hypothetical unchanging bed form in a low-Froude-number flow.

forms. Assume that the bed is in equilibrium with a steady sediment-transporting flow, and that the bed form moves downstream with unchanging size and shape. Equation 12.37 associates with the movement of the bed form a particular pattern of variation of q_s over the bed-form profile in the following way. For the bed form to move downstream it is a kinematic necessity that $\partial h/\partial t$ be negative on the upstream side of the bed form and positive on the downstream side (Figure 12-34B). Note that $\partial h/\partial t$ is zero at the crest and trough and has its greatest absolute value at points of steepest slope on the bed-form profile. By Equation 12.37, $\partial q_S/\partial x$ must vary with x in a sense just opposite to the variation in $\partial h/\partial t$ (Figure 12-34C), and therefore q_S itself must be greatest at the bed-form crest and least in the trough (Figure 12-34D). No zero point is shown on the q_S axis in Figure 12-34D, because any position of the curve is consistent with that of the curve for $\partial q_S/\partial x$ in Figure 12-34C. On ripple bed forms, q_S is zero or nearly so in the trough, and it may even be negative if the reverse flow in the separation zone is strong enough. Over antidunes, on the other hand, there may not be much relative variation in q_S over the bed-form profile. If the bed form is to move downstream q_S must increase up the stoss surface from the trough to the crest and must decrease down the lee surface from the crest to the next trough.

127 In any flow of a low-viscosity fluid like air or water with a velocity large enough to transport sediment, Reynolds numbers of flow over even small ridges or mounds on the bed are large enough for substantial front-to-back asymmetry in local bed shear stress. Recall that beginning at Reynolds numbers of about 10 the spacing of streamlines is closer, and therefore the skin friction is

greater, on the front side of a cylinder or a sphere than on the back. This becomes more pronounced with increasing Reynolds number, and when flow separation eventually develops, the skin friction on the back is negligible. The effects are qualitatively the same for any ridge or mound on a sediment bed. So provided that the free surface remains approximately planar above the bed form, any bed form—even one whose height is only a few grain diameters—should have larger q_S on the upstream side than on the downstream side, with a maximum near the crest and a minimum somewhere in the trough. From Figure 12-34D it is clear that this distribution of q_S guarantees downstream movement. This distribution of q_S is not likely to be exactly the one needed for maintenance of bed-form shape, but that is a matter for the next section; the bed form always moves downstream even if its shape tends to change at the same time.

128 If the mean-flow Froude number is close to one, surface gravity waves interact with the bed to produce stationary or slowly shifting bed waves that are in phase or almost in phase with the water-surface waves. For these upstream-shifting bed forms, which in an earlier section were called antidunes, the interaction of the free-surface wave and the bed-surface wave is such that q_S decreases up the upstream slope and increases down the downstream slope, resulting in upstream movement. No capsule statement can be made at this point that elucidates the dynamical reasons for this variation of q_S.

129 Up to this point, it has been shown:

- what the variation in q_S has to be over a bed-form profile for the bed form to move, and
- that in the case of ripples the expected variations in q_S are in accord with the bed-form movement actually observed.

This may seem like a self-evident or trivial exercise, but it shows how we can obtain some insight into the behavior of bed forms by combining ideas about sediment transport with the sediment conservation equation, and it points the way toward other problems that are not as easy to deal with.

Shape of Bed Forms

130 Introduction.—A striking characteristic of ripples and dunes is their asymmetrical profile, with a gently sloping upstream surface and a steeper, nearly angle-of-repose slip face on the downstream surface. Typically the bed profile shows a sharp angle at the top and bottom of the slip face—although reverse flow in the separation eddy can smooth out the slope break at the base. If the breaks in bed slope at the top and base of the slip face are ideally sharp, they represent jumps or discontinuities in $\partial h/\partial t$ and therefore by Equation 12.37 in $\partial q_S/\partial x$ as well. Both h and q_S show kinks in their profiles at these points.

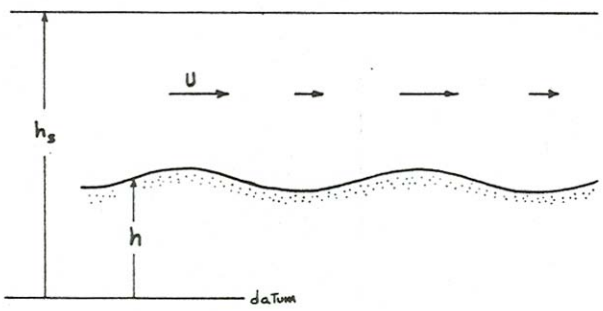

Figure 12-35. Definition sketch for analysis of the evolution of bed-form shape.

---

131 The Profile Shape of Ripples and Dunes.—In this section it is shown how the asymmetrical profile shape of ripples or dunes can be accounted for by combining the sediment conservation equation with a very general assumption about the physics of the sediment transport, namely that q_s increases with increasing flow strength. As in the preceding section, look at a hypothetical bed form in a train of identical bed forms (Figure 12-35). In this section we start with a symmetrical bed form and consider how its profile changes with time. Consideration is resticted to flows with low Froude number, so that the water surface remains nearly planar whatever the bed geometry. The following line of reasoning was first presented by Exner (1925).

132 The strategy is to develop a relationship between bed elevation h and sediment transport rate q_s, in order to put the sediment conservation equation into a form that can be solved for bed elevation as a function of position and time. As discussed above, ultimately we would like to be able to supply enough physics for this approach to lead to insights about how bed forms grow. For now we have to be content with very simple assumptions about q_s that will lead to understanding of bed-form shape but not bed-form growth.

133 The mathematically simplest assumption we can make about q_s is that it is directly proportional to some variable that describes the flow strength above the point at which q_s is measured. Using mean flow velocity U as this flow-strength variable,

$$q_s = K_2 U \tag{12.38}$$

where K_2 is some constant. This has some serious shortcomings:

- there is a finite U for which q_s becomes nonzero, and at smaller U no sediment is moved;
- q_s does not vary linearly with U even when U is strong enough to move sediment; and

- if U rather than the skin friction is to be used to characterize q_s, the flow depth d must also be specified in the function.

134 Notwithstanding these difficulties, this is a workable assumption for the task at hand, because it contains a large element of truth and it permits insight into how the bed evolves. More sophisticated assumptions would lead to the same qualitative results on the evolution of bed-form shape but would necessitate working with equations that are much more difficult to solve. Furthermore, the fact that even such an oversimplified assumption about q_s accounts well for the evolution of bed-form shape is revealing in itself.

135 Using Equation 12.38, the sediment conservation equation (Equation 12.37) can be written

$$\frac{\partial h}{\partial t} = -K_1 K_2 \frac{\partial U}{\partial x} \tag{12.39}$$

where K_1 is again the porosity correction factor $1/(1-\lambda)$. Conservation of fluid volume in the flow requires that, per unit width,

$$Ud = U(h_s - h) = K_3 \tag{12.40}$$

where h_s is water-surface elevation above the same arbitrary datum as for h, and K_3 is another constant. Equation 12.40 tells you that where the flow is deeper over some two-dimensional bed configuration the velocity is smaller, and where the flow is shallower the velocity is greater, so by Equation 12.36 there is deposition or erosion depending on the sign of $\partial U/\partial x$. Combining Equations 12.39 and 12.40,

$$\frac{\partial h}{\partial t} = -\frac{K_1 K_2 K_3}{(h_s - h)^2} \frac{\partial (h_s - h)}{\partial x} \tag{12.41}$$

136 Assuming h_s to be constant (a reasonable assumption for flows at low Froude numbers) and writing K for the constant $K_1 K_2 K_3$, Equation 12.41 becomes

$$\frac{\partial h}{\partial t} = \frac{K}{(h_s - h)^2} \frac{\partial h}{\partial x} \tag{12.42}$$

You can verify for yourself that the solution to the fairly simple partial differential equation 12.42 is

$$h_s - h = f\left[\frac{Kt}{(h_s - h)^2} - x\right] \tag{12.43}$$

where f is an arbitrary function. To investigate the change in bed geometry with time, Exner (1925) assumed an initial bed topography given by a cosine function:

$$h = A_o + A_1 \cos\frac{2\pi x}{L} \qquad (12.44)$$

where L is the spacing of the sinusoidal bed forms, and A_0 and A_1 are constants. This is what the bed profile at time $t = 0$ would be if Equation 12.43 is specialized in such a way that the bed profile as a function of x and t is

$$h = A_o + A_1 \cos\frac{2\pi}{L}\left[x - \frac{K_1 K_2 t}{(h_s - h)^2}\right] \qquad (12.45)$$

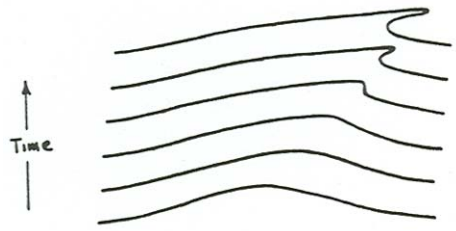

Figure 12-36. Evolution of an initially sinusoidal bed form with time. (After Exner, 1925.)

137 Figure 12-36 shows how the initial sinusoidal bed profile is modified with time according to Equation 12.45. The upstream slope of the bed form becomes gentler and the downstream slope becomes steeper, until finally the downstream slope passes through the vertical and an overhang develops. If this were a real bed form, a slip face would develop when the slope angle of the downstream side reaches the angle of repose. What is less clear from Figure 12-36 is that the bed form does not change in height as it changes in shape—but you can see from Equation 12.45 that the highest point on the bed form always has a height $h = A_0 + A_1$, because the maximum value of the cosine function is one. This just means that the oversimplified assumption about q_s is inadequate to address the problem of bed-term growth.

138 So even a very simple assumption about the dependence of q_s on the flow accounts for the tendency for an originally symmetrical bed-form profile to evolve into the markedly asymmetrical profile characteristic of ripples. If we use a different function in Equations 12.44 and 12.45 to represent a different symmetrical or nearly symmetrical initial profile, the end result is just about the same. It is easy to observe just this kind of profile development in the laboratory: mold a long and low symmetrical ridge transverse to the flow on the sand bed of your flume, turn up the discharge until the sand moves, and then watch the profile as it is transformed gradually into a ripple, just as in Figure 12-36.

Growth of Bed Forms

139 Introduction.—It is more difficult to account for the growth of bed forms than for their movement and shape. Here I will follow the same approach as before, that of combining sediment-transport dynamics with the sediment conservation equation, but it will not lead to results that are as satisfying. This is because bed-form growth and decay, or more generally the stability of bed configurations, depends on the interaction of flow and sediment transport in ways too complicated to be expressed or parameterized by local conditions like flow velocity, boundary shear stress, bed elevation, or bed slope: it involves the entire bed configuration, not just local variations in h and q_s.

140 After describing a hypothetical flume experiment to examine some of the physical effects that have to be explained, I will again examine the qualitative kinematic constraints imposed on q_s during bed-form growth and then review some of the attempts that have been made to account for the existence of bed forms by deriving and solving equations for bed-form growth based on various assumptions about transport dynamics.

141 Hypothetical Flume Experiment.—Make a long series of low transverse ridges on a sand bed in your flume (Figure 12-37). It makes no difference whether these are initially symmetrical or asymmetrical, because you have already seen that the flow soon gives the profile of a transverse ridge a ripple shape, whatever its initial shape. It helps if you give the ridges an initial spacing that's isnot greatly different from what you know beforehand about equilibrium ripple spacing (if any) corresponding to the conditions of flow and sediment size you are going to use, because then you maximize the duration of your experiment by reducing the tendency for the bed forms to change their spacing by dividing and merging. If you make the train of initial ridges very regular, the ripples stay very much alike for a long time as they evolve. Eventually the inevitable irregularities in initial bed geometry (together with the stochastic nature of the grain transport itself) lead to the irregular geometry characteristic of real bed forms, but this irregularity is not essential to the existence of the bed forms. I emphasize that this experiment is a valid way of thinking about the physics of growth and decay of ripples within the context of the initial spacing you choose, although in general you cannot expect these ripples to be happy with the given spacing forever, even if at first they grow rather than decay.

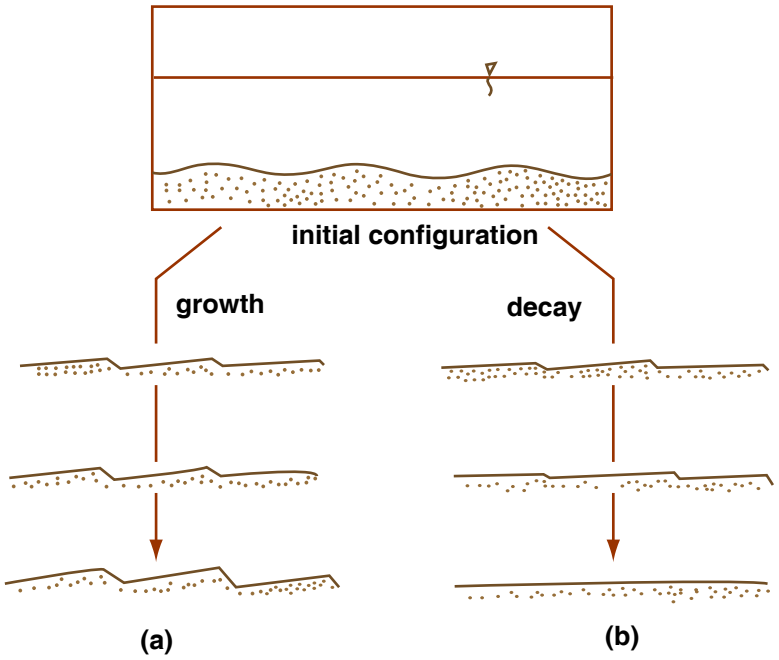

Figure by MIT OpenCourseWare.

Figure 12-37. Hypothetical flume experiment on growth and decay of a train of artificially constructed bed forms.

---

142 Pass a sand-moving current over the ridges, and keep track of the elevations of crests and troughs. Under some conditions (Figure 12-37A) bed-form height increases as the troughs become deeper and the crests become higher. Stoss surfaces become steeper as well, because bed form spacing is strongly locked in to the original value and does not change, at least not until after a long running time. The lee surface is likely to become a slip face almost from the beginning, as you have already seen, and then stay that way. Associated with the increase in crest elevation and decrease in trough elevation is an increase in the volume of sand contained in the ripple per unit width (volume being measured upward from a plane coincident with the bed-form troughs). Time-lapse motion-picture photography of the ripples as they move is a good way of appreciating the changes in bed-form height and stoss-surface steepness. If you know something beforehand about equilibrium height of ripples as a function of flow conditions and sediment size, you could first generate a set of low ripples under one set of flow conditions and then change the flow conditions to what you know will make higher ripples, and then sit back and watch.

143 Now make a second run in which you start out with a train of initially high and steep ridges (Figure 12-37B). The bed forms rapidly become asymmetrical as before, and sediment transport and ripple movement are qualitatively the same as before, but the bed forms are degraded as they move downstream: there is a gradual increase in trough elevation and decrease in crest elevation, and a corresponding gradual decrease in bed-form volume and also in the steepness of the stoss surface. Depending on sediment size and flow conditions, the ripples may stabilize at some equilibrium height, shape, and velocity, or they may become more and more like fast-moving sediment sheets

with small downstream steps until ultimately the bed is transformed into a planar transport surface.

144 Both kinds of run are an approximate simulation of what happens when an equilibrium ripple bed configuration is subjected to a change in flow conditions. They leave out the effects of adjustment in ripple spacing by gradual accentuation of inevitable small irregularities in the profile and then division of one ripple into two, or fusion of two ripples into one. But they illustrate an important principle of bed-configuration stability: if very small disturbances grow larger, then some nonplanar bed configuration is the stable one under those conditions of flow and sediment, whereas if a preexisting nonplanar bed configuration is degraded to a planar transport surface, then upper-regime plane bed or lower-regime plane bed is the stable configuration. An analysis of how the ripple trains grow or decay in experiments like this should therefore provide insight into the dynamics of bed-form stability.

145 Conditions for Growth and Decay of Bed Forms.—In this section I will reason as far as possible about the conditions for growth and decay of bed-form trains, like those in the hypothetical experiment described above. Take the x direction downstream and measure bed height from some plane parallel to the plane representing the mean bed surface and lying well below it. We will restrict ourselves to indefinitely long trains of two-dimensional flow-transverse bed forms in a transport system that's uniform in the large, in the sense that q_s averaged over an entire bed form does not change in the downstream direction (Figure 12-38).

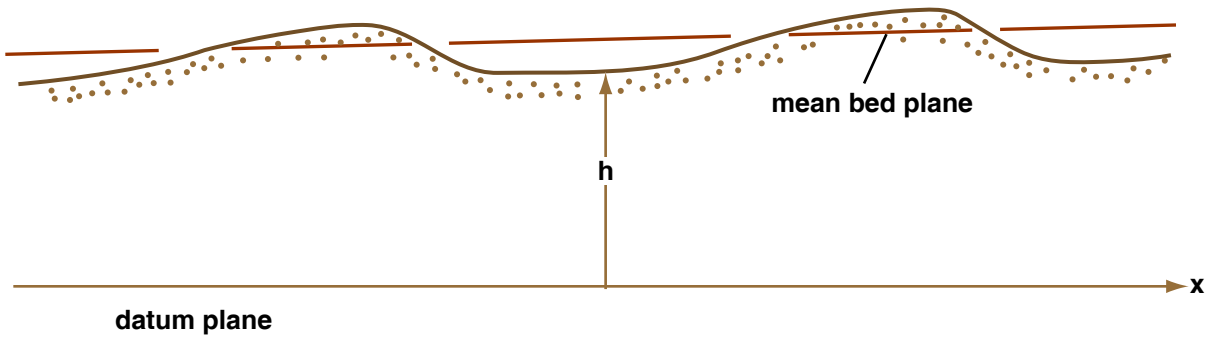

Figure 12-38. Definition sketch for analysis of growth and decay of bed-form trains in steady uniform flow.

146 The bed-form profile may or may not be changing. In either case, $\int h\,dx$ evaluated between two equivalent points on successive bed forms is constant. This expresses the condition that the bed is not aggrading or degrading on the average. If crests become higher, troughs have to become deeper in such a way that the mean bed elevation stays the same.

147 It is instructive to consider first the reference case of an unchanging profile. In the following, refer to Figure 12-39 (which is fundamentally the same as Figure 12-34). The kinematic condition for an unchanging profile is that

$$h = f(x - U_B t) \tag{12.46}$$

where U_B is a constant and f is some periodic function that represents the bed profile at a given time. The argument $x - U_B t$ in the function implies that the profile propagates or shifts downstream at speed U_B as an unchanging wave form; U_B is therefore basically the same as the bed-form velocity used earlier in this chapter. To see the consequences of this condition, assume for now that the bed profile is a sine wave:

$$H = \sin(x - U_B t) \tag{12.47}$$

There is really no loss of generality in doing this, because any periodic bed profile can be represented as a Fourier sum of sinusoidal components; at the end of this paragraph we will revert to a general periodic function f.

148 Differentiating Equation 12.47 with respect to t,

$$\frac{\partial h}{\partial t} = \frac{\partial}{\partial t} \sin(x - U_B t)$$

$$= \frac{d[\sin(x - U_B t)]}{d(x - U_B t)} \frac{\partial(x - U_B t)}{\partial t}$$

$$= U_B \cos(x - U_B t) \tag{12.48}$$

by use of the chain rule for partial differentiation. Note that $\partial h/\partial t$ in Equation 12.48 is 90° out of phase with h in Equation 12.46, if the phase angle is measured in the downstream direction. In other words, the peak of the function in Equation 12.48 is offset downstream from that of the function in Equation 12.46 by one-quarter of a wavelength. (If you are not sure about the phase relationships, plot the four curves $y = \cos x$, $y = \sin x$, $y = -\cos x$, and $y = -\sin x$ and watch the sine wave shift along the x axis by 90°, i.e., one-quarter of a wavelength, each time.) Now, to find $\partial q_s/\partial x$ substitute Equation 12.48 into the sediment conservation equation, Equation 12.37:

$$\frac{\partial q_s}{\partial x} = -\frac{1}{K_1} \frac{\partial h}{\partial t}$$

$$= -\frac{U_B}{K_1} \cos(x - U_B t) \tag{12.49}$$

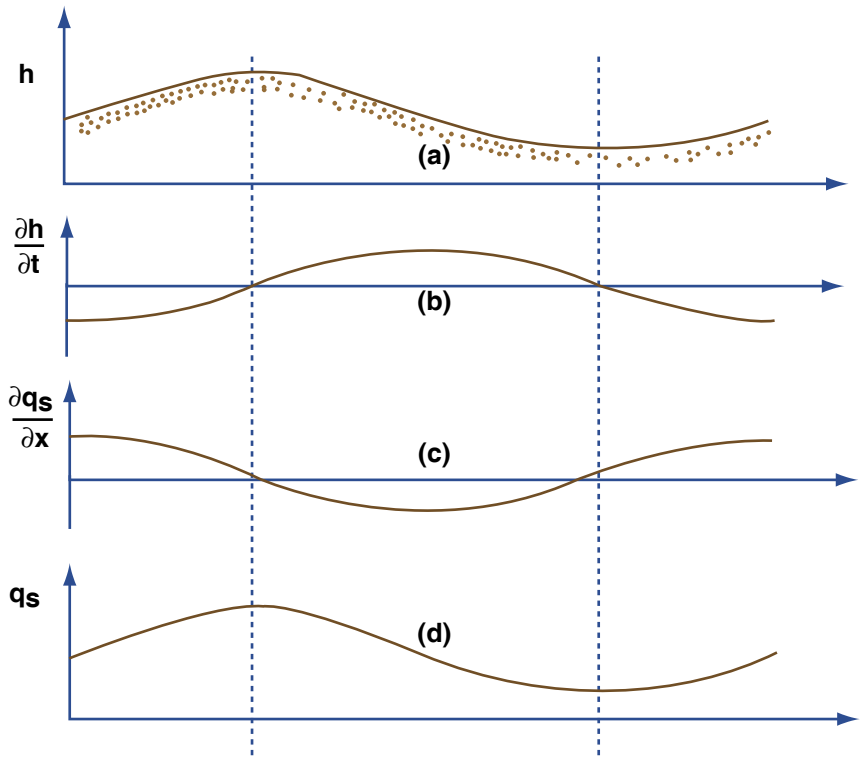

Figure by MIT OpenCourseWare.

Figure 12-39. Profiles of **A)** h, **B)** $\partial h/\partial t$, **C)** $\partial q_s/\partial x$, and **D)** q_s, for an unchanging ripple train in steady uniform flow. For simplicity, the bed-elevation profile is shown as a sine curve; the results are qualitatively the same for any periodic bed profile.

---

149 Note that $\partial q_s/\partial x$ in Equation 12.49 is 270° out of phase with h in Equation 12.46 because of the minus sign, i.e., the crest of the $\partial q_s/\partial x$ profile is one-quarter of a wavelength upstream of the crest of the bed-elevation profile. Integrating $\partial q_s/\partial x$ in Equation 12.49 with respect to x,

$$q_s(x,t) = \int \cos(x - U_B t)\,dx$$

$$= \frac{U_B}{K_1} \int \cos(x - U_B t)\,dx$$

$$= \frac{U_B}{K_1} \sin(x - U_B t) + c_1(t) \qquad (12.50)$$

where $c_1(t)$ is a constant of integration that in general could be a function of t, but is not in this case because we are assuming steady flow. (The constant of integration has to be a function of t because the integration is a "partial integration" of a function of two variables with respect to just one of those variables. while holding $U_B t$ constant.) Note that q_s is in phase with the bed profile and differs only by a multiplicative constant U_B/K_1 and an additive constant c_1.

150 To summarize, for an unchanging bed profile

$$h(x,t) = f(x - ct) \qquad (12.51)$$

and

$$q_s(x,t) = \frac{U_B}{K_l} f(x - U_B t) + c_1 \qquad (12.52)$$

where c_1 is just a constant that relates the average bed elevation to the average sediment transport rate. The variation of q_s is in phase with the bed profile and has the same shape except for the constant factor U_B/K_1. Remember that this is all just a kinematic necessity; we have not specified anything about how q_s and h interact dynamically to produce the particular patterns observed.

151 From here on I will concentrate on lower-flow-regime ripple or dune bed forms. You have seen that if suspended-load transport is unimportant, lower-regime bed forms are dominated by slip faces that represent shock discontinuities. These discontinuities are associated with major flow separation over the bed form, but in a sense they are independent of the flow separation, in that they are a consequence of the steep increase in q_s with flow strength. Disregarding minor reverse flow in the lee eddy, q_s is zero from the toe of the slip face downstream to the reattachment point. If the profile is unchanging with time, this stretch of bed must be horizontal: within it q_s is independent of both x and t because it is identically zero there, so h, which differs from q_s only by a multiplicative and an additive constant (compare Equations 12.46 and 12.50), is constant in x and t there. This stretch of bed with $q_s = 0$ may not be quite the lowest in the profile. because of some upchannel-directed sediment transport just upchannel of the reattachment zone, but it can safely be assumed so without affecting the conclusions of this section. Likewise, there is no dynamical requirement that the brink at the top of the slip face is the highest point on the profile, even if the profile is unchanging with time, but, because there is such a strong tendency for flow separation to develop upstream of a negatively sloping surface, the brink should be just about the highest point on the profile. It is therefore convenient to let the slip face represent the bed-form height H, and it is also convenient to let the rate of downstream advance of the brink represent the velocity U_B of the ripple.

152 The presence of the shock discontinuity represented by the slip face imposes a further kinematic relationship that must hold among bed-form height, bed-form velocity, and the value of q_s at the brink:

$$(q_s)_{brink} = K_1 H U_B \qquad (12.53)$$

This is exactly the same as Equation 12.31; if you go back and review the derivation of that equation, you will see that it holds for the present situation as well, provided that all of the load is dumped at the break in slope at the brink to build the slip face forward. Equation 12.53 holds generally, not just for an unchanging profile. Note that the slip-face angle drops out of the expression. This is consistent with the idea that the slip face is just the physical manifestation of a shock discontinuity in q_s. The sediment delivered to the crest could just as well be falling off a cliff, in terms of the kinematics of the phenomenon!

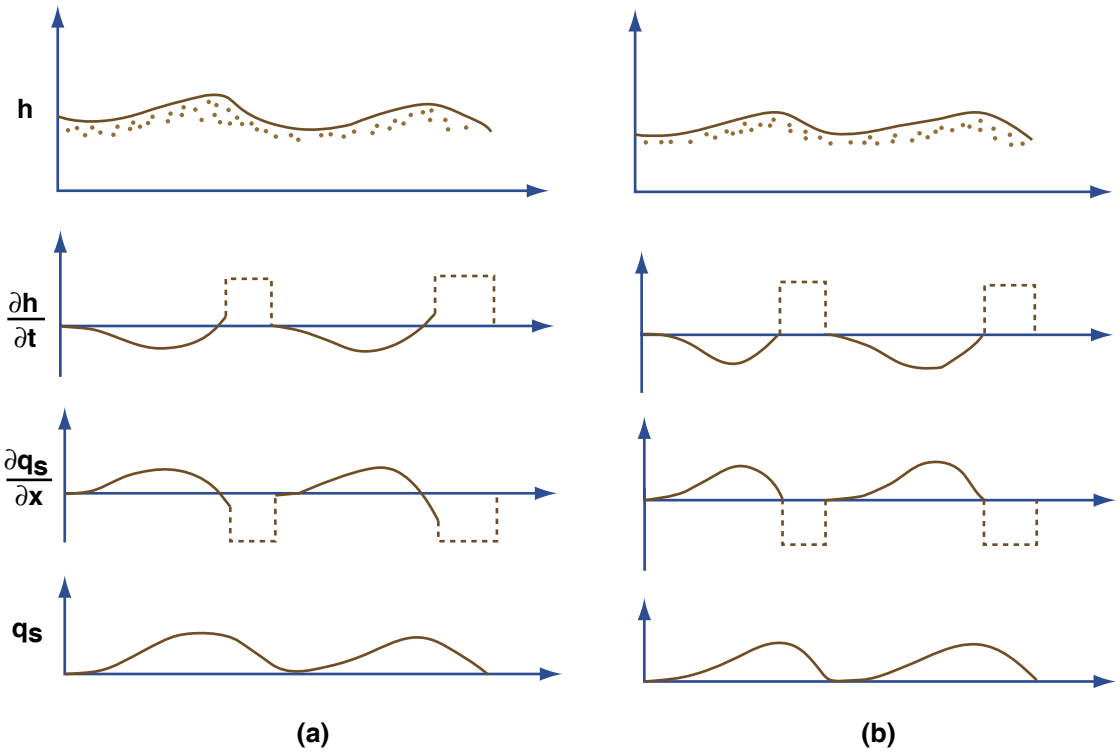

Figure by MIT OpenCourseWare.

Figure 12-40. Profiles of **A)** h, **B)** $\partial h/\partial t$, **C)** $\partial q_s/\partial x$, and **D)** q_s, for a train of ripples increasing in height. **A)** Ripples are adjusting in height; **B)** ripples have reached equilibrium. See text for explanation.

---

153 In the light of all this bed-form kinematics, what can be done about accounting for the results of the hypothetical experiment? In the first run the bed forms started out too low and grew to some stable greater height, and they changed their shape in the process. After the bed forms reached equilibrium, the distributions of h, $\partial h/\partial t$, $\partial q_s/\partial x$, and q_s must have been as shown in Figure 12-40B, which is qualitatively the same as Figure 12-34. Note the discontinuities in $\partial h/\partial t$ and $\partial q_s/\partial x$, reflecting the sharp kinks in bed elevation and transport rate at the top and bottom of the slip face. While the ripple train was adjusting, these curves must have been as shown in Figure 12-40A. The differences between Figure 12-40A and Figure 12-40B look minor, but they are very significant for ripple growth. Large differences should not be expected anyway, because change in ripple shape and height is slow relative to ripple movement. The maximum in q_s on the stoss slope is located a little upstream of the brink rather than right at it. This leads to upward growth of the upper stoss surface during migration. Also, there is a downchannel slope to the bed between the base of the slip face and the low point on the profile. These two differences reflect stronger-than-equilibrium scour in the reattachment zone and just downstream, leading to a temporal lowering of bed elevation in the trough. The extra sediment produced by this scour is transported up the stoss surface to steepen the upper part. The slip face lengthens as it builds into the deepening trough, making ripple height greater. By Equation 12.53, U_B

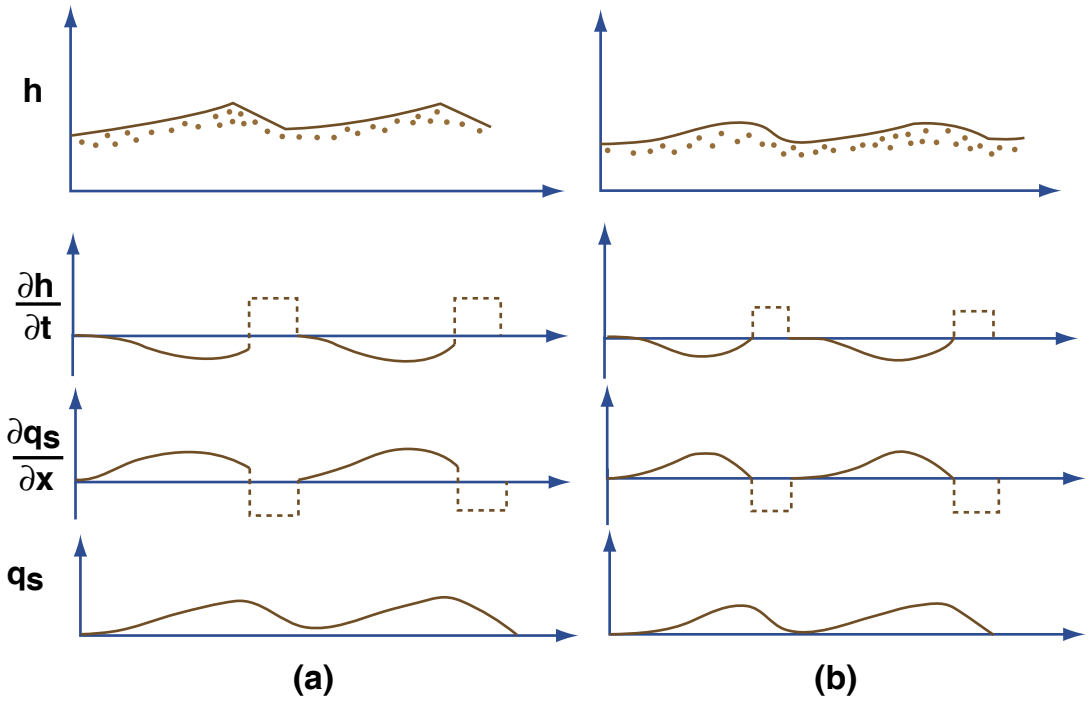

Figure by MIT OpenCourseWare.

Figure 12-41. Profiles of **A)** h, **B)** $\partial h/\partial t$, **C)** $\partial q_s/\partial x$, and **D)** q_s, for a train of ripples decreasing in height. **A)** Ripples are adjusting in height; **B)** ripples have reached equilibrium. See text for explanation.

---

tends to decrease as the slip face lengthens, and this augments the tendency for increased trough scour, because the reattachment zone passes more slowly along the bed in the trough as it is driven downstream by the next ripple coming along. Eventually the geometry and sediment transport adjust to the new flow, and a picture qualitatively like that of Figure 4-40B is reestablished with a greater ripple height and a different ripple shape.

154 In the second run, the bed forms started out too large and shrank either to some stable smaller height or were degraded completely. Figure 12-41 shows the distributions of h, $\partial h/\partial t$, $\partial q_s/\partial x$, and q_s as the ripples were changing. If the ripples reached equilibrium in the run, Figure 12-41A can be compared with Figure 12-41B for the stable smaller ripples. If not, then Figure 12-41A evolves into an uninteresting graph, not shown, in which h and q_s are positive and constant, and $\partial h/\partial t$ and $\partial q_s/\partial x$ are zero. Note in Figure 12-41A that q_s is increasing at all points up the stoss surface from reattachment. Because $\partial q_s/\partial x$ is still positive at the brink, $\partial h/\partial t$ is negative there, so the crest elevation is decreasing with time. Scour in the trough is weaker than needed to maintain trough depth, so the bed slopes upward at all points downchannel of the base of the slip face, although no sediment is moved on the stretch of bed from there to the reattachment point. Trough elevation increases as the slip face becomes shorter by building onto the upsloping trough surface, so both ripple height and ripple volume decrease. By Equation 12.53, U_B tends to increase as the slip face becomes shorter, and this augments the weakening of scour in the trough because it causes the reattachment zone to sweep more rapidly downchannel.

155 In summary, changes in ripple height, shape, and velocity can be viewed in terms of the interaction among three related but distinguishable factors:

- the dependence of q_S on flow structure along the reach of bed extending from the reattachment point up the stoss surface to the brink;
- the rate at which the zones of differing flow structure downstream of the point of flow separation are swept along the bed surface by the advancing crest upstream, as specified by the relation expressed by Equation 12.53 among slip-face height, ripple velocity, and sediment transport rate at the brink; and
- the slope of the trough surface onto which the slip face builds.

156 We have not solved any problems of bed-form stability here; we have only shown what factors are involved. Nonetheless, this line of approach is nonetheless useful, in that it aids in an understanding of the problem.

157 **Stability Analyses.—**In order to understand the existence of bed forms, various investigators have resorted to stability analysis, a mathematical technique, useful in many areas of applied mathematics, whereby a partial differential equation is somehow developed that gives the rate of growth of a periodic disturbance or perturbation introduced onto the bed surface. The assumption is that if the rate of growth of the perturbation is positive the perturbation is amplified with time, and bed forms eventually develop. If, on the other hand, the perturbation is damped, then a plane bed should be the only stable bed configuration. The differential equation is of the same kind as used in the preceding sections. It comes about by supplying a relationship for q_s as a function of flow, which can be used to put the sediment conservation equation into a solvable form. This equation has to go beyond the oversimplified assumptions made in the section on shape of ripples, because we saw that those assumptions account only for change in ripple shape, not in ripple volume.

158 The great advantage of the stability approach is that it can be developed for perturbations with amplitude very small compared to wavelength, so that bed slopes are very small. It is then more likely that relationships for sediment transport that are not grossly unrealistic can be specified. By the same token, however, without further analysis this approach gives no information on the nature of the resulting bed configuration when the perturbation is amplified to the extent that that the small-amplitude assumption is no longer valid. There is the possibility, however, that an estimate of the spacing of the resulting bed forms can be obtained by determining the wavelength of the perturbation that shows the fastest rate of growth.

159 It is worth mentioning several attempts, along the above lines to account for observed bed configurations: those by Kennedy (1963, 1969), Smith (1970), Engelund (1970; see also Engelund and Fredsøe, 1974), Richards (1980), McLean (1990), Ji and Mendoza (1997), and Jerolmack et al. (2006). (You can see, from that list, that the pursuit of the fundamental dynamics by means of

stability analysis has had a long history. The last word has not been spoken on that topic—a manifestation of the enduring obstacles to a unified and generally accepted theory.)

160 Kennedy's analysis, which is most relevant to bed configurations at mean-flow Froude numbers close to one, assumes inviscid flow with a wavy free surface over a wavy boundary. By making simple assumptions about sediment transport rate as a function of near-bed velocity, Kennedy developed a framework that accounts well for the occurrence of antidunes—bed forms whose behavior is dependent upon the presence of the free surface. The theory does not so much predict the bed configuration as provide a rational framework in which to account for it: as do many later analyses by others, the analysis involves a parameter called the lag distance (the distance by which local sediment transport rate lags behind the local velocity at the bed) that would have to be supplied by either experiment or additional theory. For the stability of antidunes, the theory works well with physically realistic assumptions about the lag distance in that it succeeds in accounting for the observed spacing of antidunes. As might be expected from the essential role of the presence of the wavy free surface in the analysis, the theory is less successful in accounting for dunes. Kennedy's work stimulated many subsequent attempts along the same lines.

161 Smith (1970) developed a stability analysis to deal specifically with flow at Froude numbers low enough that free-surface effects are negligible. Making suitable assumptions about nature of the flow (eddy-viscous flow of real fluid) and about sediment transport rate as a function of flow, Smith developed an equation that, when linearized by retaining only the most significant terms, is amenable to stability analysis. The result is that, for these not grossly unrealistic assumptions about flow and sediment transport, a positive growth rate, and therefore development of ripple-like bed configurations, is predicted for all flows strong enough to transport sediment. This is a rather fundamental and satisfying way to account for the existence of ripple-like bed configurations under reasonably realistic assumptions about flow and sediment transport. Even aside from the usual problem of not being able to take finite-amplitude effects into account without further theory, however, the analysis does not account for the existence of plane-bed stability at the higher flow strengths.

162 Engelund (1970; see also Fredsøe, 1974, and Engelund and Fredsøe, 1974), in a somewhat different approach also involving an eddy-viscous fluid, but taking account of the distinction between suspended-load transport and bed-load transport, was able to account well for the transition from dunes to plane bed as a function of both grain size and flow strength. Richards (1980), using a more realistic description of the structure of turbulence near the bed, was able to account for the separate existence of ripples and dunes by predicting the occurrence of two separate modes of instability, one (for ripples) dependent on the bed roughness and the other (for dunes) dependent on the flow depth. More recently, McLean (1990) and Li and Mendoza (1997) have gone beyond linear stability analysis to account also for nonlinear finite-amplitude effects. Even more recently, Jerolmack et al. (2006) have developed a model of bed-form development that unifies the dynamics of ripples and dunes.

Are Ripples and Dunes Different?

163 Of course, the answer is "yes": dunes are larger than ripples. I should rephrase the question: Are the dynamics of ripples and dunes different? Most investigators have assumed that the answer to that question is also "yes". Those who have attempted to account for the existence of ripples and dunes by means of a stability analysis (see the preceding section) have invoked a short-wavelength instability that leads to the development of ripples and a long-wavelength instability that leads to the development of dunes. In that approach, the key to the development of ripples is a spatial (downstream) lag between bed shear stress and sediment transport rate (that is, the sedimentary transport rate lags the bed shear stress) in the case of ripples, and a spatial lag between bed shear stress that also involves suspended-load transport, in the case of dunes.

164 It has commonly been believed that there is a gap in spacing between what are considered to be ripples and what are considered to be dunes. In reporting a consensus among the "experts", Ashley (1990) chose a cutoff of 0.6 m spacing for the boundary between ripples and dunes. There indeed seems to be a paucity of bed forms with spacings in the range between a few decimeters and one meter (Figure 12-42).

165 Clearly there is not a complete absence of ripple or dune bed forms in that range—but it is still uncertain whether there is a continuum in spacing between undoubted ripples and undoubted dunes, or whether those intermediate cases are stunted dunes (in very shallow flow) or newly developing dunes. The matter has not yet reached the stage of a general consensus. There have been only a few studies aimed particularly at describing the transition between ripples and dunes (Boguchwal and Southard, 1990; Bennett and Best, 1996; Lopez et al., 2000; Robert and Uhlman, 2001). The range of mean flow velocity, for a given flow depth, over which the transition is completed is rather narrow. Within that narrow range, there is a large change in bed-form geometry as well as the associated flow characteristics. What all of these studies seem to agree upon is that there is a real dynamical distinction between ripples and dunes.

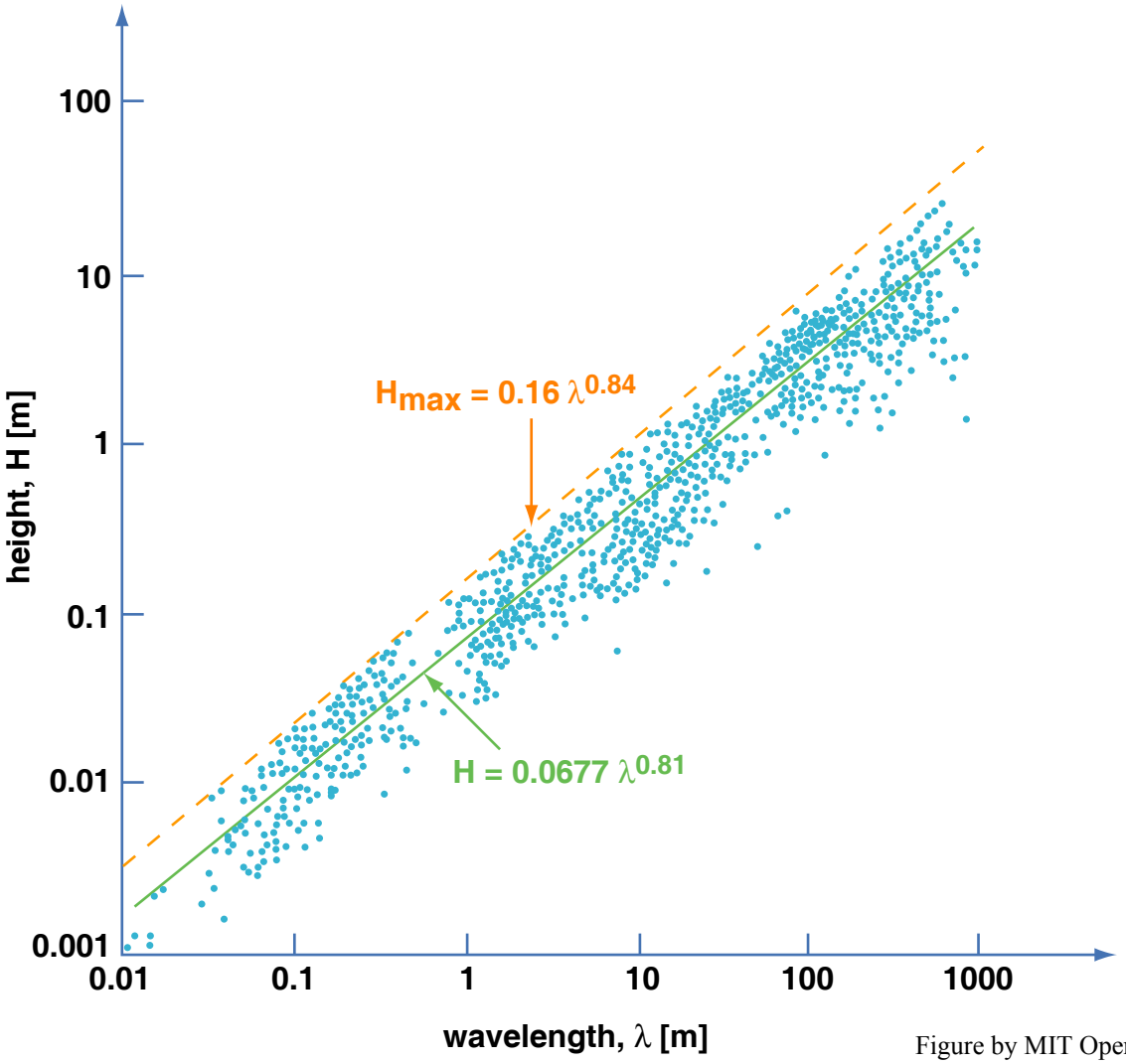

Figure by MIT OpenCourseWare.

Figure 12-42. Plot of bed-form height vs. bed-form spacing. The dashed line is the maximum best-fit power-law relationship, and the solid line is the mean best-fit power-law relationship. (From Jerolmack et al., 2006, based on the work of B.W. Flemming.)

OSCILLATORY-FLOW AND COMBINED-FLOW BED CONFIGURATIONS

Introduction

166 As described in Chapter 6, water-surface waves propagating in water much shallower than the wavelength cause a back-and-forth motion of the water at the bottom. If the maximum speed of the water (which is attained in the middle of the oscillation) exceeds the threshold for sediment movement, oscillatory-flow bed forms develop. This is common in the shallow ocean. Swell from distant storms causes bottom oscillatory motion even though the weather is fine and calm locally. More importantly, bottom-water motions under large storm waves cause bed forms also. In that situation there is likely to be a non-negligible unidirectional current as well, resulting in a combined flow.

A Tank Experiment on Oscillatory-Flow Bed Configurations

167 There are three ways to make oscillatory-flow bed configurations in the laboratory. One is to build a big long tank and make waves in it by putting a

wave generator at one end and a wave absorber at the other end (Figure 12-43). The generator does not need to be anything more than a flap hinged at the bottom and rocked back and forth in the direction of the tank axis at the desired period. This arrangement makes nice bed forms, but the trouble is that you are limited to short oscillation periods.

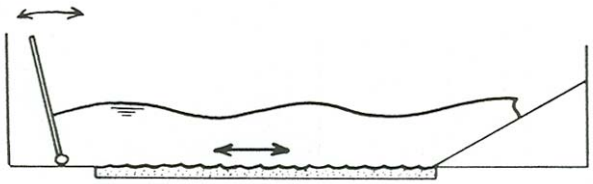

Figure 12-43. Making an oscillatory-flow bed configuration in a wave tank.

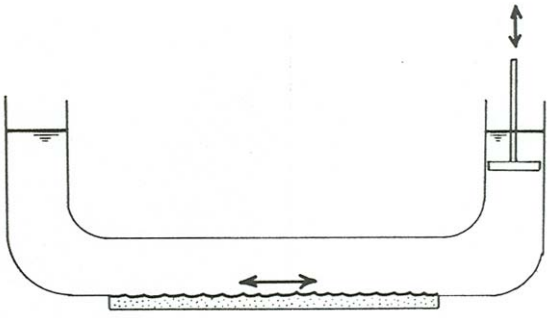

Figure 12-44. Making an oscillatory-flow bed configuration in an oscillatory-flow duct.

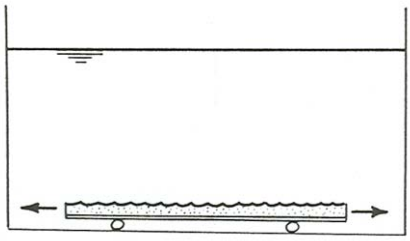

Figure 12-45. Making an oscillatory-flow bed configuration in an oscillatory bed beneath still fluid.

168 Another good way to make oscillatory-flow bed configurations is to build a horizontal closed duct that connects smoothly with reservoir tanks at both ends, fill the whole apparatus with water, and then put a piston in contact with the water surface in one of the reservoir tanks and oscillate it up and down at the desired period (Figure 12-44). This allows you to work with much longer-period oscillations, but there is the practical problem that the apparatus has its own natural oscillation period, and if you try to make oscillations at a much different period you have to fight against what the duct wants to do, and that means large forces.

169 The third way should seem elegant and ingenious to you: place a sand-covered horizontal tray at the bottom of a large tank of water, and oscillate the tray back and forth underneath the water (Figure 12-45). The problem is that the details of particle and fluid accelerations are subtly different from the other two devices, and it turns out that the bed configurations produced in this kind of apparatus do not correspond well with those produced in the other two kinds of apparatus.

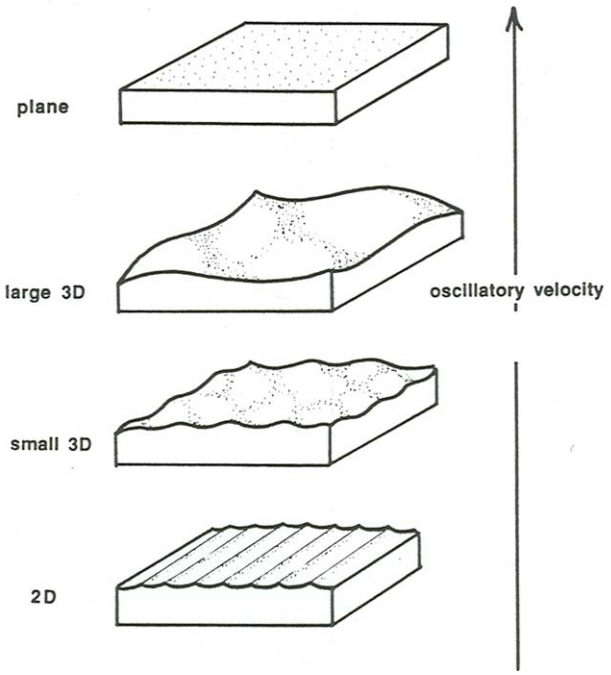

Figure 12-46. Sequence of oscillatory-flow bed configurations sin fine sands with increasing oscillation velocity, for an oscillation period of several seconds.

170 Imagine making an exploratory series of runs in an oscillatory-flow duct of the kind shown in Figure 12-44 to obtain a general idea of the nature of oscillatory-flow bed configurations. Work at just one oscillation period, in the range from three to five seconds. Start at a low maximum oscillation velocity and increase it in steps. Figure 12-46 shows the sequence of bed configurations you would observe.

171 Once the movement threshold is reached, a pattern of extremely regular and straight-crested ripples develops on a previously planar bed. The ripples are symmetrical in cross section, with sharp crests and broad troughs. In striking contrast to unidirectional-flow bed configurations, the plan pattern is strikingly regular: ripple size varies little from ripple to ripple, and the ripples are straight and regular. At fairly low velocities the ripples are relatively small, with

spacings of no more than several centimeters, but with increasing velocity the become larger and larger.

172 In a certain range of moderate velocities, the ripples become noticeably less regular and more three-dimensional, although they are still oriented dominantly transverse to the oscillatory flow. These three-dimensional ripples continue to grow in size with increasing velocity, until eventually they become flattened and are finally washed out to a planar bed. Therefore, just as in unidirectional flows, rugged bed configurations pass over into a stable plane-bed mode of transport with increasing velocity.

173 Oscillatory-flow bed configurations at longer oscillation periods are much less well studied, especially at high oscillatory velocities. Some comments on bed configurations produced under those conditions, which are very important in natural environments, are given in a later section.

Dimensional Analysis

174 Assume again, as we did earlier with unidirectional flow bed configurations, that the sediment is described well enough by its density ρ_s and average size D. The oscillatory flow is specified by any two of the following three variables: oscillation period T, orbital diameter d_o (the distance traveled by water particles during one-half of an oscillation), and maximum orbital velocity U_m; I'll use T and U_m here. As with unidirectional-flow bed configurations, we also need to include ρ, μ, and γ'. The number of independent variables is seven, so we should expect a set of four equivalent dimensionless variables.

175 One dimensionless variable can again be the density ratio ρ_s/ρ, and the other three have to include U_m, T, and D as well as ρ, μ, and γ'. Adopting the same strategy as for unidirectional flow, we can form a dimensionless maximum oscillation velocity, a dimensionless oscillation period, and a dimensionless sediment size:

$$\left(\frac{\rho^2}{\mu\gamma'}\right)^{1/3} U_m\,,\ \left(\frac{\gamma'^2}{\rho\mu}\right)^{1/3} T\,,\ \left(\frac{\gamma'\rho}{\mu^2}\right)^{1/3} D$$

Then we can plot another three-dimensional graph to show the stability fields of oscillatory-flow bed phases, just as for unidirectional-flow bed phases (Figure 12-47). Relationships are best revealed by looking at a series of velocity–period sections through the graph for various values of sediment size (Figure 12-47). Figure 12-48 shows three such sections, one for very fine sands, 0.1–0.2 mm (Figure 12-48A), one for medium sands, 0.3–0.4 mm (Figure 12-48B), and one for coarse sands (0.5–0.6 mm (Figure 12-48C). As with the graphs for unidirectional flows presented earlier, the axes are labeled with the 10°C values of velocity and period corresponding to the actual dimensionless variables. The data shown in Figure 12-48 are from laboratory experiments on oscillatory-flow bed configurations, made in both wave tanks and oscillatory-flow ducts, by several different investigators.

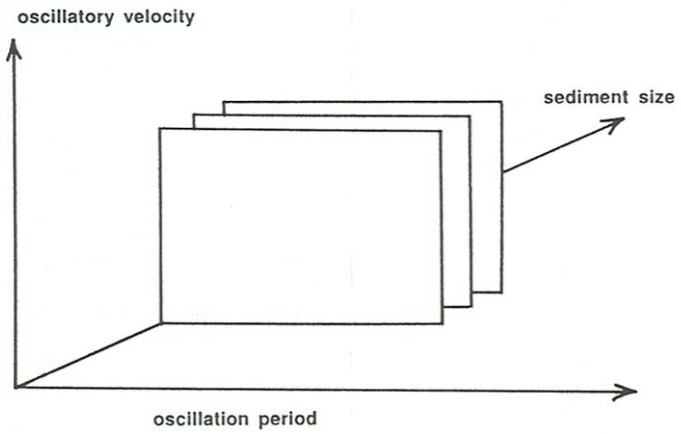

Figure 12-47. The velocity–period–size diagram, showing velocity–period sections for three sediment sizes.

176 In each section in Figure 12-48, there is no movement at low velocities and a plane-bed mode of transport at high velocities. The intervening stability region for oscillation ripples narrows with decreasing oscillation period. As with ripples in unidirectional flows, there really are two different kinds of lower boundary of the stability field for oscillation ripples: one represents the threshold for sediment movement on a preexisting planar bed, and the other represents the minimum oscillation velocity needed to maintain the equilibrium of a preexisting ripple configuration. Existing data are not extensive enough to define the exact nature of these boundaries.

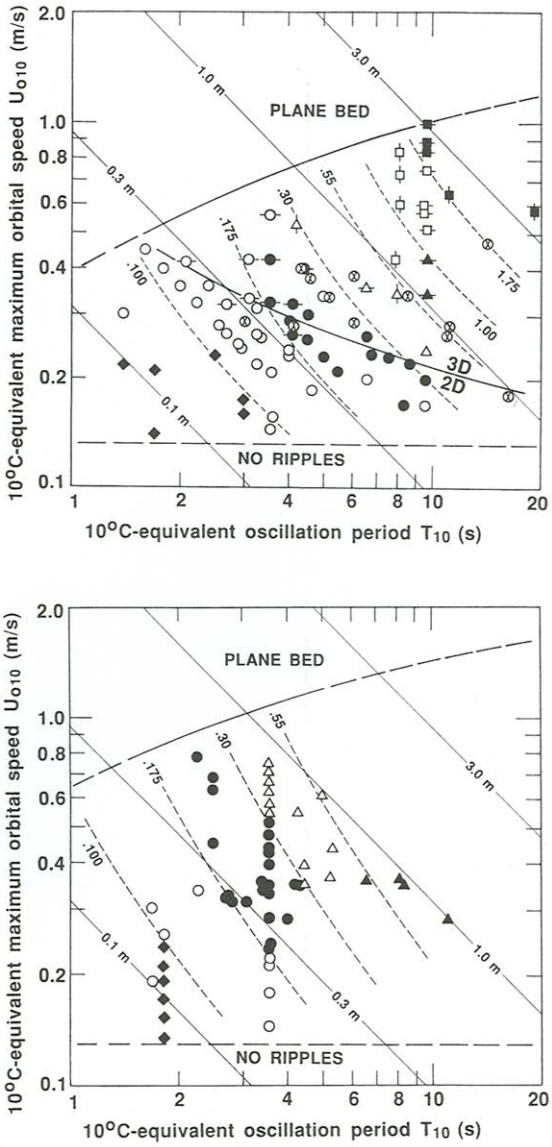

Figure 12-48. Velocity–period sections for sand sizes of **A)** 0.01–0.02 mm and **B)** 0.50–0.65 mm sand. Symbols for spacing: solid diamonds, < 0.100 mm; open circles, 0.100–0.175 mm; solid circles, 0.175–0.30 mm; open triangles, 0.30–0.55 mm; solid triangles, 0.55–1.00 mm; open squares, 1.00–1.75 mm; solid squares, > 1.75 mm. Horizontal tick marks indicate a three-dimensional configuration. Symbols without tick marks indicate a two-dimensional configuration, except that circles with enclosed X's represent a three-dimensional configuration for which a characteristic ripple spacing was not measured. Vertical tick marks indicate ripples whose spacing is much greater than duct width, so that the three-dimensional geometry of the ripples could not be observed. (From Southard, 1991.)

177 The most prominent feature of each of the sections in Figure 12-48 is the regular increase in ripple spacing from lower left to upper right, with increasing velocity and period. The contours of ripple spacing are close to being parallel to the lines of equal orbital diameter except near the transition to plane bed.

178 An important feature of the section for fine sands is a transition from extremely regular straight-crested ripples (which I will call two-dimensional ripples) at relatively low oscillation velocities to rather irregular ripples (which I will call three-dimensional ripples) with short and sinuous crest lines at relatively high oscillation velocities. The most three-dimensional bed configurations show only a weak tendency for flow-transverse orientation, and it is difficult or impossible to measure an average ripple spacing. In medium sands (Figure 12-48B) the transition from two-dimensional ripples to three-dimensional ripples takes place at velocities closer to the transition to plane bed, and the tendency for three-dimensionality is not as marked as in fine sands.

179 Superimposed smaller ripples are prominent in the troughs and on the flanks of the larger ripples formed at long oscillation periods and high oscillation velocities in fine sands. These small superimposed ripples have spacings of about 7 cm, and they seem to dynamically related to ripples in unidirectional flows. The one-way flow during each half of the oscillation lasts long enough and transports enough sediment so that a pattern of current ripples becomes established in local areas on the bed. The flow in the other direction reverses the asymmetry of these small ripples but does not destroy them.

180 Experimental data are least abundant for long periods and high velocities, but preliminary data show the existence of three-dimensional rounded bed forms with spacings of well over a meter in fine sands under these conditions. In contrast to the smaller two-dimensional ripples, these large ripples are not static but show a tendency to change their shape and shift their position with time, even after the bed configuration has stopped changing on the average.

181 In coarse sands (Figure 12-48C), no experiments have been made at the longest periods and highest velocities, but evidence from observations in modern shallow marine environments, and also from the ancient sedimentary record, suggests that ripples in coarse sands are two-dimensional over the entire range of periods and velocities characteristic of natural flow environments.

182 The flow over oscillation ripples is characteristic (Figure 12-49). During half of the oscillation cycle, the flow separates over the sharp crest of the ripple, putting abundant suspended sediment in suspension in the separation vortex over the downflow side. As the flow reverses, the vortex is abruptly carried over the crest of the ripple and deposits its suspended sediment. Flow separation is then rapidly reestablished on the other side of the ripple, and a new vortex develops. For this reason, these ripples have been called ***vortex ripples***.

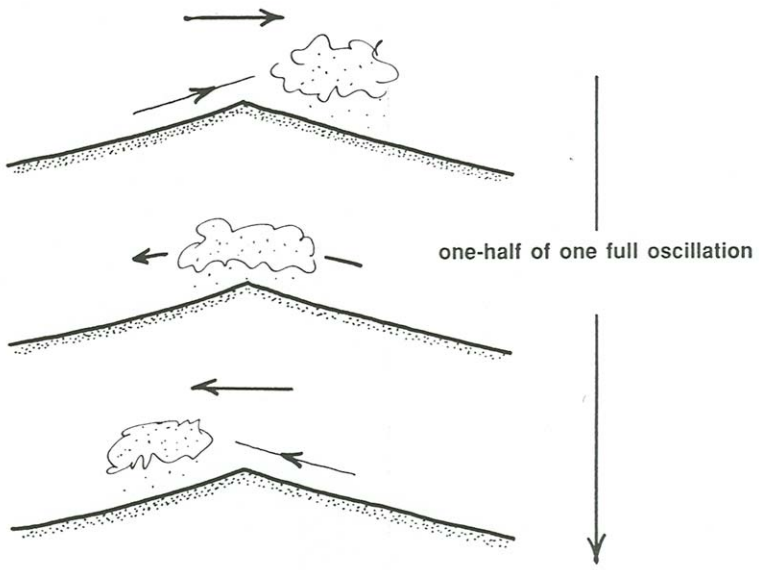

Figure 12-49. Sediment transport in suspension over the crest of an oscillation ripple.

---

183 Purely oscillatory flows that involve a discrete or continuous range of oscillatory components with different directions, periods, and velocities must be common in the shallow ocean. For example, when a storm passes a given area, strong winds tend to blow from different directions at different times. Some time is needed for the sea state to adjust itself to the changing wind directions, and during those times the sea state is complicated, with superimposed waves running in different directions. The nature of bed configurations under even simple combinations of two different wave trains is little known. Much more observational work needs to be done on this topic.

Combined-Flow Bed Configurations

184 So far we have considered only the two "end-member cases" of flows that make bed configurations. Even aside from the importance of time-varying unidirectional and oscillatory flows, and of purely oscillatory flows with more than just one oscillatory component, there is an entire range of combined flows that generate distinctive bed configurations. Observations in the natural environment are scarce, and systematic laboratory work (Arnott and Southard, 1990; Yokokawa, 1995; Dumas et al., 2005) has so far explored only a small part of the wide range of relevant conditions. This section is therefore necessarily shorter than the previous sections. Up to now, systematic observations have been made only for combined flows in which a single oscillatory component is superimposed on a current flowing with the same orientation as the oscillation.

There is therefore still a major gap in our knowledge of combined-flow bed configurations.

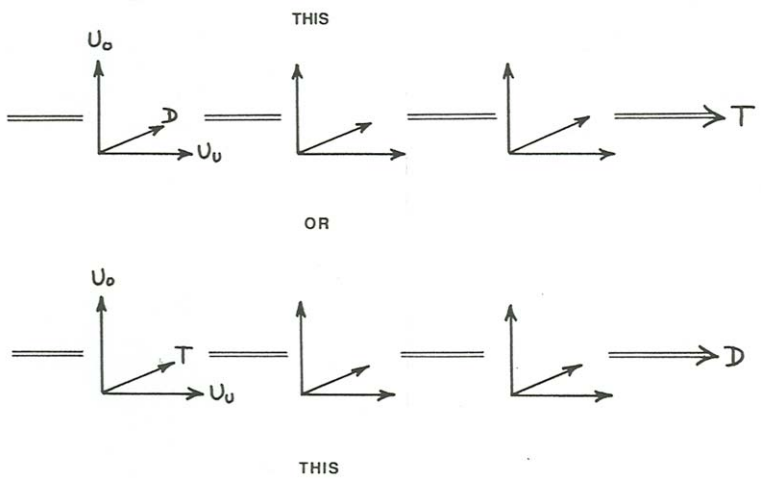

Figure 12-50. Ways of representing combined-flow bed configurations graphically.

185 Figure 12-50 is an inadequate attempt to provide a conceptual framework for thinking about combined-flow bed configurations. Ideally we would like to be able to plot observational data on combined-flow bed configurations on a graph with axes representing the four important independent variables: oscillatory velocity, unidirectional velocity, oscillation period, and sediment size. Unfortunately it is impossible for human beings to visualize four-dimensional graphs. A substitute approach (Figure 12-50) is to imagine one or the other of two equivalent kinds of graphs:

- a continuous series of three-dimensional graphs with the two velocity components and sediment size along the axes, one such graph for each value of oscillation period; or
- a continuous series of three-dimensional graphs with the two velocity components and oscillation period along the axes, one such graph for each value of sediment size.

186 Systematic laboratory experiments on combined-flow configurations have been carried out by Arnott and Southard and, more recently, covering wider range of flow and sediment conditions, by Dumas et al. (2005). The experiments by Dumas et al. (2005) were done in large oscillatory-flow ducts with oscillation

periods ranging from about 8 s to 11 s (scaled to 10°C water temperature), with well-sorted sediments ranging in size from 0.10 to 0.23 mm (scaled to 10°C water temperature). Figure 12-51 shows three phase diagrams, for three combinations of oscillation period and sediment size, showing data points and phase boundaries. The boundaries within the field for ripples are gradual rather than abrupt. Bear in mind, when looking at these diagrams, that they are still an extremely "thin" representation of the graphic framework shown in Figure 12-50.

Image removed due to copyright restrictions.
Dumas, S., R. W. C. Arnott, and J. B. Southard. "Experiments on Oscillatory-flow and Combined-flow Bed Forms: Implications for Interpreting Parts of the Shallow-marine Sedimentary Record." *Journal of Sedimentary Research* 75 (2005): 501-513.

Figure 12-51. Bed-phase diagrams for combined-flow bed phases, with oscillatory velocity component on the vertical axis and unidirectional velocity component on the horizontal axis. **A)** sediment size 0.14 mm, oscillation period 10.5 s; **B)** sediment size 0.14 mm, oscillation period 8.0 s; **C)** sediment size 0.22 mm; oscillation period 10.5 s.

187 Here are some of the features of Figure 12-51. At combinations of low oscillatory velocities and low unidirectional velocities, there is no sediment movement. At combinations of high oscillatory velocities and high unidirectional velocities, a planar bed with strong sediment movement is the stable bed configuration. Note that when even a small unidirectional component is present, the oscillatory velocity for the transition from ripples to plane bed is substantially lower than in purely oscillatory flow.

188 In the lower part of the region of ripple stability, the ripples are relatively small. Only a small unidirectional component is needed to make the small ripples fairly asymmetrical. Except when the unidirectional component is very weak, small combined-flow ripples are not greatly different in geometry from ripples in purely unidirectional flow.

189 In the upper part of the region of ripple stability, the ripples are relatively large. Only a small unidirectional flow component is needed to make the large three-dimensional oscillatory-flow bed forms produced at these oscillation periods and sediment sizes noticeably asymmetrical. For relatively large oscillatory velocities, especially in the finer sand size, the bed forms acquire a three-dimensional hummocky appearance; this region is shown by the shading in Figures 12-51A, B, and C; it is a feature that seems to become superimposed on the symmetrical to symmetrical large combined-flow ripples under those values of the velocity components.

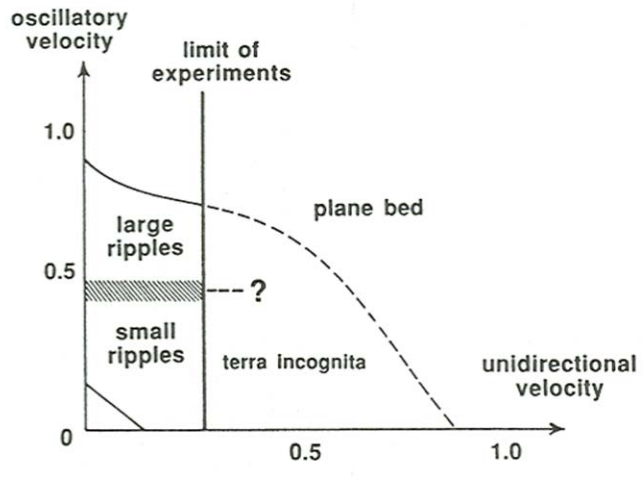

Figure 12-52. Hypothetical extrapolation of the results shown in Figure 12-51 to a wider range of combined-flow conditions. (From Southard, 1991.)

190 At unidirectional velocities greater than are shown in this graph, the field for large combined-flow ripples must pinch out, because small ripples are known to be the only stable bed configuration in purely unidirectional flows in these fine sand sizes. Figure 12-52 shows a speculative extrapolation of Figure 12-51 to higher unidirectional velocities. The effect of an increasingly strong oscillatory velocity component on unidirectional-flow dunes in medium and coarse sands is an intriguing problem for which no experimental data are yet available.

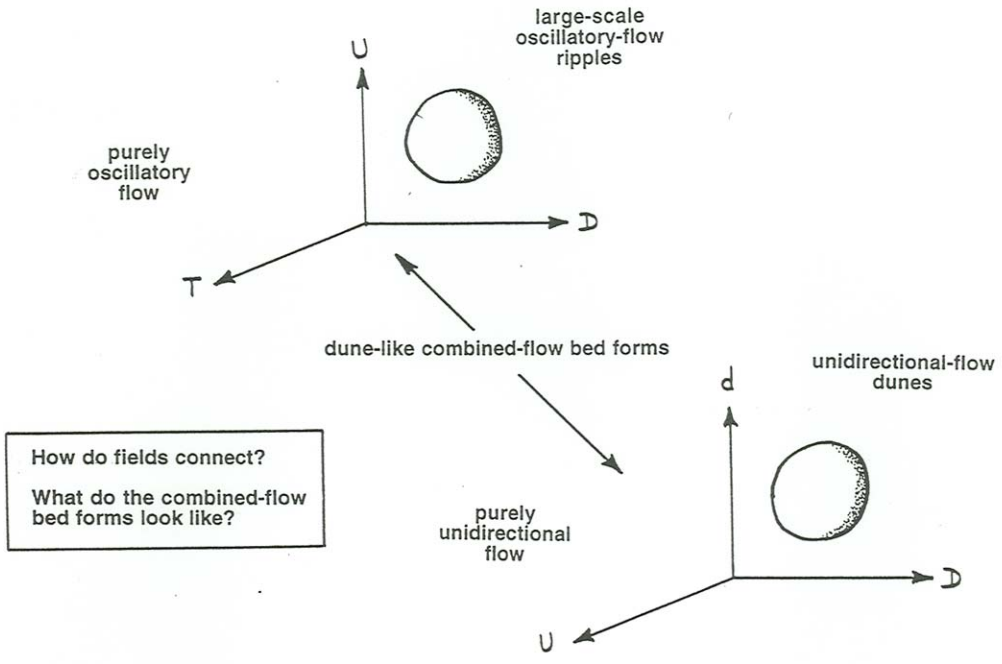

Figure 12-53. Relationship between large-sale ripples in purely oscillatory flow and dunes in purely unidirectional flow.

---

191 When the oscillation period is large, medium to high oscillation velocities produce large symmetrical ripples. Even a slight unidirectional component is known (e.g., Arnott and Southard, 1990; Dumas et al., 2005) to make these large ripples noticeably asymmetrical, to the point where they are not greatly different in geometry and internal stratification from unidirectional-flow dunes. That leads to an important question: *what do the large-scale bed forms in the intermediate range of flow conditions and sediment sizes look like?* There has been almost no systematic study of such bed forms, and yet deductively it seems that they should be important, and that a lot of the cross stratification we see in the ancient sedimentary record must have been produced under such conditions. Figure

WIND RIPPLES

Introduction

192 When a sand-moving wind lows across a surface of loose sand, wind ripples soon make their appearance. In their classic manifestation, wind ripples are almost

perfectly straight-crested low ridges extending for long distance transverse to the wind. In places, a wind ripple ends abruptly, and in other places there are "tuning fork" junctions at which a single ripple branches into two. Ripple spacing range mostly between a few centimeters and ten centimeters—although in coarser particle sizes the spacing increases up to a few meters and the ripple become much less regular in their geometry. Such ripples have been called ***granule ripples***. Upwind (stoss) surfaces of common wind ripples have slope angles of X, and downwind(lee surface have slopes of X, much less than the angle of repose for loose sand. Crests as well as troughs are rounded. As with subaqueous current ripples, wind ripples move downwind at speeds orders of magnitude slower than the driving wind. In contrast to subaqueous current ripples, particle size at the crests of the ripples are coarser than in the troughs. It is in the troughs that finer particles—of very fine sand size down into silt size—find resting places, sheltered from the wind.

193 As with so many aspects of eolian sedimentation, modern study of wind ripples began with Bagnold (1941), who studied them both in the field and in laboratory wind tunnel. (It is especially easy to make wind ripples even in a short wind tunnel.) A later classic paper is that by Sharp (1963). Two of the most extensive wind-tunnel studies of wind ripples are those of Seppälä and Lindé (1978) and Walker (1981). In what to my knowledge is the most extensive and systematic wind-tunnel study of wind ripples to date, Walker (1981) found that ripple spacing increases with both mean particle size and wind velocity, and, for a given particle size, ripple spacing increases as the sorting become less good.

194 The dynamics of wind ripples has had a long history of controversy. Bagnold theorized that the spacing of wind ripples was set by a certain "characteristic" saltation jump length. Later workers, beginning with Sharp (1963), rejected Bagnold's concept and emphasized the role of surface creep, driven by saltation impacts, in forming and maintaining the ripples. This line of thought culminated in a stability analysis of ripple development by Anderson (1987). A rather different approach to wind ripples was taken by Werner and Gillespie (1993) and by Landry and Werner (1994).

195 In recent years, physicists and applied mathematicians have been attracted to the dynamics of wind ripples, perhaps in part because it is such an intriguing example of dynamical self-organization, and perhaps in part because it lends itself to theoretical and numerical modeling in which the messiness of turbulence does not have a direct effect on the process. This interest has resulted in numerous papers, published mainly in physics periodicals; see, in particular, papers by Nishimori and Ouchi (1993), Ouchi and Nishimori (1995), Prigozhin (1995), Stam (1996), Hoyle and Woods (1997), Hoyle and Mehta (1999), Valance and Rioual (1999), Terzidis et al. (1998), Kurtze et al. (2000), Valdewalle and Galam (2000) Miao et al. (2001), Niño et al. (2002), and Yizhaq et al. (2004). In contrast, observational studies of wind ripples seem to have been scarce in recent times; see Andreotti et al. (2006).

EOLIAN DUNES

Introduction

196 In areas covered widely by movable sand, the wind shapes the sand into large-scale features called ***dunes***. In contrast to the subaqueous case, for which there is controversy about the dynamical distinction between ripples and dunes, it is clear that there is a fundamental dynamical distinction between wind ripples and eolian dunes. This was first made explicit in a widely cited paper by Wilson (1972) (Figure 12-54). Eolian dunes range in spacing from many meters, at a minimum, to thousands of meters. There seems to be no upper limit to dune size, given sufficient sand and a sufficient reach on which the wind can do its work. For a thorough exposition of eolian dune types, see Pye and Tsoar (1990).

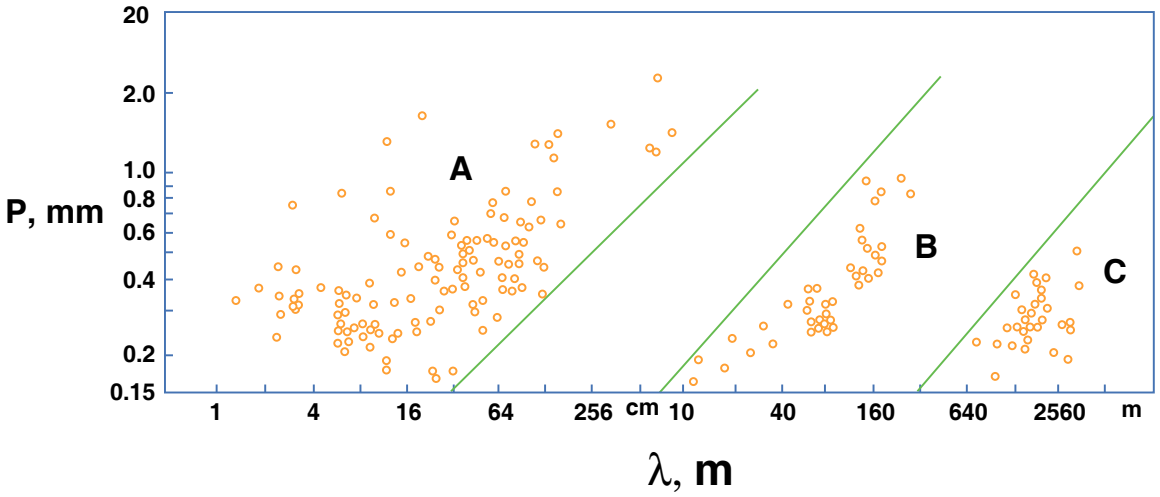

Figure by MIT OpenCourseWare.

Figure 12-54. Bed-form spacing λ against P_{20}, the coarse-twentieth-percentile particle diameter. A = wind ripples, B = dunes, C = draas. (From Wilson, 1972.)

197 In sharp contrast to subaqueous dunes, the shapes of eolian dunes, and their orientation elative to the sand-moving wind, range very widely. Features that are classified under the term *dune* range from those that are strictly transverse to the wind, to those that are extremely regular in geometry and are closely parallel to the wind—hence the distinction between transverse dunes and longitudinal dunes. In regions where the winds are highly variable in direction, star dunes, with arms oriented in various directions, form. Smaller dunes can be superimposed upon larger dunes.

198 A thought experiment seems in order here. In the case of subaqueous dunes, much of what we know comes from studies of dunes generated by unidirectional flows of water under equilibrium conditions in flumes. In the case of eolian dunes, no experimental programs of that sort have ever been conducted, to my knowledge at least. The basic problem is that because of the minimum size of dunes is so large, it would take an extraordinarily large wind tunnel to make experiments on the equilibrium characteristics of eolian dunes. And even then, of course, the presence of the roof in the

wind tunnel would make the results less applicable to the natural environment, in which, in the context of eolian dunes, is effectively unlimited in height.

199 What would we find if we built a long quonset-hut-like building, perhaps a large fraction of a kilometer long, with a roof a few tens of meters high, over a deep bed of loose sand, and passed a controlled, steady wind through the tunnel, perhaps by means of a propeller driven by an old-fashioned airplane engine mounted at the downwind end of the tunnel, while at the same time adding new sand at the upwind end of the tunnel? Presumably, dunes would develop; how would their spacing depend on wind velocity and sand size? Would they grow to the point of constriction by the height of the tunnel for all wind speeds, or would their spacing increase with wind speed? Would dune size vary with sand size? The answers to those questions, which are fairly clear for subaqueous dunes, are not known.

200 Nature provides us with much less controlled conditions: everywhere on Earth, even in the least variable climatic conditions, the wind varies in both speed and direction. That variability makes any conclusions about how dune geometry depends on wind conditions fraught with uncertainty.

201 In areas where the availability of movable sand is limited, eolian dunes take the form of ***barchans***: crescent-shaped dunes, with horns pointing downwind, that move across a non-moveable surface. Sand is supplied to the barchans from upwind; the barchans lose sediment, at about the same rate, from the downwind tips of the horns. Barchans are not restricted to eolian environments: it is easy to make miniature barchans in water flows in a flume in which limited quantities of fine sand or silt move across a the rigid floor of the flume.

202 *Are eolian dunes and subaqueous dunes identical, in terms of the fundamental dynamics?* This question is not explicitly addressed in the literature, to my knowledge, but I would speculate that the specialists, if asked, would say that they indeed are. The only way to know for sure would be to make a systematic series of observations over the range of intermediate ratios of particle density to fluid density—and that has never been done and is unlikely ever to happen.

READING LIST:

References cited:

Allen, J.R.L., 1970, A quantitative model of climbing ripples and their cross-laminated deposits: Sedimentology, v. 14, p. 5-26.

Anderson, R.S., 1987, A theoretical model for aeolian impact ripples: Sedimentollgy, v. 34, p. 943-956.

Andreotti, B., Claudin, P., and Pouliquen, O., 2006, Aeolian sand ripples: experimental study of fully developed states: Physical Review Letters, v. 96, 028001, 4 p.

Arnott, R.W., and Southard, J.B., 1990, Exploratory flow-duct experiments on combined-flow bed configurations, and some implications for interpreting storm-even stratification: Journal of Sedimentary Petrology, v. 60, p. 211-219.

Ashley, G.M., 1990, Classification of large-scale subaqueous bed forms: a new look at an old problem: Journal of Sedimentary Petrology, v. 60, p. 160-172.

Ashley, G.M., Southard, J.B., and Boothroyd, J.C., 1982, Deposition of climbing-ripple beds: A flume simulation: Sedimentology, v. 29, p. 67-79.

Bagnold, R.A., 1941, The Physics of Blown Sand and Desert Dunes: London, Methuen, 265 p.

Bagnold, R.A., 1941, The Physics of Blown Sand and desert Dunes: Chapman & Hall, 265 p.

Bennett, S.J., and Best, J.L., 1996, Mean flow and turbulence strcture over fixed ripples and the ripple–dune transition, *in* Ashworth, P.J., Bennett, S.J., Best, J.L., and McLelland, S.J., Coherent Flow Structures in Open Channels: Wiley, p. 281-304.

Boguchwal, L.A., and Southard, J.B., 1990, Bed configurations in steady unidirectional water flows. Part 3. Effects of temperature and gravity: Journal of Sedimentary Petrology, v. 60, p. 680-686.

Dillo, H.G., 1960, Sandwanderungen in Tideflussen: Technische Hochschule Hannover, Franzius-Institut für Grund- und Wsserbau, Mitteilungen, v. 17, p. 135-253.

Dumas, S., Arnott, R.W.C., and Southard, J.B., 2005, Experiments on oscillatory-flow and combined-flow bed forms: implications for interpreting parts of the shallow-marine sedimentary record: Journal of Sedimentary Research, v. 75, p. 501-513.

Engelund, F., 1970, Instability of erodible beds: Journal of Fluid Mechanics, v. 42, p. 225-244.

Engelund, F., and Fredsøe, J., 1974, Transition from dunes to plane bed in alluvial channels: Technical University of Denmark, Institute of Hydraulic Engineering, Series Paper 4.

Exner, F.M., 1925, Über die Wechselwirkung zwischen Wasser und Geschiebe in Flussen: Vienna, Austria, Akademie der Wissenschaften, Sitzungsberichte, Mathematisch-Naturwissenschaftliche Klasse, Abteilung IIa, v. 134, p. 166-204.

Fredsøe, J, 1974, On the development of dunes in erodible channels: Journal of Fluid Mechanics, v. 64, p. 1-16.

Gilbert, G.K., 1914, The transportation of debris by running water: U.S. Geological Survey, Professional paper 86, 263 p.

Guy, H.P., Simons, D.B., and Richardson, E.V., 1966, Summary of alluvial channel data from flume experiments: U.S. Geological Survey, Professional paper 462-I, 96 p.

Harms, J.C., Southard, J.B., and Walker, R.G., 1982, Structures and Sequences in Clastic Rocks: Society of Economic Paleontologists and Mineralogists, Short Course 9, variously paged.

Hoyle, R.B., and Mehta, A, 1999, Two-species continuum model for aeolian sand ripples: Physical Review Letters, v. 83, p. 5170-5173.

Hoyle, R.B., and Woods, A.W., 1997, Analytical model of propagating sand ripples: Physical Review E, v. 56, p. 6861-6868.

Jackson, P.S., 1981, On the displacement height in the logarithmic velocity profile: Journal of Fluid Mechanics, v. 111, p. 15-25.

Jerolmack, D.J., Mohrig, D., and McElroy, B., 2006, A unified description of ripples and dunes in rivers, *in* Parker, G., and García, M.H., eds., River, Coastal and Estuarine Morphodynamics: London, Taylor & Francis Group, p. 843-851.

Ji, Z.G., and Mendoza, C., 1997, Weakly nonlinear stability anaoysis for dune formation: Journal of Hydraulic Engineering, v, 123, p. 979-985.

Kennedy, J.F., 1963, The mechanics of dunes and antidunes in erodible channels: Journal of Fluid Mechanics, v. 16, p. 521-544.

Kennedy, J.F., 1969, The formation of sediment ripples, dunes, and antidunes: Annual Review of Fluid Mechanics, v. 16, p. 147-168.

Kurtze, D.A., Both, J.A., and Hong, D.C., 2000, Surface instability in windblown sand: Physical Review E, v. 61, p. 6750-6758.

Landry, W., and Werner, B.T., 1994, Computer simulations of self-organized wind ripple patterns: Physica D, v. X, p. X-X.

Lopez, F., Fernandez, R., and Best, J., 2000, Turbulence and coherent flow structure associated with bedform amalgamation: an experimental study of the ripple–dune transition: American Society of Civil Engineers, Joint Conference on Water Resources Engineering and Water Resources Planning and Management, Minneapolis, Minnesota.

McLean, S.R., 1990, The stability of ripples and dunes: Earth-Science Reviews, v. 129, p. 131-144.

Miao, T.D., Mu, Q.S., and Wu, S.Z., 2001, Computer simulation of aeolian sand ripples and dunes: Physics Letters A, v. 288, p. 16-22.

Middleton, G.V., and Southard, J.B., 1984, Mechanics of Sediment Movement, Second Edition: SEPM (Society for Sedimentary Geology), variously paged.

Monin, A.S., and Yaglom, A.M., 1971, Statistical Fluid Mechanics, Volume 1: Cambridge, Massachusetts, MIT Press, 769 p.

Niño, Y., Atala, A., Barahona, M., and Aracena, D., 2002, Discrete particle model for analyzing bedform development: Journal of Hydraulic Engineering, v. 128, p. 381-389.

Nishimori, H., and Ouchi, N., 1993, Formation of ripple patterns and dunes by wind-blown sand: Physical Review Letters, v. 71, p. 197-201.

Nordin, C.F., 1976, Flume studies with fine and coarse sands: U.S. Geological Survey, Open-File Report 76-762.

Ouchi, N.B., and Nishimori, H., 1995, Modeling of wind-blown sand using cellular automata: Physical Review E, v. 52, p. 5877-5880.

Paola, C., 1983, Flow and skin friction over natural rough beds: Cambridge, Massachusetts, Massachusetts Institute of Technology, Department of Earth and Planetary Sciences, Ph.D. dissertation, 347 p.

Prigozhin, L. 1995, Nonlinear dynamics of aeolian ripples: Physical review E, v. 60, 041302, 6 p.

Pye, K., and Tsoar, H., 1990, Aeolian Sand and Sand Dunes: Unwin Hyman, 396 p/

Richards, K.J., 1980, The formation of ripples and dunes on an erodible bed: Journal of Fluid Mechanics, v. 99, p. 597-618.

Robert, A, and Uhlman, W., 2001, An experimental study on the ripple–dune transition: Earth Surface Processes and Landforms, v. 26, p. 615-629.

Rubin, D.M., and Hunter, R.S., 1982, Bedform climbing in theory and nature: Sedimentology, v. 29, p. 121-138.

Rubin, D.M., and McCulloch, D.S., 1980, Single and superimposed bedforms: A synthesis of San Francisco Bay and flume observations: Sedimentary Geology, v. 26, p. 207-231.

Seppälä, M., and Lindé, K., 1978, Wind tunnel studies of ripple formation: Geografiska Annaler, v. A60, p. 29-42.

Sharp, R.P., 1963, Wind ripples: Journal of Geology, v. 71, p. 617-636.

Simons, D.B., and Richardson, E.V., 1966, Resistance to flow in alluvial channels: U.S. Geological Survey, Professional paper 422-J, 61 p.

Simons, D.B., and Richardson, E.V.,1963, Forms of bed roughness in alluvial channels: American Society of Civil Engineers, Transactions, v. 128, Part I, p. 284-302.

Simons, D.B., Richardson, E.V., and Nordin, C.F., Jr., 1965, Bedload equation for ripples and dunes: U.S. Geological Survey, Professional paper 462-H.

Smith, J.D., 1970, Stability of a sand bed subjected to a shear flow of low Froude number: Journal of Geophysical Research, v. 75, p. 5928-5939.

Smith, J.D., and McLean, S.R., 1977, Spatially averaged flow over a wavy surface: Journal of Geophysical research, v. 82, p. 1735-1746.

Southard, J.B., 1971, Representation of bed configurations in depth-velocity-size diagrams: Journal of Sedimentary petrology, v. 41, p. 903-915.

Southard, J.B., 1991, Experimental determination of bed-form stability: Annual Review of Fluid Mechanics, v. 19, p. 423-455.

Southard, J.B., and Boguchwal, L.A., 1990, Bed configurations in steady unidirectional water flows. Part 2. Synthesis of flume data: Journal of Sedimentary Petrology, v. 60, p. 658-679.

Southard, J.B., and Dingler, J.R., 1971, Flume study of ripple propagation behind mounds on flat sand beds: Sedimentology, v. 16, p. 251-263.

Southard, J.B., Boguchwal, L.A., and Romea, R.D., 1980, Test of scale modeling of sediment transport in steady unidirectional flow: Earth Surface Processes, v. 5, p. 17-23.

Stam, J.M.T., 1996, Migration and growth of aeolian bedforms: Mathematical Geology, v. 28, p. 519-536.

Terzidis, O., Claudin, P., and Bouchaud, J.P., 1998, A model for ripple instabilities in granular media: European Physical Journal B, v. 5, p. 245-249.

Thom, A.S., 1971, Momentum absorption by vegetation: Royal Meteorological Society, Journal, v. 97, p. 414-428.

Valance, A., and Rioual, F., 1999, A nonlinear model for aeolian sand ripples: European Physical Journal B, v. 10, p. 543-548.

Valdewalle, N., and Galam, S., 2000, A 1D Ising model for ripple formation: Journal of Physics A, v. 33, p. 4955-4962.

van den Berg, J.H., and van Gelder, A., 1993, A new bedform stability diagram, with emphasis on the transition of ripples to plane bed over fine and ssilt, *in* Marzo, M., and Puigdefàbregas, C., eds., Alluvial Sediments: International Association of Sedimentologists, Special Publication 17, p. 11-21.

Vanoni, V.A., and Brooks, N.H., 1957, Laboratory studies of the roughness and suspended load of alluvial streams: California Institute of Technology, Sedimentation Laboratory, Report E-68, MRD Sediment Series no. 11.

Vanoni, V.A., ed., 1975, Sedimentation Engineering: American Society of Civil Engineers, Manuals and Reports on Engineering Practice, no. 54, 745 p.

Walker, J.D., 1981, An experimental study of wind ripples: M.S., thesis, Massachusetts Institute of Technology, Cambridge, Massachusetts, USA, 145 p.

Werner, B.T., and Gillespie, D.T., 1993, Fundamentally discrete stochastic model for wind ripple dynamics: Physical review Letters, v. 71, p. 3230-3233.

Willis, J.C., Coleman, N.L., and Ellis, W.M., 1972, Laboratory study of transport of fine sand: American Society of Civil Engineers, Proceedings, Journal of the Hydraulics Division, v. 98, p. 489-502.

Yizhaq, H., Balmforth, N.J., and Provenzale, A., 2004, Blown by wind: nonlinear dynamics of aeolian sand ripples: Physica D, v. 195, p. 207-228.

Yokokawa, M., 1995, Combined-flow ripples: genetic experiments and applications for geologic records: Kyushu University, Faculty of Science, Memoirs, v. 29, no. 1, p. 1-38.

Recent papers on bed configurations, not cited:

Alexander, J., Bridge, J.S., Cheel, R.J., and Leclair, S.F., 2001, Bedforms and associated sedimentary structures formed under supercritical water flows over aggrading sand beds: Sedimentology, v. 48, p. 133-152.

Arnott, R.W.C., and Hand, B.M., 1989, Bedforms, primary structures and grain fabric in the presence of suspended sediment rain: Journal of Sedimentary Petrology, v. 59, p. 1062-1069.

American Society of Civil Engineers Task Committee, 2002, Flow and transport over dunes: Journal of Hydraulic Engineering, v. 128, p. 726-728.

Baas, J.H., 1999, An empirical model for the development and equilibrium morphology of current ripples in fine sand: Sedimentology, v. 46, p. 123-138.

Bartholdy, J., Bartholomae, A., and Flemming, B.W., 2002, Grain-size control of large compound flow-transverse bedforms in a tidal inlet of the Danish Wadden Sea: Marine Geology, v. 188, p. 391-413.

Bartholdy, J., Flemming, B.W., Bartholomä, A., and Ernstsen, V.B., 2005, Flow and grain size control of depth-independent simple subaqueous dunes: Journal of Geophysical Research, v. 110, F04S16, 12 p.

Bennett, S.J,, and Best, J.L., 1995, Mean flow and turbulence structure over fixed, two-dimensional dunes: implications for sediment transport and bedform stability: Sedimentology, v. 42, p. 491-513.

Besio, G., Blondeaux, P., Brocchini, M., and Vittori, G., 2004, On the modeling of sand wave migration: Journal of Geophysical Research, v 109, C04018, 13 p.

Best, J., 2005, The fluid dynamics of river dunes: A review of some future research directions: Journal of Geophysical Research, v. 110, F04S02, 21 p.

Best, J., and Bridge, J., 1992, The morphology and dynamics of low amplitude bedwaves upon upper stage plane beds and the preservation of planar laminae: Sedimentology, v. 39, p. 737-752.

Best, J.L., and Kostaschuk, R., 2002, An experimental study of turbulent flow over a low-angle dune: Journal of Geophysical Research, v. 107(C9), 3135, 19 p.

Blom, A., 2006, The impact of variability in dune dimensions on sediment sorting and morphodynamics, *in* Parker, G., and García, M.H., eds., River, Coastal and Estuarine Morphodynamics: London, Taylor & Francis Group, p. 873-881.

Blom, A., and Parker, G., 2004, Vertical sorting and the morphodynamics of bed form–dominated rivers: A modeling framework: Journal of Geophysical Research, v. 109, F02007, 15 p.

Blom, A., Ribberink, J.S., and de Vriend, H.J., 2003, Vertical sorting in bed forms: Flume experiments with a natural and a trimodal sediment mixture: Water Resources Research, v. 39 (2), 1025, ESG 1, 13 p.

Bridge, J.S., and Best, J.L., 1988 Flow, sediment transport and bedform dynamics over the transition from dunes to upper-stage plane beds: implications for the formation of planar laminae: Sedimentology, v. 35, p. 753-763.

Cacchione, D.A., Wiberg, P.L., Lynch, J., Irish, J., and Traykovski, P., 1999, Estimates of suspended-sediment flux and bedform activity on the inner portion of the Eel continental shelf: Marine Geology, v. 154, p. 83-97.

Carling, P.A., 1999, Subaqueous gravel dunes: Journal of Sedimentary Research, v. 69, p. 534-545.

Carling, P.A., and Shvidchenko, A.B., 2002, A consideration of the dune:antidune transition in fine gravel: Sedimentology, v. 49, p. 1269-1282.

Carling, P.A., Gölz, E., Orr, H.G., and Radecki-Pawlik, A., 2000, The morphodynamics of fluvial sand dunes in the River Rhine, near Mainz, Germany. I. Sedimentology and morphology: Sedimentology, v. 47, p. 227-252.

Carling, P.A., Williams, J.J., Gölz, E., and Kelsey, A.D., 2000, The morphodynamics of fluvial sand dunes in the River Rhine, near Mainz, Germany. II. Hydrodynamics and sediment transport: Sedimentology, v. 47, p. 253-278.

Cataño-Lopera, Y.A., and García, M.H., 2006, Geometric and migrating characteristics of amalgamated bedforms under oscillatory flows, *in* Parker G, and García M, eds., River, Coastal and Estuarine Morphodynamics: London, Taylor & Francis Group, p. 1017-1026.

Chang, Y.S., and Hanes, D.M., 2004, Suspended sediment and hydrodynamics above mildly sloped long wave ripples: Journal of Geophysical Research, v. 109, C07022, 16 p.

Chang, Y.S., and Scotti, A., 2004, Modeling unsteady turbulent flows over ripples: Reynolds-averaged Navier-Stokes equations (RANS) versus large-eddy simulation (LES): Journal of Geophysical Research, v. 109, C09012, 16 p.

Cheel, R.J., 1990, Horizontal lamination and the sequence of bed phases and stratification under upper-flow-regime conditions: Sedimentology, v. 37, p. 517-529.

Clarke, L.B., and Werner, B.T., 2004, Tidally modulated occurrence of megaripples in a saturated surf zone: Journal of Geophysical Research, v. 109, C01012, 15 p.

Coleman, S.E., Fedele, J.J., and Garcia, M.H., 2003, Closed-conduit bed-form initiation and development: Journal of Hydraulic Engineering, v. 129, p. 956-965.

Coleman, S.E., Schlicke, E., and Blackbourn, S., 2006, Growth of wave-induced ripples, *in* Parker, G., and García, M.H., eds., River, Coastal and Estuarine Morphodynamics: London, Taylor & Francis Group, p. 963-971.

Crawford, A.M., and Hay, A.E., 2001, Linear transition ripple migration and wave orbital velocity skewness: Observations: Journal of Geophysical Research, v. 106, p. 14,113-14,128.

Damgaard, J., Soulsby, R., Peet, A., and Wright, S., 2003, Sand transport on steeply sloping plane and rippled beds: Journal of Hydraulic Engineering, v. 129, p. 706-719.

Davis, J.P., Walker, D.J., Townsend, M., and Young, I.R., 2004, Wave-formed sediment ripples: Transient analysis of ripple spectral development: Journal of Geophysical Research, v. 109, C07020, 15 p.

Dinehart, R.L., 1992, Evolution of coarse gravel bed forms: field measurements at flood stage: Water Resources Research, v. 28, p. 2667-2689.

Doucette, J.S., 2000, The distribution of nearshore bedforms and effects on sand suspension on low-energy, micro-tidal beaches in Southwestern Australia: Marine Geology, v. 165, p. 41-61.

Doucette, J.S., 2002, Geometry and grain-size sorting of ripples on low-energy sand beaches: field observations and model predictions: Sedimentology, v. 49, p. 483-503.

Duffy, G.P., and Hughes-Clarke, J.E., 2005, Applications of spatial cross correlation to detection of migration of submarine sand dunes: Journal of Geophysical Research, v. 110, F04S12.

Elhakeem, M., and Imran, J., 2006, A bedload model for uniform sediment derived from the movement of bed forms, *in* Parker, G., and García, M.H., eds., River, Coastal and Estuarine Morphodynamics: London, Taylor & Francis Group, p. 853-860.

Ernstsen, V.B., Noormets, R., Winter, C., Hebbeln, D., Bartholomä, A., Flemming, B.W., and Bartholdy, J., 2005, Development of subaqueous barchanoid-shaped dunes due to lateral grain size variability in a tidal inlet channel of the Danish Wadden Sea: Journal of Geophysical Research, v. 110,F04S08, 13 p.

Flemming, B.W., 1992, Bed phases in bioclastic sands exposed to unsteady, non-equilibrated flows: an experimental flume study: Senckenbergiana Maritima, v. 22. p. 95-108.

Giménez-Curto, L.A., and Corniero, M.A., 2003, Highest natural bed forms: Journal of Geophysical Research, v.108(C2), 3046, 7 p.

Gonzalez, R., and Eberli, G., 1997, Sediment transport and bedforms in a carbonate tidal inlet; Lee Stocking Island, Exumas, Bahamas: Sedimentology, v. 44, p. 1015-1030.

Ha, H.K., and Chough, S.K., 2003, Intermittent turbulent events over sandy current ripples: a motion-picture analysis of flume experiments: Sedimentary Geology, v. 161, p. 295-308.

Harbor, D.J., 1998, Dynamics of bedforms in the lower Mississippi River: Journal of Sedimentary Research, v. 68 , p. 750-762.

Héquette, A., and Hill, P.R., 1995, Response of the seabed to storm-generated combined flows on a sandy Arctic shoreface, Canadian Beaufort Sea: Journal of Sedimentary Research, v. A65, p. 461-471.

Hersen, P., 2005, Flow effects on the morphology and dynamics of aeolian and subaqueous barchan dunes: Journal of Geophysical Research, v. 110, F04S07, 10 p.

Hoekstra, P., Bell, P., van Santen, P., Roode, N., Levoy, F., and Whitehouse, R., 2004, Bedform migration and bedload transport on an intertidal shoal: Continental Shelf Research, v. 24, p. 1249-1269.

Hulscher, S.J.M.H., 1996, Tidal-induced large-scale regular bed form patterns in a three-dimensional shallow water model: Journal of Geophysical Research, v. 101, p. 20,727-20,744.

Hulscher, S.J.M.H., and Dohmen-Janssen, C.M., 2005, Introduction to special section on Marine Sand Wave and River Dune Dynamics: Journal of Geophysical Research, v. 110, F04S01, 6 p.

Jerolmack, D., and Mohrig, D., 2005, Interactions between bed forms: Topography, turbulence, and transport: Journal of Geophysical Research, v. 110, F02014, 13 p.

Kleinhans, M.G., 2001, The key role of fluvial dunes in transport and deposition of sand–gravel mixtures, a preliminary note: Sedimentary Geology, v. 143, p. 7-13.

Kleinhans, M.G., 2005, Upstream sediment input effects on experimental dune trough scour in sediment mixtures: Journal of Geophysical Research, v. 110, F04S06, 8 p.

Kleinhans, M.G., Wilbers, A.W.E., de Swaaf, A., and van den Berg, J.H., 2002, Sediment supply–limited bedforms in sand–gravel bed rivers: Journal of Sedimentary Research, v. 72, p. 629-640.

Kostaschuk, R., 2000, A field study of turbulence and sediment dynamics over subaqueous dunes with flow separation: Sedimentology, v. 47, p. 519-531.

Kostaschuk, R., 2006, Sediment transport mechanics and subaqueous dune morphology, *in* Parker G,, and García M., eds, River, Coastal and Estuarine Morphodynamics: London, Taylor & Francis Group, p. 795-801.

Kostaschuk, R., and Best, J., 2005, Response of sand dunes to variation in tidal flow: Fraser Estuary, Canada: Journal of Geophysical Research, v. 110, F04S04, 10 p .

Langlois, V., and Valance, A., 2005, Three-dimensionality of sand ripples under steady laminar shear flow: Journal of Geophysical Research, v. 110, F04S09, 12 p.

Larcombe, P., and Jago, C.F., 1996, The morphological dynamics of intertidal megaripples in the Mawddach Estuary, North Wales, and the implications for palaeoflow reconstructions: Sedimentology, v. 43, p. 541-559.

Lawless, M., and Robert, A., 2001, Three-dimensional flow structure around small-scale bedforms in a simulated gravel-bed environment: Earth Surface Processes and Landforms, v. 26, p.507-522.

Leclair, S.F., 2002, Preservation of cross-strata due to the migration of subaqueous dunes: an experimental investigation: Sedimentology, v. 49, p. 1157-1180.

Leclair, S.F., and Bridge, J.S., 2001, Qualitative interpretation of sedimentary structures formed by river dunes: Journal of Sedimentary Research, v. 71, p. 713-716.

Leclair, S.F., and Miller, J.Z., 2006, Time variation of probability distributions of dune-bed elevation in a large river, *in* Parker, G., and García, M.H., eds., River, Coastal and Estuarine Morphodynamics: London, Taylor & Francis Group, p. 803-812.

Lee, H.J., Jo, H.R., and Chu, Y.S., 2006, Dune migration on macrotidal flats under symmetrical tidal flows: Garolim Bay, Korea : Journal of Sedimentary Research, v. 76, p. 284-291.

Li, M.Z., 1994, Direct skin friction measurements and stress partitioning over movable sand ripples: Journal of Geophysical Research, v. 99, p. 791-799.

Li, M.Z., and Amos, C.L., 1998 Predicting ripple geometry aned bed roughness under combined waves and currents in a continental shelf environment Continental Shelf Research 18 941-970 .

Li, M.Z., and Amos, C.L., 1999a, Field observations of bedforms and sediment transport thresholds of fine sand under combined waves and currents: Marine Geology, v. 158, p. 147-160.

Li, M.Z., and Amos, C.L., 1999b, Sheet flow and large wave ripples under combined waves and currents: field observations, model prediction and effects on boundary layer dynamics: Continental Shelf Research, v. 19, p. 637-663.

Maddux, T.B., McLean, S.R., and Nelson, J.M., 2003a, Turbulent flow over three-dimensional dunes: 2. Fluid and bed stress: Journal of Geophysical Research, v.108 (F1), 6010, 11, 17 p.

Maddux, T.B., Nelson, J.M., and McLean, S.R., 2003b, Turbulent flow over three-dimensional dunes: 1. Free surface and flow response: Journal of Geophysical Research, v. 108, F1, 6009, 20 p.

Malarkey, J., and Davies, A.G., 2004, An eddy viscosity formulation for oscillatory flow over vortex ripples: Journal of Geophysical Research, v. 109, C12016, 13 p.

Mantz, P.A., 1992, Cohesionless fine-sediment bed forms in shallow flows: Journal of Hydraulic Engineering, v. 118, p. 743-764.

Marin, F., Abcha, N., Brossard, J., and Ezersky, A.B., 2005, Laboratory study of sand bed forms induced by solitary waves in shallow water: Journal of Geophysical Research, v. 110, F04S17.

Mazumder, R., 2000, Turbulence–particle interactions and their implications for sediment transport and bedform mechanics under unidirectional current: some recent developments: Earth-Science Reviews, v. 50, p. 113-124.

Mazumder, R., 2003, Sediment transport, aqueous bedform stability and morphodynamics under unidirectional current: a brief overview: Journal of African Earth Sciences, v. 36, p. 1-14.

McLean, S.R., and Nelson, J.M., 2006, Sediment transport over ripples and dunes, *in* Parker, G., and García, M.H., eds., River, Coastal and Estuarine Morphodynamics: London, Taylor & Francis Group, 821-829.

McLean, S.R., Nelson, J.M., and Wolfe, S.R., 1994, Turbulence structure over two-dimensional bed forms: Implications for sediment transport: Journal of Geophysical Research, v. 99, p. 12,729-12,747.

McLean, S.R., Wolfe, S.R., and Nelson, J.M., 1999, Predicting boundary shear stress and sediment transport over bed forms: Journal of Hydraulic Engineering, v. 125, p. 725-736.

Morris, S.A., Kenyon, N.H., Limonov, A.F., and Alexander, J., 1998, Downstream changes of large-scale bedforms in turbidites around the Valencia channel mouth, north-west Mediterranean: implications for palaeoflow reconstruction: Sedimentology, v. 45, p. 365-377.

Murray, A.B., Coco, G., Green, M., Hume, T., and Thieler, R., 2006, Different approaches to modeling inner-shelf 'sorted bedforms', *in* Parker, G., and García, M.H., eds., River, Coastal and Estuarine Morphodynamics: London, Taylor & Francis Group, p. 1009-1015.

Narteau, C., Lajeunesse, E., Métivier, F., and Rozier, O., 2006, Modelling of dune patterns by short range interactions, *in* Parker, G,, and García, M., eds., River, Coastal and Estuarine Morphodynamics: London, Taylor & Francis Group, p. 1035-1046.

Nelson, J.M., Shreve, R.L., McLean, S.R., and Drake, T.G., 1995, Role of near-bed turbulence structure in bed load transport and bed form mechanics: Water Resources Research, v. 31, p. 2071-2086.

Nelson, J.M., Burman, A.R., Shimizu, Y., McLean, S.R., Shreve, R.L., and Schmeeckle, M., 2006, Computing flow and sediment transport over bedforms, *in* Parker, G., and García, M.H., eds., River, Coastal and Estuarine Morphodynamics: London, Taylor & Francis Group, p. 861-872.

Németh, A.A., Hulscher, S.J.M.H., and van Damme, R.M.J., 2006, Simulating offshore sand waves: Coastal Engineering, v. 53, p. 265-275.

Ngusaru, A.S., and Hay, A.E., 2004, Cross-shore migration of lunate megaripples during Duck94: Journal of Geophysical Research, v. 109, C02006, 16 p.

Oost, A.P., and Baas, J.H., 1994, The development of small scale bedforms in tidal environments: an empirical model for unsteady flow and its applications: Sedimentology, v. 41, p. 883-903.

Paarlberg, A.J., Dohmen-Janssen, C.M., and Hulscher, S.J.M.H., 2006, A parameterization for flow separation in a river dune development model, *in* Parker, G., and García, M.H., eds., River, Coastal and Estuarine Morphodynamics: London, Taylor & Francis Group, p. 883-895.

Parsons, D.R., Best, J.L., Orfeo, O., Hardy, R.J., Kostaschuk, R., and Lane, S.N., 2005, Morphology and flow fields of three-dimensional dunes, Rio Paraná, Argentina: Results from simultaneous multibeam echo sounding and acoustic Doppler current profiling: Journal of Geophysical Research, v. 110, F04S03, 9 p.

Passchier, S., and Kleinhans, M.G., 2005, Observations of sand waves, megaripples, and hummocks in the Dutch coastal area and their relation to currents and combined flow conditions: Journal of Geophysical Research, v. 110, F04S15, 15 p.

Ramsay, P.J., Smith, A.M., and Mason, T.R., 1996, Geostrophic sand ridge, dune fields and associated bedforms from the Northern KwaZulu–Natal shelf, south-east Africa: Sedimentology, v. 43, p. 407-419.

Robert, A., and Uhlman, W., 2001, An experimental study on the ripple–dune transition: Earth Surfsce Processes and Landforms, v. 26, p. 615-629

Schindler, R.J., and Robert, A., 2004, Suspended sediment concentration and the ripple–dune transition: Hydrological Processes, v. 18, p. 3215-3227.

Schindler, R.J., and Robert, A., 2005, Flow and turbulence structure across the ripple–dune transition: an experiment under mobile bed conditions: Sedimentology, v. 52, p. 627-649.

Serra, S.G., and Vionnet, C.A., 2006, Migration of large dunes during extreme floods of the Paraná River, Argentina, *in* Parker, G., and García, M.H., eds., River, Coastal and Estuarine Morphodynamics: London, Taylor & Francis Group, p. 897-908.

Smyth, C.E., and Li, M.Z., 2005, Wave-current bedform scales, orientation, and migration on Sable Island Bank: Journal of Geophysical Research, v. 110, C02023, 12 p.

Smyth, C., Hay, A.E., and Zedel, L., 2002, Coherent Doppler Profiler measurements of near-bed suspended sediment fluxes and the influence of bed forms: Journal of Geophysical Research, v. 107(C8), 3105, 20 p.

Storms, J.E.A., van Dam, R.L., and Leclair, S.F., 1999, Preservation of cross-sets due to migration of current ripples over aggrading and non-aggrading beds: comparison of experimental data with theory: Sedimentology, v. 46, p. 189-200.

Tjerry, S., and Fredsøe, J., 2005, Calculation of dune morphology: Journal of Geophysical Research, v. 110, F04013, 13 p.

Trouw, K., Williams, J.J., and Rose, C.P., 2000, Modelling sand resuspension by waves over a rippled bed: Estuarine, Coastal and Shelf Science, v. 50, p. 143-151.

van den Berg, J.H., and van Gelder, A., 1998, Flow and sediment transport over large subaqueous dunes: Fraser River, Canada: Sedimentology, v. 45, p. 217-221.

van der Mark, C.F., Blom, A., and Hulscher, S.J.M.H., 2006, On modeling the variability of bedform dimensions, *in* Parker, G., and García, M.H., eds., River, Coastal and Estuarine Morphodynamics: London, Taylor & Francis Group, p. 831-841.

van Dijk, T.A.G.P., and Kleinhans, M.G., 2005, Processes controlling the dynamics of compound sand waves in the North Sea, Netherlands: Journal of Geophysical Research, v. 110, F04S10, 15 p.

Vanwesenbeeck, V., and Lanckneus, J., 2000, Residual sediment transport paths on a tidal sand bank: a comparison between the modified McLaren model and bedform analysis: Journal of Sedimentary Research, v. 70, p. 470-477.

Venditti, J.G., and Bauer, B.O., 2005, Turbulent flow over a dune: Green River, Colorado: Earth Surface Processes and Landforms, v. 30, p. 289-304.

Venditti, J.G., Church, M., and Bennett, S.J., 2005a, On the transition between 2D and 3D dunes: Sedimentology, v. 52, p. 1343-1359.

Venditti, J.G., Church, M.A., and Bennett, S.J., 2005b, Bed form initiation from a flat sand bed: Journal of Geophysical Research, v. 110, F01009, 19 p .

Villard, P.V., and Church, M., 2005, Bar and dune development during a freshet: Fraser River Estuary, British Columbia, Canada: Sedimentology, v. 52 , p. 737-756.

Villard, P., and Kostaschuk, R., 1998, The relation between shear velocity and suspended sediment concentration over dunes: Fraser Estuary, Canada: Marine Geology, v. 148, p. 71-81.

Villard, P.V., and Osborne, P.D., 2002, Visualization of wave-induced suspension patterns over two-dimensional bedforms: Sedimentology, v. 49, p. 363-378.

Walgreen, M., Calvete, D., and de Swart, H.E., 2002, Growth of large-scale bed forms due to storm-driven and tidal currents: a model approach: Continental Shelf Research, v. 22, p. 2777-2793.

Werner, S.R., Beardsley, R.C., and Williams, A.J., III, 2003, Bottom friction and bed forms on the southern flank of Georges Bank: Journal of Geophysical Research, v. 108(C11), 8004, 21 p.

Whitehouse, R.J.S., Bassoullet, P., Dyer, K.R., Mitchener, H.J., and Roberts, W., 2000, The influence of bedforms on flow and sediment transport over intertidal mudflats: Continental Shelf Research, v. 20, p. 1099-1124.

Williams, J.J., Bell, P.S., and Thorne, P.D., 2003, Field measurements of flow fields and sediment transport above mobile bed forms: Journal of Geophysical Research, v. 108(C4), 3109, 36 p.

Williams, J.J., Bell, P.S., and Thorne, P.D., 2005, Unifying large and small wave-generated ripples: Journal of Geophysical Research, v. 110, C02008, 18 p.

Wilson, I.G., 1972, Universal discontinuities in bedforrms produced by the wind: Journal of Sedimentary Petrology, v. 42, p. 667-669.

Yamaguchi, S., and Izumi, N., 2006, Weakly nonlinear analysis of dunes by the use of a sediment transport formula incorporating the pressure gradient, *in* Parker, G., and García, M.H., eds., River, Coastal and Estuarine Morphodynamics: London, Taylor & Francis Group, p. 813-820.

Zedler E.A,, and Street, R.L., 2002, Large-eddy simulation of sediment transport: currents over ripples: Journal of Hydraulic Engineering, v. 127, p. 444-452.

Zedler, E.A., and Street, R.L., 2006, Sediment transport over ripples in oscillatory flow: Journal of Hydraulic Engineering, v. 132, p. 180-193.